ARCHITECTURE OF THE BETA2/BETA4-NAV CHANNEL SIGNALING COMPLEX

by

John Michael Gilchrist

"A dissertation submitted to Johns Hopkins University in conformity with the requirements for the degree of Doctor of Philosophy"

Baltimore, Maryland

April 2017

Abstract

The voltage-gated sodium (Nav) channel complex is comprised of a channel-forming, ion-conducting α-subunit and one or multiple accessory β-subunits. The latter has been shown to influence the function of Nav channels and mutations within the β-subunit have been tied to cardiac and neurologic disorders. We show here that β-subunits can also affect the pharmacology of Nav channels, particularly in relation to toxins derived from animal venoms. In this work we combine our knowledge of toxin binding sites with novel crystal structures of two β-subunits to determine the cysteine residues responsible for forming the disulfide bridge between the β2/β4 subunits and the Nav1.2 channel. In doing so, we provide a basis for understanding the interaction between the β-subunits and Nav channels and the functional consequences of this interaction.

Thesis Advisor: Dr. Frank Bosmans

Thesis Reader: Dr. Michael Caterina

Acknowledgements

I would like to thank the following people:

Thomas Gilchrist and Deborah Dawson: for producing, supporting, and encouraging me throughout my life thus far.

Dr. Frank Bosmans: for providing incomparable scientific training, introducing me to the scientific community, and being an incredibly supportive mentor

Dr. Alan Schenkel: for introducing me to scientific research, encouraging my independence as a researcher, and generally preparing me for my scientific endeavors to date

Dr. Suzi Schweitzer: for helping me realize I would pursue a PhD

Dr. Michael Caterina: for serving on my thesis committee, writing letters of recommendation, and being a remarkably timely and forbearing thesis reader

Drs. Jeremy Nathans, Kenton Swartz, and David Yue: for graciously serving on my thesis committee and giving me the constructive input that helped me successfully complete my graduate studies

Drs. Samir Das and Filip Van Petegem: for being generous and patient collaborators without whom this work would be incomplete

Dr. Blythe Shepard, Dr. YaWen Lu, Dr. Carlitos Villalba-Galea, Ms. Elizabeth Calzada, and Mr. Jesse Yoder: for invaluable technical assistance

The others too many to enumerate: everything else too long to list here

Table of Contents

ABSTRACT……..……ii

ACKNOWLEDGEMENTS……..……iii

LIST OF FIGURES…….…vi

LIST OF TABLES……..…viii

CHAPTER 1: Introduction……1

The voltage-gated sodium channel signaling complex……..……2

Figures……..…19

CHAPTER 2: Crystallographic insights into sodium-channel modulation by the β4 subunit…….…….20

Summary and Contributions…….……21

Introduction……..……22

Results…….……24

β-subunits shape Nav channel pharmacology……..……24

The β4 subunit structure reveals an exposed cysteine……26

Mutating 58Cys in β4 restores Nav1.2 sensitivity to ProTx-II……..……27

Mapping clinically relevant β-Subunit mutations onto the β4 structure.…29

The C131W mutation alters the influence of β4 on Nav1.2 toxin pharmacology…….…..…32

Discussion……34

Materials and Methods…….……37

Acknowledgments ……..……43

Figures…….……44

Tables……....…61

CHAPTER 3: Binary architecture of the Nav1.2-β2 signaling complex……..…65

Summary and Contributions……66
Introduction……67
Results……70
Crystal structure of the human β2 extracellular region……70
Mutating 55Cys in hβ2 restores hNav1.2 toxin susceptibility……72
The S5-S6 loop in domain II of hNav1.2 contains an anchoring point for hβ2……74
Positioning β2 in relation to Nav1.2……78
Discussion……80
Materials and Methods……84
Acknowledgments……91
Figures……92
Tables……119
CHAPTER 4: Conclusion……127
Summary of findings……128
Future directions……134
Figures……136
REFERENCES……137
CURRICULUM VITAE……176

List of figures

Figure 1-1: A general depiction of the Nav channel……..…19

Figure 2-1: Influence of β-subunits on the ligand susceptibility

of the voltage-gated sodium channel Nav1.2……..…..…44

Figure 2-2: Influence of β4 on the ligand susceptibility of Nav1.2……..……46

Figure 2-3: Sensitivity of Nav1.2 paddle chimaeras to LqqIV……..…48

Figure 2-4: Crystal structure of the β4 extracellular domain……49

Figure 2-5: Omit map of the β4 core……51

Figure 2-6: Surface representation and thermal stability of the β4

extracellular domain……..…52

Figure 2-7: Reducing ^{58}Cys abolishes the effect of β4 on ProTx-II binding……..54

Figure 2-8: Influence of β4 C58A on ProTx-II susceptibility of Nav1.2……..……55

Figure 2-9: β4 and the C58A mutant are glycosylated and trafficto the membrane……57

Figure 2-10: Disease-related mutations mapped onto the β4 extracellular

domain structure and crystal structure of the β4 C131W variant……..……58

Figure 2-11: Gel-filtration chromatograms of β4, C131W, and C131A……..……59

Figure 2-12: Influence of β4 C131W on ProTx-II susceptibility of Nav1.2…….60

Figure 3-1: Crystal structure of hβ2……..…92

Figure 3-2: Structural comparison of hβ2 to hβ3 and hβ4……..……94

Figure 3-3: ProTx-II does not bind directly to β4……..……96

Figure 3-4: G-V and SSI relationships for hβ2 mutants……97

Figure 3-5: Effect of hβ2 on hNav1.2 toxin pharmacology……..……99

Figure 3-6: Amino acid sequence alignment of the β2 protein

found in various organisms……..……..……101

Figure 3-7: hβ2 forms a disulfide bond with ^{910}Cys in hNav1.2……103

Figure 3-8: G-V and SSI relationships for hNav1.2 mutants……105

Figure 3-9: Activity of the μO§-conotoxin GVIIJ is affected by hβ2……107

Figure 3-10: Biochemical assessment of rβ2 oligomer formation……109

Figure 3-11: Biochemical verification of the β2 and β4 disulfide bond with ^{910}Cys in Nav1.2……110

Figure 3-12: Mutation of ^{910}Cys in rNav1.2a disrupts rβ4 influence on ProTx-II effect……112

Figure 3-13: ProTx-II inhibits hNav1.5 in the presence of hβ2……114

Figure 3-14: hβ2 influences hNav1.2 VSDI toxin pharmacology……116

Figure 3-15: Activity of spider and scorpion toxins on hNav1.2……118

Figure 4-1: Potential location of β-subunits within the Nav channel signaling complex……136

List of tables

Table 2-1: Influence of ligands on the gating properties of Nav1.2 and Nav1.2/βx……..……61

Table 2-2: Data collection and refinement statistics……62

Table 2-3: Disease mutations mapped on the Navβ4 structure……..……64

Table 3-1: Data collection and refinement statistics……...…119

Table 3-2: Table providing values for fits of the data presented in Fig. 3-4 and Fig. 3-5……120

Table 3-3: Table providing values for fits of the data presented in Fig. 3-7 and Fig. 3-8……121

Table 3-4: Table providing values for fits of the data presented in Fig. 3-9……..123

Table 3-5: Table providing values for fits of the data presented in Fig. 3-12……..……124

Table 3-6: Table providing values for fits of the data presented in Fig. 3-13……125

Table 3-7: Table providing values for fits of the data presented in Fig. 3-14 and Fig. 3-15……126

ARCHITECTURE OF THE BETA2/BETA4-NAV CHANNEL SIGNALING COMPLEX

Chapter 1: Introduction

The voltage-gated sodium channel signaling complex

The voltage-gated sodium (Nav) channel signaling complex is a critical component of electrical signaling within the body. As the Nav complex is responsible for axonal nerve conduction, initiation of the (cardiac) action potential, and a host of other roles, the importance of the Nav complex is reflected in the number of diseases resulting from or associated with mutations of its constituents [1]. These diseases range from neurologic syndromes like epilepsy [2] and migraine [3] to cardiac disorders such as Brugada syndrome [4] and Long QT syndrome [5] and even extreme pain [6] or total insensitivity to pain [7]. Despite the long history of Nav channel research, only in the past two decades has the role of auxiliary subunits come to light, illuminating their ability to modify channel gating as well as other Nav channel-independent roles [8-10]. The Nav complex is composed of several integral membrane proteins [11], including the pore-forming α-subunit (the Nav channel) and the auxiliary β-subunit. A description of each follows.

The voltage-gated sodium channel

Structure

The voltage-gated sodium (Nav) channel (α-subunit, referred to henceforth as the Nav channel) is a transmembrane glycoprotein with 24 transmembrane (TM) segments, organized into four domains with six TM segments each, with the first four TM segments comprising the voltage-sensor and the latter two

contributing to the formation of the central ion-conducting pore. The pore is a cavity within the center of the Nav channel α-subunit circumscribed by eight TM helices with each domain contributing two helices [12] (Fig. 1-1). Within the pore, a selectivity filter formed by an Asp-Glu-Lys-Ala (DEKA) motif dictates specificity for Na^+ over K^+ [13-15].

The fourth TM segment (S4) of each voltage-sensing domain (VSD) carries a number of positive charges, borne on the basic side chains of Arg and Lys contained in the S4 [16, 17]. These basic side chains, termed gating charges, provide the voltage sensor with its ability to sense voltage, migrating through the membrane in response to a change in the electric field [18, 19].

Both the N- and C-termini reside inside the cell, and the channel spans roughly 1900 amino acids between them [20], resulting in a molecular mass of approximately 280 kDa, contributed by both the peptide and its glycosylation [21-23]. The Nav1 family is populated by the related isoforms Nav1.1 through Nav1.9, as well as the distantly related Nax [24]. While their discovery was aided by the potent Nav-specific blocker tetrodotoxin (TTX) [25, 26], three of the isoforms are resistant to this toxin: the cardiac isoform Nav1.5 is somewhat resistant [27], while the peripheral nervous system (PNS) isoforms Nav1.8 and Nav1.9 are highly resistant [28]. All isoforms are believed to conform to the same structural archetype, with very similar TM segments, particularly those of the voltage sensor, while the extra- and intracellular loops are highly variable, differing in both sequence and length [29].

One of the defining features of Nav channels, and one critical to proper function, is their characteristic fast inactivation process, where the activated channel terminates its sodium conductance and becomes refractory to subsequent depolarizations. While not unique to Nav channels, the inactivation process is found in all Nav isoforms [30]. Inactivation has been linked to activation of the slower-moving domain IV (DIV) voltage sensor [31-36]. The intracellular III-IV linker provides the termed “inactivation gate”, which uses an Ile-Phe-Met (IFM) motif presumably to occlude the pore and prevent further Na^+ flux [37-41]. Subsequent to inactivation, the Nav channel is refractory to activation and cannot be opened until after a hyperpolarization event [42]. This refractory period is critical for unidirectional conduction of an action potential along the axon, preventing a return of depolarization “upstream” from which the action potential originated. DI-III are primarily tied to opening; VSDI-III, which are believed to move first in response to membrane depolarization, migrate in the membrane, driven by the charged S4 helix and opening the channel [18, 31, 33].

As the Nav channel family is related of the the voltage-gated potassium (Kv) channel family, early structural insights into Kv structures were a boon to the Nav channel field. Like the Nav channel, the Kv channel also has a central pore and four voltage-sensing domains but instead of being formed from a single polypeptide chain, the complete Kv channel is a homotetramer of smaller subunits that each bear 6 TM domains [43, 44]. As a result, the Kv and Nav channels adopt a similar geometry, but the latter exhibits substantial heterogeneity between domains [29]. The crystal structures of the KvAP [44] and

Kv1.2 [43] channels (2003 and 2005, respectively), propelled many new insights into ion channel structure and function. Between then and 2011, when the first prokaryotic Nav channel was crystallized [16], the Kv channel served as primary structural model for much of what was understood about Nav channel structure. Multiple bacterial Nav channel structures were solved [16, 17, 45, 46], but as homotetramers themselves, they provided only an incremental improvement on the Kv channel. While many new insights were gained, the structure of the mammalian Nav channel remained elusive. It was not until 2017 that a eukaryotic Nav channel structure was revealed by cryo-EM [47], providing a first glance into the channel's actual pseudoheterotetramer tertiary structure.

While unique insights into the Nav channel were afforded by the cryo-EM structure, much of what was observed in these studies was a confirmation of what had been anticipated from the Kv channel. One of the more interesting revelations from the Kv channel structure was of the "domain-swap" architecture [44, 48, 49], where the two pore-forming segments S5 and S6 sit not next to S1-4 of the voltage-sensor but instead by the VSD of the retrograde domain. The domains are oriented in a clockwise fashion and the domain swap arrangement has the pore domain of DIV sitting by VSDIII, and the DIII pore domain by the DII voltage-sensor, etc. This same configuration was observed in the bacterial Nav channels, highlighting a degree of structural conservation between the voltage-gated channel family [16, 17, 45, 46].

Physiology

Found throughout the body on in nerves and muscles, the Nav channel is responsible for rapid depolarizations of the cellular membrane, generated by the influx of Na^+ from outside the cell through the channel [12, 50]. In response to small depolarizations of the cell or a rising resting membrane potential, the Nav channel activates and by creating a permeability to Na+, quickly shifts the membrane potential (Vm) nearer to that of the Na^+ Nernst potential, typically around +60 mV. The elevation of Vm in the local area can induce other Nav channels to open, propagating an action potential down the length of a neuronal axon, or it might stimulate voltage-gated calcium (Cav) channels to open, triggering muscle contraction or neurotransmitter release. The Nav channels' involvement in neuronal signaling, muscle contraction, and pain makes them ideal targets for drug classes including antiepileptics, antiarrhythmics, and anaesthetics [51]. Outside of the β-subunits, Nav channels have also been observed to interact with other proteins within the cell, such as calmodulin [52], contactin [53], ankyrin [54], and several fibroblast growth factor homologous factors [55].

In the brain, the primary neuronal Nav isoforms found are Nav1.1, Nav1.2, and Nav1.6, as well as Nav1.3 to a lesser extent. Nav1.3 is primarily expressed embryonically, although it is still present in adult nervous tissue [56]. Sodium

channel distribution is complicated, however, and these proteins are subject to spatial and temporal regulation [57-59]. Nav1.1 was recently revealed to have a role in peripheral pain sensation [60], consistent with its detection in the PNS, albeit at low levels. Nav1.6 has been found in the brain, spinal cord, and PNS [61-63], primarily at the axon initial segments, somata, and nodes of Ranvier. It is thought to be a major component of persistent and resurgent current within Purkinje cells [64].

Nav1.4 and Nav1.5 are the principal isoforms found in skeletal and cardiac muscle, respectively. Nav1.4 is found on skeletal muscle fibers, responding to nerve stimulation to initiate excitation-contraction coupling [20, 65, 66]. Nav1.5 is required for the initial depolarization of the action potential of cardiac myocytes, and is also responsible for conduction of action potentials through the heart. This Nav channel is also unique in that it is moderately TTX-resistant [67].

The primary PNS isoforms Nav1.7, Nav1.8, and Nav1.9 [68-70] are largely associated with their roles in pain sensation. The Nav1.7 subunit is found in nociceptive neurons of the dorsal root ganglia (DRG) and sympathetic neurons, as well as olfactory neurons and trigeminal ganglia [71]. Generally clustered at nerve termini, Nav1.7 serves to amplify small depolarizations, setting the threshold for action potential initiation or neurotransmitter secretion [72]. Nav1.8 and Nav1.9 are also heavily involved in nociception and while being the most distantly related to other Nav isoforms they, like other isoforms, are also susceptible to modulation by animal toxins [73].

Nav channels have also been found to play roles in tissues or cells traditionally regarded as unexcitable. In the immune system, for example, Nav1.7 has been postulated to establish a resting Vm in dendritic cells, tuning them for proper activation in response to antigens [74]. Nav1.5, on the other hand, has been suggested to play multiple roles: in developing T-cells, the channel is essential for activation during positive selection of T-lymphocytes [75] whereas in macrophages the channel resides in lysosomes, possibly enabling more extensive acidification of the degradative lumen [76]. Nav1.1 and Nav1.6 have been found to play multiple roles in mouse microglial cells [77].

Given the importance of Nav channels in nervous system and muscle control it is unsurprising they are a primary target for animal toxins. Spiders, scorpions, and other venomous animals use toxins specific for ion channels to incapacitate and kill prey, or protect themselves from predation. Venoms contain components targeting many ion channels and hundreds of millions of years of evolution have provided researchers with tools to very specifically activate or inhibit ion channels, discriminating between ion channel subtypes, even between Nav isoforms [78]. Toxins are able to modify Nav channel function through two primary mechanisms: pore blockade to directly impair Na+ conductance and gating modification, through binding to voltage sensors, to shape the gating properties of the cell [78-80].

It is difficult to overstate the importance of animal toxins in Nav channel research. The first isolations of the Nav channel were done with the neurotoxins TTX and LqTx [25, 81, 82], and subsequent mapping of the extracellular topology

was done with the aid of LqTxV [83, 84]. The blocker TTX is routinely used to eliminate Na^+ conductances through subtraction in electrophysiological recordings of Nav channels and combinations of Nav isoform-specific animal toxins can be used to isolate specific channel isoforms during nerve recordings [85-87].

Pathology

Considering the roles of Nav channels in normal physiology, it is to be expected that most diseases related to them affect the nervous or muscular systems. While the disease mechanisms of pathogenic Nav channel mutations can be difficult to untangle in neurologic disorders [88], such as epileptic syndromes, the pathogenesis is often much better understood in cardiac or skeletal muscles disorders [89, 90]. The severity of Nav-related disorders varies, as some pose no serious risks to patients while others are frequently disabling or even fatal. Generally, the more severe mutations manifest in systems less robust to mutation [91].

Among the most prevalent and visible Nav channel disorders are the various epileptic syndromes arising from mutations in Nav1.1 and Nav1.2 [2, 88, 92, 93]. Both isoforms have been implicated in epilepsy, but it is the Nav1.1 isoform that has been most extensively linked to epilepsy [2, 88, 94, 95] and is thus a major target in neurologic pharmacy [96]. Nav1.3 and Nav1.6, which are also found in the adult CNS, have been linked to epilepsy [97, 98]. The

mechanism by which these mutations drive epilepsy is still unclear but is believed to involve reduced activity of inhibitory neurons [99-101]. In addition, a mutant form of an Nav channel found in the brain, Nav1.6, was found to be involved in cerebellar ataxia in mice [102].

The chief Nav isoform expressed in skeletal muscle, Nav1.4, has been linked to several myotonic and paralytic conditions [103, 104], defects of increased and decreased electrical excitability, respectively. Mutations in this channel frequently affect the III-IV linker, impairing fast inactivation and leading to aberrant contractility of the muscle cell [105, 106]. In the heart, the cardiac isoform Nav1.5 is responsible for initiation of the cardiac action potential and mutations within this isoform predictably lead to cardiac disorders [107]. Mutations can affect the channel by impairing cardiac conduction [108, 109] or arrhythmias [110-112] culminating in a descent into ventricular fibrillation and death. Idiopathic ventricular fibrillation syndromes can result from Nav1.5 mutations, such as Brugada syndrome [113-115] or Sudden Unexplained Death Syndrome (SUDS) [116-119].

Perhaps the most debilitating Nav channel disorders are a result of their role in pain signaling, as mutations in Nav1.7, Nav1.8, and Nav1.9 have been shown to alternatively lead to heightened pain sensation or complete insensitivity to pain. Mutations of Nav1.7 [120, 121] and Nav1.9 [7, 122] have both been linked to an insensitivity to pain. To anyone who has broken a bone or even stubbed a toe, a lack of pain sensation would seem a blessing, but these conditions can in fact be dangerous to their sufferers. As children, patients

suffering from this condition suffer frequent chewing-induced damage to fingers and tongues, and unwitting burns are common [123]. Curiously, in those lacking a functional Nav1.7 isoform, many patients lose their sense of smell in addition to that of pain, arising from a role for Nav1.7 in olfactory nerve conduction [124].

On the other side of the spectrum, mutations in Nav1.7 [6, 125], Nav1.8 [126], and recently Nav1.9 [127, 128] can lead to hyperactive pain sensations, the former contributing to erythromelalgia, in which the burning sensation experienced in their extremities has earned the moniker “Man on Fire” syndrome [129]. As such, Nav1.7 has become one of the most pharmaceutically relevant Nav channel isoforms, and specific modulators of Nav1.7 are some of the most sought after compounds in drug research [130]. Nav1.8 has been found to be important in chronic and inflammatory pain [131-134]. Other channels have also been shown to play a role in pain. The Nav1.3 isoform, typically expressed during embryonic development, displays upregulation in injured nerves and contributes to neuropathic pain under those circumstances [135, 136]. The neuronal isoform Nav1.1, which has been heavily implicated in epilepsy, has also recently been shown to play a role in mechanical allodynia [60], offering a new life for established Nav1.1-specific antiepileptic drugs in pain modulation [96].

Within the Nav signaling complex, the Nav channel appears to be the heavy lifter; it senses voltage changes, passes Na+ ions, and is targeted by gating-modifier toxins and thus it seems reasonable that disease mutations would primarily manifest in the Nav channel itself. However, the β-subunit plays a critical role in modifying channel gating and properly localizing the Nav channel,

and as such mutations in the β-subunit can have drastic effects on human health and disease.

The β-subunit

Structure

The β-subunit is a single-pass transmembrane protein of approximately 230 amino acids and a peptide molecular weight about 28 kDa, with an extracellular N-terminal domain and a short C-terminal tail inside the cell. The extracellular domain adopts an immunoglobulin-like V-type fold [10, 137]. Of the four β-subunit isoforms (β1-4), encoded by the genes *SCN1B-SCN4B* [138-142], the internal disulfide is conserved in all of them, but two (β2 and β4) share a conserved cysteine that is presumed to be free. The β2 and β4 subunits are believed to bind covalently to the Nav channel with a disulfide bridge formed in part by this free cysteine (^{55}Cys in β2, ^{58}Cys in β4) [22, 142-145]. The other two β-subunits, β1 and β3, are thought to interact with the Nav channel non-covalently [9, 21, 143, 146-149]. While it is not known where the β2/β4 bind to the channel, β1 is believed to interact with VSDIV, explaining some of its functional effects on channel inactivation [150, 151].

Like the Nav channel α-subunit, the β-subunits are glycosylated and several putative N-linked glycosylation sites have been identified [152]. Some of these glycosylation sites are thought to have their sugar moieties capped with

sialic acid, which has been suggested to play a role in β1 and β2 modification of channel gating [153, 154]. At the present time, knowledge of the extent and composition of β-subunit glycosylation is limited and the role it plays in β-subunit function or folding is uncertain.

Knowledge of the three-dimensional structure of the β-subunit is limited, but the β1 extracellular domain has been placed by the DI and DIV pore loops through cross-linking studies [150, 151] as well as scorpion toxin assays [155]. Knowledge of β-subunit function has outpaced that of structure, but structural insights would prove invaluable in advancing understanding of their function.

Physiology

As a subunit of the Nav channel signaling complex, the most prominent effects of the β-subunit are on Nav channel gating [8] and in this way to alter the electrical aspects of the cell [8, 145, 156-158]. The β1 subunit is the most pronounced in this regard, having been shown to affect the kinetics of fast inactivation as well as the voltage sensitivity of the channel [151, 152, 159-161], the former suggesting an interaction with the Nav channel DIV [150, 151, 162]. In addition, β-subunits have been shown to play a role in cell adhesion and migration [163].

The literature has been divided on the way β1 affects the channel; some reports suggest the extracellular domain is responsible for mediating functional effects while others purport it is instead the cytoplasmic tail that does so, and

some researchers argue both [152, 164, 165]. Regardless, β1 is regarded as the most functionally relevant of the β-subunits, being the best characterized biophysically and seemingly with the most substantial gating effects, namely a hyperpolarizing shift in steady-state inactivation, and an increase in the rate of both fast inactivation and recovery from fast inactivation [138]. It is found throughout the body, in the brain, spinal cord, heart, and skeletal muscle [138]. β1 KO mice show lengthened QT intervals, indicating a critical role in the heart [166]. Curiously, despite its significant functional effect in heterologous systems, β1 appears to have more subtle effects *in vivo* and the β1 KO mouse is still viable [167]. Presently alone amongst the β-subunits, β1 has an alternatively spliced β1b isoform, consisting solely of the extracellular domain of the protein [168]. The β1b is believed to be secreted by the cell [141].

The β2 subunit, through its covalent linkage to the channel, appears to play a role in modulating currents in DRG neurons, possibly by controlling the assembly and trafficking of the Nav channel signaling complex [169]. Generally, this subunit is found in brain and spinal cord [139] although others have found it in the heart as well [170]. Research has shown a role for glycosylation-mediated gating effects of β2 on the cardiac Nav1.5 [153, 154]. *SCN2B* KO mice are generally healthy, beyond a few seizures [171]. While it is believed β2's effect is mediated through stabilization of the Nav channel complex at the cell surface, this effect appears cell-type specific and is inconsistent *in vivo* [172].

β3 remains perhaps the least appreciated of the β-subunits, and although its role is still uncertain, β3 may behave similarly to β1. Like β1, β3 causes a

leftward shift in steady-state inactivation, and accelerates both the rate of fast inactivation as well as the recovery from fast inactivation [140]. Multiple reports have reported shifts in the conductance-voltage (G-V) and steady-state inactivation (SSI) curves of co-expressed Nav channels [158, 173], reflecting roles in activation and inactivation, respectively, but reports are often contradictory and can vary depending upon the expression system [174, 175]. The β3 subunit has been found throughout the body, in the brain, heart, and kidney [140] as well as in DRGs [176]. Like β2 KO mice, β3 KO mice are typically healthy, but do display some cardiac arrhythmias, suggesting a role for β3 in modifying the gating of a cardiac Nav channel [177, 178].

Possibly the most unconventional subunit, β4 has been implicated in several cardiac disorders and appears to play an important role in normal heart function. Whether this effect is mediated through a change in gating remains uncertain; initial characterizations of the channel suggested the β4 could impart a very minor shift in voltage-sensitivity [142]. Apparently unique to β4 is its ability to endow a resurgent current onto the Nav channel, allowing the channel to reactivate during a timeframe when it would normally be inactivated, enabling high frequency firing [179]. The mechanism by which this occurs is still unclear but is believed to involve the cytoplasmic tail of β4 interfacing with the internal pore of the Nav channel. The β4 cytoplasmic tail is also targeted by secretase enzymes, similar to β2 but not seen for β1 or β3, suggesting a possible role for β4 in Alzheimer's [180]. The β4 subunit also plays a role alongside Nav1.5 in a cell with a presumably non-excitable membrane -- the developing lymphocyte.

During T-cell positive selection in the thymus, β4 was shown to be essential for proper production of CD4+ T-cells [75], and has also been seen to be expressed during some stages of B-cell development in bone marrow. Clearly, the functional roles of β-subunits extend well beyond the nervous system, and even independent of Nav channels. Widespread in tissues, β4 is found in brain, spinal cord, DRGs, skeletal muscle, and the heart [142]. Thus far a viable β4 KO mouse has not been successfully produced, as these mice present a phenotype of sudden unexpected death, perhaps mimicking the effect of β4 mutations in the heart [181].

Outside their role in the Nav channel complex, several β-subunits have been found to have roles in cell adhesion [8]. Sequence comparisons to the cell-adhesion molecule myelin protein zero reinforce these findings [139, 140, 152]. Aligned with this role in cell adhesion, several of the β-subunits demonstrate interactions with structural and cytoskeletal elements such as contactin [182], tenascin [183], and ankyrin [184, 185]. In some cases, the β-subunits have been revealed to participate in cis- or trans-homophilic or heterophilic engagements [184, 186, 187].

Pathology

Considering their role supporting the Nav channel it comes as no surprise that many β-subunit mutations give rise to the same kinds of disease as do mutations in Nav channels. The β1 isoform is heavily implicated in epilepsy and

the β1 C121W mutation was in fact the first β-subunit mutation to be linked to a disease, in this case generalized epilepsy febrile seizures plus (GEFS+) [188], with which the R125L mutation is also associated [189]. Other mutants have been linked to Dravet syndrome [190, 191], atrial fibrillation [192], and Brugada syndrome [193], possibly as a result of their interaction with the neuronal Nav channel isoforms Nav1.1 and Nav1.2.

While the β2 subunit KO mouse is nonlethal and generally healthy [171], the appearance of mild seizures indicates the channel plays some role in the brain, though whether this is by directing modulating channel gating or by altering localization remains to be seen. Like Nav channels, β2 is also suggested to play a part in neuropathic pain [169]. Curiously, the β2 subunit is a target of amyloidogneic secretase enzymes, hinting at a potential role in Alzheimer's disease [194, 195]. However, most disease mutations are found near the transmembrane region or within the signal peptide, suggesting that the disease mechanism may result from a misfolding or mistargeting of the protein [196-200].

Mutations in β3 are suggested to play a role in cardiac arrhythmias [201] and Brugada syndrome [202, 203]. However, several mutations in β3 have been found in the amino terminus, suggesting their pathogenesis is derived not from gating modifications of the Nav1.5 channel but instead by the absence of β3 subunits [204]. Whether this impacts the function of trafficking of the channel is not yet known.

Given the diverse roles β4 plays throughout the body, diseases arising from its malfunction are varied. Thus far, the β4 subunit has been implicated in

atrial fibrillation [196], long-QT syndrome (LQTS) [197], and LQTS-associated Sudden Infant Death Syndrome [198]. Additionally, evidence has suggested a role in Huntington's disease [205] and, as a result of its targeting by β- and γ-secretase enzymes similar to β2, Alzheimer's disease [180].

Unfortunately, for many of the diseases in which β-subunit mutations play a participatory role, the mechanism remains unclear. The functional consequences of Nav channel mutants are often more obvious and easily assessed, but the β-subunits exert their effects subtly and mechanisms can be more difficult to decipher. Knowledge of Nav channel structure has greatly aided the interpretation of mutations and their predicted outcomes, but the paucity of β-subunit structural knowledge has greatly hindered our knowledge of pathogenesis. Hopefully, insights into the β-subunit structures, in conjunction with those of the Nav channel structure, will enable a deeper understanding of the means by which the Nav channel/β-subunit signaling complex operates and malfunctions.

Figures

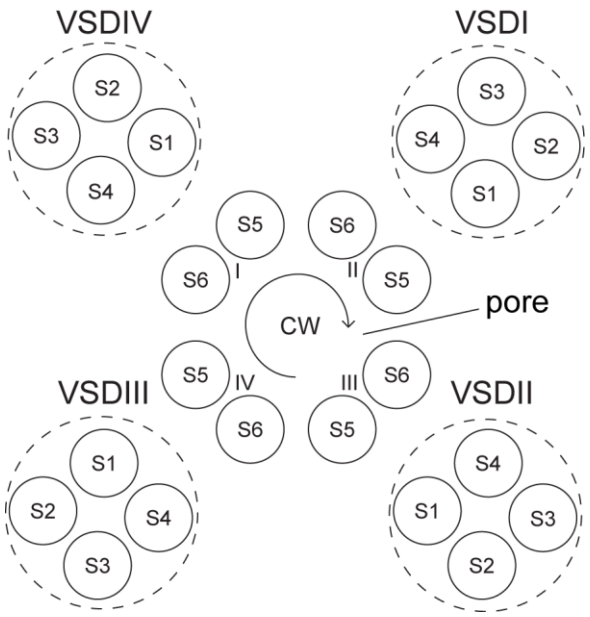

Figure 1-1: A general depiction of the Nav channel. The central pore of the channel is defined by the eight TM segments that delineate it, two (S5 and S6) from each domain. The voltage sensors are organized in clockwise fashion while the two pore-lining segments of each domain are located adjacent to the preceding voltage sensor. A dashed circle indicates the segments (S1-S4) that constitute the voltage sensors.

ARCHITECTURE OF THE BETA2/BETA4-NAV CHANNEL SIGNALING COMPLEX

Chapter 2: Crystallographic insights into sodium-channel modulation by the β4 subunit

This chapter adapted from:

Gilchrist, J., et al., *Crystallographic insights into sodium-channel modulation by the β4 subunit.* Proceedings of the National Academy of Sciences of the United States of America, 2013. **110**(51).

Summary

Nav channels are embedded in a multicomponent membrane signaling complex that plays a crucial role in cellular excitability. Although the mechanism remains unclear, β-subunits modify Nav channel function and cause debilitating disorders when mutated. While investigating whether β-subunits also influence ligand interactions, we found that β4 dramatically alters toxin binding to Nav1.2. To explore these observations further, we solved the crystal structure of the extracellular β4 domain and identified ^{58}Cys as an exposed residue that, when mutated, eliminates the influence of β4 on toxin pharmacology. Moreover, our results suggest the presence of a docking site that is maintained by a cysteine bridge buried within the hydrophobic core of β4. Disrupting this bridge by introducing a β1 mutation implicated in epilepsy repositions the ^{58}Cys-containing loop and disrupts β4 modulation of Nav1.2. Overall, the principles emerging from this work (*i*) help explain tissue-dependent variations in Nav channel pharmacology; (*ii*) enable the mechanistic interpretation of β-subunit–related disorders; and (*iii*) provide insights in designing molecules capable of correcting aberrant β-subunit behavior

Contributions: The contents of figures 2-4, 2-5, 2-6, 2-10, and 2-11 and Table 2-2 were courteously provided by Samir Das and Filip Van Petegem.

Introduction

Nav channels play a key role in cellular communication by manipulating the transmembrane voltage gradient to encode and propagate vital information rapidly over long distances [24]. Consequently, mutations that modify Nav channel activity underlie debilitating neurological diseases, muscular disorders, and pain syndromes [72, 103]. Typically, Nav channels are part of a membrane-embedded signaling complex that involves various integral membrane proteins [11]. The significance of this environment for proper channel function is highlighted by divergent Nav channel responses to changes in membrane voltage when expressed in native tissues or in heterologous systems. β-Subunits are prominent members of the Nav channel signaling complex but do not contribute to the ion-conducting pore [8]. Instead, they are multifunctional single-transmembrane segment glycoproteins that (*i*) modulate the gating properties of voltage-gated ion channels; (*ii*) regulate Nav channel trafficking and expression levels; and (*iii*) promote cell adhesion and migration [8, 145, 147, 148, 152, 156, 157, 206-208]. Of the four known β-subunits and their splice variants [138-142, 209], β4 is unique in that it enables resurgent current, a feature that renders certain Nav channel isoforms capable of high-frequency firing in excitable tissues [179]. Moreover, aberrant behavior of the ubiquitously expressed β4 subunit has been implicated in long-QT syndrome (LQTS) [197], LQTS-associated Sudden Infant Death Syndrome [198], atrial fibrillation [196], Huntington's disease [205], and prostate cancer [210], possibly through dysregulation of the Nav channel signaling complex. β4 also is targeted by β- and γ-secretase enzymes from the

amyloidogenic pathway, a recent observation that suggests a potential contribution of this particular subunit to the development of Alzheimer's disease [211].

Despite accumulating evidence supporting an important contribution to neuronal excitability and various health disorders [212], fundamental questions about the molecular mechanisms underlying β4 interaction with Nav channels remain unanswered. Moreover, the notion that the β4 subunit shapes the overall pharmacological sensitivities of the Nav channel signaling complex remains unexplored. However, altered ligand interactions may be exploited to detect the presence of β4 in normal or pathological conditions [213]. Here, we investigated whether β-subunits influence Nav channel sensitivity to molecules isolated from animal venom and discovered that β4 can drastically alter the response of the neuronal Nav1.2 isoform to spider and scorpion toxins that target paddle motifs within Nav channel voltage sensors. To elucidate the machinery underlying this observation, we solved the crystal structure of the extracellular β4 domain and found a ^{58}Cys-containing binding interface that is involved in Nav channel modulation of toxin pharmacology by β4. Remarkably, dismantling the strictly conserved internal cysteine bridge in β4 by introducing a β1 mutation implicated in epilepsy [188] does not preclude protein folding and trafficking to the membrane. However, conformational changes induced by the mutation perturb the ^{58}Cys-containing loop and disrupt β4 interaction with Nav1.2, in turn altering the functional and pharmacological properties of the larger Nav channel signaling complex.

Results

β-subunits shape Nav channel pharmacology.

Although the influence of β-subunits on ion channel gating is well documented [8], little is known about their ability to manipulate the pharmacological sensitivities of Nav channel signaling complexes [172, 213, 214]. To investigate the extent to which these versatile glycoproteins modify ligand interactions, we applied seven toxins from spider, scorpion, sea anemone, and wasp venom (ProTx-I, ProTx-II, TsVII, AaHII, LqqIV, ATX-II, and β-PMTX) as well as two drugs (lidocaine and ambroxol) to *Xenopus* oocytes expressing the neuronal Nav1.2 isoform and determined potential changes in ligand susceptibility induced by the presence of each of the four β-subunits. We uncovered multiple conditions in which Nav1.2's sensitivity to a particular toxin was modified by β-subunits, whereas sensitivity to neither drug was significantly affected (Fig. 2-1, Fig. 2-2, and Table 2-1). For example, the sea anemone toxin ATX-II interacts exclusively with the Nav1.2 domain IV voltage sensor to inhibit fast inactivation, resulting in a large increase in inward sodium ion flow [215]. When β2 is present, 100 nM ATX-II still prevents Nav1.2 from inactivating rapidly; however, the peak sodium current increases only marginally (Fig 2-1). A similar effect is seen when 100 nM of the domain IV-targeting scorpion toxin LqqIV is applied to Nav1.2 coexpressed with β1 [binding site identification is given in Fig. 2-3 [31]]. In this instance, however, LqqIV also shifts the steady-state inactivation curve to more positive potentials (V1/2 from −57 mV to −48 mV; $P \leq 0.001$),

thereby increasing channel availability to open in response to membrane depolarizations (Fig. 2-1). In contrast, the related scorpion toxin AaHII [31] decreases Nav1.2 availability when coexpressed with β2 (V1/2 from −42 mV to −61 mV; $P \leq 0.001$) or β4 (V1/2 from −45 mV to −63 mV; $P \leq 0.001$).

Interestingly, the most striking effects on toxin susceptibility are observed when Nav1.2 is expressed together with the β4 subunit. First, the tarantula toxin ProTx-II has been shown to interact with the voltage sensors in domains I, II, and IV of Nav1.2 and to inhibit channel opening [31, 216]. However, in the presence of β4, Nav1.2 is dramatically less inhibited, suggesting that β4 may prevent ProTx-II from interacting with one or more of its receptor sites (Fig. 2-2*B*). Second, the structurally unrelated scorpion toxin TsVII promotes Nav channel opening by preferentially interacting with the voltage sensor in domain II and stabilizing it in an activated state [31, 217]. Without β-subunits present, 500 nM TsVII causes Nav1.2 to open at more negative voltages, although the maximal conductance of the channel is not affected. In contrast, TsVII greatly decreases Nav1.2 maximal conductance with a smaller shift in activation voltage when β4 is present (Fig. 2-2*C*), raising the possibility that this β-subunit exerts an influence on the domain II voltage sensor. Next, we crystallized the extracellular β4 domain to explore the mechanisms underlying the influence of this particular β-subunit on Nav1.2 pharmacology.

The β4 subunit structure reveals an exposed cysteine.

Despite their impact on the functional and pharmacological properties of Nav channels, tertiary structural information about β-subunits has been lacking. To address this inadequacy, we solved the crystal structure of the extracellular β4 domain (residues 32–157) at 1.7 Å resolution (Fig. 2-4, Fig. 2-5, and Table 2-2) and found that this subunit has a compact fold, similar to that of immunoglobulins, that consists of 10 β-strands and two 3_{10} helices [187, 218]. A low sequence complexity suggests that the upstream region of this domain (residues 1–31) is likely to be disordered in the absence of a binding partner, because constructs containing this particular segment result in protein aggregation. Moreover, a large portion of this region also may serve as a membrane-targeting signal sequence that is proteolytically cleaved during cellular processing [142]. Overall, the structure is held together by a buried disulfide bridge connecting the β2–β3 loop with the β8-strand which is flanked by ^{68}Trp, a residue conserved among all β-subunit isoforms. On the other side, it packs against ^{114}Ile and ^{133}Val, both of which correspond to the similar Ile, Val, or Leu residues in other β-subunits (Fig. 2-4*C*). Because of the strictly conserved nature of the protein core (Fig. 2-4*D*). it is likely that the buried disulfide bond has a major effect on the stability of the protein. Another stabilizing element in the β4 structure is an ion-pair network involving two hydrogen bonds between ^{98}Asp and ^{100}Arg, which forms two additional bonds with ^{125}Asp, as well as a hydrogen bond between ^{77}Lys and ^{125}Asp that is mediated by a water molecule (Fig. 2-4*E*). Such networks of ionic pairs are more stabilizing than individual salt bridges because

of lower desolvation penalties [219]. Next, we examined the surface of β4 for unique structural features that may contribute to an interaction with Nav1.2.

The β4 extracellular domain consists of solvent-accessible surface area of ~6,600 $Å^2$ with one side exposing multiple hydrophobic side chains as well as residue 58, a Cys in WT protein but replaced by Ala to facilitate crystallization (Fig. 2-6*A*). ^{58}Cys is located in a loop between the β2- and β3-strands and is lined by two hydrophobic pockets, thereby placing it in an ideal position to form a disulfide bond with another free Cys (Fig. 2-4*A*). Nonetheless, conformational changes resulting from the C58A mutation are unlikely, because the residue is located at the protein surface, and the mutant has a thermal stability similar to that of WT β4 (Fig. 2-6*B*). Strikingly, the position of ^{58}Cys in β4 corresponds to that of the Cys (^{26}Cys) thought to be involved in linking β2 to Nav1.1 [144]. Here, removing the covalent bond with Nav1.1 by mutating ^{26}Cys to Ala results in an altered subcellular localization pattern of β2. Given the prominent position of ^{58}Cys in the β4 crystal structure and the functional importance of the corresponding residue in β2, we asked whether ^{58}Cys plays a role in determining the influence of β4 on Nav1.2 toxin pharmacology.

Mutating ^{58}Cys in β4 restores Nav1.2 sensitivity to ProTx-II.

To examine whether the ability of β4 to alter Nav1.2 toxin susceptibility depends on a disulfide bond involving ^{58}Cys, we initially incubated Nav1.2/β4-expressing oocytes with a reducing agent (DTT) for 60 min. Subsequently, we transferred the oocyte to a physiological recording solution and tested whether

Nav1.2 regains sensitivity to ProTx-II (Fig. 2-7). Even though all exposed cysteines may have been reduced, channel-gating behavior is not affected significantly; however, we observe that the toxin now inhibits Nav1.2 as if no β4 is present, suggesting that the disulfide bond between ^{58}Cys and Nav1.2 is crucial in modifying channel susceptibility to ProTx-II in the presence of β4.

Next, we replaced ^{58}Cys in β4 with Ala and exploited the presence of an intracellular Myc-tag to determine whether cellular trafficking of this mutant is altered. By doing so, we discovered that the WT β4 protein and the C58A mutant are produced in large quantities (Fig. 2-8*A*). Moreover, biotinylation experiments reveal the presence of both variants within the lipid membrane, most likely in a glycosylated form [220]. When β4 glycosylation is removed using peptide-*N*-glycosidase F (PNGase F), an amidase that releases N-linked oligosaccharides, the molecular weight of the protein on the membrane surface corresponds to the predicted mass of β4 (28 kDa) (Fig. 2-9) [142]. Having established the membrane insertion of β4 and the C58A mutant (without or in the presence of Nav1.2; Fig. 2-9), we next applied 100 nM ProTx-II to cells expressing Nav1.2/β4 C58A and observed a level of inhibition similar to that obtained when no β4 is present (Fig. 2-8 *B* and *C*). When comparing the affinities of ProTx-II for Nav1.2 in more detail, we note an approximately fivefold decrease in the presence of β4 compared with control conditions without β4 (IC_{50} from 32 ± 1 nM to 164 ± 33 nM with slopes of 1.9 ± 0.1 and 1.6 ± 0.3, respectively). Moreover, the affinity of ProTx-II for Nav1.2 coexpressed with the C58A mutant (IC_{50} = 33 ± 2 nM with a slope of 1.7 ± 0.1) is comparable to the IC50 obtained on cells lacking β4 (Fig. 2-8*D*). Taken together,

our results identify ^{58}Cys as a reactive residue that, when mutated, eliminates the influence of β4 on Nav1.2 toxin pharmacology by perturbing a unique disulfide bond with the Nav channel.

Mapping clinically relevant β-subunit mutations onto the β4 structure.

Reflecting its medical importance, atypical β-subunit behavior has been implicated in various epilepsy syndromes and cardiac disorders [8]. However, little is known about the relationship between the structural and functional consequences of mutations and a particular clinical phenotype. Our results presented here provide a unique opportunity to map abnormalities within the extracellular domain onto a high-resolution β4 crystal structure and to explore their mode of action (Fig. 2-10 and Table 2-3). For example, R85H and E87Q in β1 have been associated with atrial fibrillation and Brugada syndrome, respectively [192, 193]. Both residues are located near or within the β5–β6 loop and form a patch of solvent-accessible surface area (Fig. 2-10*A*), suggesting that these amino acids are part of an important functional interface that may be targeted by therapeutics [212]. Similarly, the R125L variant has been identified in patients who have generalized epilepsy plus febrile seizures plus (GEFS+) [189], whereas R125C may contribute to the occurrence of Dravet syndrome [190]. Because this residue lines a pocket near the conserved ^{58}Cys, the addition of a Cys may interfere with the formation of a proper disulfide bond with the Nav channel (Fig. 2-10*A*).

Surface-exposed mutations may hint at a disruption of a functional interface, whereas buried substitutions are likely to affect overall protein folding. For instance, in patients who suffer from Dravet syndrome [191] a Pro residue replaces a concealed Ile at position 106 in β1, where it is likely to interfere with protein folding (Fig. 2-10*A*). The V110I mutation in β3 has been linked to Brugada syndrome and also affects a residue buried within a hydrophobic core, resulting in reduced channel expression [202]. Interestingly, the first epileptogenic mutation attributed to Nav channel β-subunits is a Cys-to-Trp substitution that disrupts the disulfide bridge within the extracellular domain of β1 [188]. Although the protein traffics to the membrane, the precise mechanism relating this C121W variant to the resulting GEFS+ disease phenotype is still a matter of debate [221-223]. We chose to mutate the corresponding residue in β4 (C131W and C131A) to determine whether disrupting this strictly conserved internal disulfide bond repositions ^{58}Cys to such an extent that it cannot interact with the Nav channel.

Even though a lack of space for a Trp side chain at the ^{131}Cys position suggests that this mutant should be unable to fold properly and aggregate, both the C131W and the C131A construct can be purified to obtain nonaggregated protein, as indicated by size-exclusion chromatography (Fig 2-11). Moreover, thermal stability measurements in the presence of reducing agent [14 mM 2-mercaptoethanol (2-ME)] only show ~4-°C and ~7-°C decreases in melting temperatures for C131W and C131A, respectively, compared with WT (Fig. 2-6*B*). The presence or absence of 2-ME did not affect the melting curves for the

two mutants, and we did not observe an interpretable melting curve for WT β4 without reducing agent, an observation that is consistent with the major stabilizing effect of a disulfide bond. Taken together, these results demonstrate that, although the disulfide bond adds to stability, it is not strictly required for folding.

To explore this surprising result further, we next solved the crystal structure of the C131W construct at a resolution of 1.7 Å and found that the mutation results in conformational changes at multiple positions (Fig. 2-10*B*). Because the location of ^{144}His in the β9–β10 loop would clash with the bulky Trp residue, this residue has swung away completely, and the β9–β10 loop adopts a β-strand conformation that results in a merged β9–β10 strand. In addition, ^{53}Cys no longer is constrained by the disulfide bond, resulting in a dramatic shift of the β2–β3 loop (~5.2 Å) within the main chain. This shift of the β2–β3 loop in turn shifts the positions of the neighboring β4–β5 loop (~6 Å) and the β6–β7 loop (~6.8 Å), resulting in complete remodeling of the surface. Because the β2–β3 loop contains the functionally important ^{58}Cys residue, the C131W mutation remodels the Nav channel-binding interface, potentially altering the functional and pharmacological properties of the Nav channel signaling complex. To substantiate this notion, we tested whether the C131W mutant indeed loses its ability to modify Nav1.2 sensitivity to ProTx-II.

The C131W mutation alters the influence of β4 on Nav1.2 toxin pharmacology.

To examine the effect of the C131W substitution on Nav1.2 toxin susceptibility, we first determined whether cellular trafficking of this mutant is altered. Similar to WT β4, C131W is produced in large amounts (Fig. 2-12*A*); however, a nonquantitative Western analysis of total cell lysate uncovers potential alterations in glycosylation patterns that may complicate protein separation from the endoplasmatic reticulum. Nonetheless, biotinylation experiments reveal the presence of C131W within the oocyte membrane (Fig. 2-12*A*). Indeed, when glycosylation is removed using PNGase F, the molecular mass of the C131W mutant on the membrane surface closely matches the predicted mass of β4 [142]. These results are consistent with previously reported observations with the β1 C121W mutant in a mouse model for epilepsy [224] and in human embryonic kidney cells stably expressing Nav1.1 [156]. Subsequently, we applied 100 nM ProTx-II to cells expressing Nav1.2/β4 C131W and observed a level of inhibition over a wide voltage range similar to that obtained when neither β4 nor the C58A mutant is present (Fig. 2-12 *B* and *C*). Because the C131W mutant traffics to the membrane surface in oocytes, results from the ProTx-II experiment suggest that ^{58}Cys no longer may be able to interact with Nav1.2. It is worth noting that our Western blot analysis (Fig. 2-12*A*) does not rule out the possibility that impaired C131W trafficking in oocytes may contribute, at least in part, to the restoration of Nav1.2 toxin sensitivity. Together with our crystallographic data, these functional results show that, although the conserved

cysteine bond is not strictly required to produce folded protein, it does dictate the overall conformation, including the position of the important ^{58}Cys-containing bioactive surface.

Discussion

β-Subunits are vital members of the larger Nav channel signaling complex in which they modify channel function to fine-tune the electrical excitability of native tissues [8, 145, 156-158]. The goal of the present study was to investigate the interaction of β-subunits with Nav channels on a molecular level and the role of these ancillary proteins in shaping the pharmacological sensitivities of the neuronal Nav1.2 isoform. Our experiments with an extensive collection of animal toxins establish that β-subunits can alter Nav1.2 pharmacology drastically and that the resulting effects vary among β-subunit–toxin pairs (Fig. 2-1, Fig. 2-2, and Table 2-1). For example, β4 coexpression results in an approximately fivefold decrease in the affinity of ProTx-II for Nav1.2, whereas the same subunit reduces sodium influx upon TsVII application, an effect that is not observed with the WT channel or in the presence of β1–3. It is worth considering potential principles underlying β-subunit modulation of Nav channel pharmacology. For example, a toxin may compete with a β-subunit for binding to a particular region within Nav1.2. For instance, LqqIV interacts with the domain IV voltage sensor (Fig. 2-3), and its effect is influenced by β1, suggesting a direct or allosteric interaction of this particular subunit with domain IV within Nav1.2 [150, 151, 162]. Alternatively, ligands may bind directly to β-subunits [225], an intriguing concept that also has been observed with the voltage-gated calcium channel inhibitor gabapentin, which acts through the transmembrane $\alpha_2\delta$ subunit [226]. Interestingly, β3 is unable to modulate Nav1.2 susceptibility to any of the toxins we tested, but this particular subunit influences lidocaine binding to the neonatal

Nav1.3 and cardiac Nav1.5 isoform [227, 228]. This result highlights the unique character of the interaction between a particular β-subunit and a given Nav channel isoform [229].

Because the most striking effects on Nav1.2 toxin susceptibility are observed with the β4 subunit, we crystallized its extracellular domain and identified ^{58}Cys as a surface-exposed residue that, when mutated, abolishes the impact of β4 on ProTx-II binding to Nav1.2 (Fig 2-4 and 2-6). Because this Cys is conserved in β2 and β4, it likely belongs to a universal docking site for multiple Nav1 channel isoforms. The two other conserved cysteines (^{53}Cys and ^{131}Cys) are buried within a hydrophobic core where they form a disulfide bond. When ^{131}Cys is mutated to Trp or Ala (Fig. 2-6*B*), we surprisingly find that the extracellular domain is still folded, thus demonstrating that the cysteine bridge is not strictly required for protein folding. However, the crystal structure of the C131W mutant, which mimics a well-established epileptogenic mutation found in β1, reveals conformational changes at multiple locations, including the loop that contains the conserved ^{58}Cys (Fig. 2-10*B*). Subsequently, an important role of the buried cysteine bridge may be to maintain a specific local structure that allows an interaction with the Nav channel and that, when disrupted (Fig 2-12), creates a loss-of-function phenotype that relates to disorders such as GEFS+ [188].

Collectively, the functional and crystallographic results reported here shed light on the intricate interactions of β4 within the Nav channel signaling complex and establish a key role for β-subunits in shaping Nav1.2 pharmacology. As

such, an important concept emerging from our work is that β-subunits provide exciting opportunities for designing new therapeutic strategies to correct their abnormal behaviors.

Materials and Methods

Toxin Acquisition and Purification.

ProTx-I and ProTx-II [230] were acquired from Peptides International, β-PMTX [231] was obtained from Alomone Laboratories, and ATX-II [232], lidocaine, and ambroxol were from Sigma-Aldrich. AaHII from *Androctonus australis* hector venom, TsVII from *Tityus serrulatus* venom, and LqqIV from *Leiurus quinquestriatus* were purified as described previously [233-235]. Toxins were kept at −20 °C, and aliquots were dissolved in appropriate solutions containing 0.1% BSA.

Two-Electrode Voltage-Clamp Recording from *Xenopus* Oocytes.

The DNA sequences of rNav1.2a [236], rβ1–4 (acquired from Origene and modified for oocyte expression), and of the C58A and C131W mutants were confirmed by automated DNA sequencing, and cRNA was synthesized using T7 polymerase (mMessage mMachine kit; Ambion) after linearizing the DNA with appropriate restriction enzymes. LqqIV binding site experiments on chimeric voltage-gated potassium channels were carried out as previously described [31]. Channels were expressed together with a β-subunit (1:5 molar ratio) in *Xenopus* oocytes that were incubated at 17 °C in 96 mM NaCl, 2 mM KCl, 5 mM Hepes, 1 mM $MgCl_2$, 1.8 mM $CaCl_2$, and 50 g/mL gentamycin (pH 7.6) with NaOH for 1–2 d after cRNA injection, and then were studied using two-electrode voltage-clamp

recording techniques (OC-725C; Warner Instruments) with a 150-μL recording chamber. Data were filtered at 4 kHz and digitized at 20 kHz using pClamp 10 software (Molecular Devices). Microelectrode resistances were 0.5–1 MΩ when filled with 3 M KCl. The external recording solution (ND100) contained 100 mM NaCl, 5 mM Hepes, 1 mM $MgCl_2$, and 1.8 mM $CaCl_2$ (pH 7.6) with NaOH. All experiments were performed at room temperature (~22 °C). Leak and background conductances, identified by blocking the channel with tetrodotoxin (Alomone Laboratories), have been subtracted for all Nav channel currents. All chemicals used were obtained from Sigma-Aldrich unless otherwise indicated.

Analysis of Channel Activity and Toxin–Channel Interactions.

Voltage–activation relationships were obtained by measuring steady-state currents and calculating conductance (G). In representative cases a Boltzmann function was fitted to the data according to: $G/G_{max} = (1 + e^{-zF(V-V_{1/2})/RT})^{-1}$ where *G*/*Gmax* is the normalized conductance, *z* is the equivalent charge, $V_{1/2}$ is the half-activation voltage, *F* is Faraday's constant, *R* is the gas constant, and *T* is temperature in Kelvin. Occupancy of closed or resting channels by ProTx-II and other toxins was examined using negative holding voltages when open probability was very low, and the fraction of uninhibited channels (F_u) was estimated using depolarizations that are too weak to open toxin-bound channels, as described previously [31]. After the toxin was added to the recording chamber, the equilibration between the toxin and the channel was monitored using weak depolarizations elicited at 5-s intervals. Concentration dependence for ProTx-II

inhibition of Nav channels is plotted as Fu measured at negative voltages versus toxin concentration. A Hill equation was fitted the data to obtain affinity values. Off-line data analysis was performed using Clampfit 10 (Molecular Devices) and Origin 8 (OriginLab).

Nonquantitative Biochemical Assessment of β4 Production in *Xenopus* Oocytes.

Batches of 20 oocytes expressing Nav1.2, Nav1.2/β4, Nav1.2/β4 C58A, and Nav1.2/β4 C131W were washed with ND100 and incubated with 0.5 mg/mL Sulfo-NHS-LC-biotin (Pierce) for 30 min. Oocytes were thoroughly washed again (by pipetting up and down) in ND100 before lysis in 400 µL buffer H (1% Triton X-100, 100 mM NaCl, 20 mM Tris·HCl, pH 7.4) plus protease inhibitors (Clontech). All subsequent steps were performed at 4 °C. Lysates were shaken gently for 15 min and then were centrifuged at 16,200 × *g* for 3 min. The pellet was discarded, and the supernatant was transferred to a fresh 1.5-mL Eppendorf tube; 40 µL of supernatant was stored at −80 °C for later use as the whole-cell protein aliquot. Then 200 µL of hydrophilic streptavidin magnetic beads (New England Biolabs) was added, and the sample was shaken gently at 4 °C overnight. Beads were washed six times with buffer H and were resuspended in 40 µL buffer H, after which biotinylated protein was dissociated from the beads by the addition of 40 uL 1× LDS loading buffer plus reducing agent [final concentration: 10% (vol/vol) 2-ME, 50 mM DTT] and boiling at 95 °C for 5 min. Deglycosylated samples were prepared by incubating the surface protein aliquot with PNGase-F and 1%

Nonidet P-40 at 37 °C for I h. All samples were diluted appropriately in buffer H to give roughly equal protein concentrations, as measured by absorbance at 280 nM. Then 7.5 µL of the supernatant was run on a 10% (wt/vol) Bis-Tris NuPAGE Novex Mini-Gel (Invitrogen) with 3-(*N*-morpholino)propanesulfonic acid running buffer and were analyzed by Western blot analysis. Nitrocellulose membranes were probed with 1:1,000 mouse anti-Myc antibody (Cell Signaling Technologies) as the primary antibody and 1:10,000 goat anti-mouse HRP-conjugated antibody (Thermo-Fisher Scientific) as the secondary antibody. Membranes were incubated for 5 min with an enhanced chemiluminescent substrate [237] before imaging.

Production of the β4 Extracellular Domain.

Human β4 (hβ4) (32-157) acquired from OriGene was cloned into pET28HMT [238]. Mutations were introduced using the QuikChange kit from Stratagene according to the manufacturer's instructions. Proteins were expressed at 18 °C in *Escherichia coli* Rosetta (DE3) pLacI strains (Novagen), were induced at an OD600 of ~0.6 with 0.3 mM isopropyl β-D-1-thiogalactopyranoside, and were grown overnight before harvesting. Cells were lysed via sonication in buffer A (250 mM KCl and 10 mM Hepes, pH 7.4) supplemented with 25 µg/mL DNaseI and 25 µg/mL lysozyme. After centrifugation, the supernatant was applied to a PorosMC column (Tosoh Biosep), washed with buffer A plus 10 mM imidazole, and eluted with buffer B (250 mM KCl plus 500 mM imidazole, pH 7.4). The protein was dialyzed

overnight against buffer A and cleaved simultaneously with recombinant TEV protease. Next, the samples were run on another PorosMC column in buffer A, and the flowthrough was collected and dialyzed against buffer C (50 mM KCl plus 20 mM Tris·Cl, pH 8.0), applied to a HiloadQ column (GE Healthcare), and eluted with a gradient from 0–30% buffer D (2 M KCl plus 20 mM Tris·Cl, pH 8.0). Finally, the samples were run on a Superdex200 gel-filtration column (GE Healthcare) in buffer A. The protein samples were exchanged with 25 mM KCl plus 10 mM Hepes (pH 7.4), concentrated to 10–20 mg/mL using Amicon concentrators (3 K molecular weight cut off; Millipore), and stored at −80 °C.

Crystallization, Data Collection, and Structure Solution.

Crystals were grown using the sitting-drop method at 4 °C. β4 (32-157) C58A was crystallized in 0.1 M Hepes (pH 7) and 15% (wt/vol) PEG 20000. The C131W mutant was crystallized in 0.2 M ammonium formate, 20% (wt/vol) PEG formate, and 20% (wt/vol) PEG 3350 at 4 °C. Crystals were flash-frozen after transfer to the same solution supplemented with 30% (vol/vol) glycerol. Diffraction experiments were performed at the Advanced Photon Source (Chicago) beamline 23-ID-D-GM/CA, and datasets were processed using XDS [239]. A search model was created by using only β-strands from Protein Data Bank (PDB) ID code 1NEU and with all side chains truncated to Ala. Molecular replacement was performed using Phaser [240], yielding poor initial phases which were improved via autobuilding in ARP/wARP [241]. The model was completed by successive rounds of manual model building in COOT [242] and

refinement using Refmac5.5 [243]. A simulated annealing composite omit map was calculated with CNS [244] to verify the absence of residual model bias. No residues were found to be in disallowed regions of the Ramachandran plot. All structure figures were prepared using PYMOL (DeLano Scientific). Coordinates are available in the PDB database (ID codes 4MZ2 and 4MZ3).

Thermal Melting Experiments.

The protein melting curves were measured by means of ThermoFluor experiments [238, 245]. Samples for melting curves contained 50 μL of 0.1 mg/mL protein and 1× SYPRO Orange solution (Invitrogen) using the manufacturer's instructions. The curves were measured in a DNA engine Opticon 2 real-time PCR machine (Bio-Rad), using the SYBR green filter option. The temperature was ramped from 25–95 °C in 0.5-°C steps, with 15 s at each step. The melting temperatures were taken as the midpoint of each transition.

Acknowledgments

We thank Al Goldin for sharing the rNav1.2a clone; Marie-France Martin-Eauclaire and Pierre Bougis for sharing TsVII, AaHII, and LqqIV; YaWen Lu for assistance with biochemistry; the staff of the Advanced Photon Source (Chicago) GM/CA-CAT beamline 23-iD-D; the staff at the SSRL beamlines (Menlo Park); and the members of the F.B. and F.V.P. laboratories for helpful discussions. This work was supported in part by the National Institute of Neurological Disorders and Stroke of the National Institutes of Health under Award R00NS073797 (to F.B.) and by Human Frontier Science Program Grant RGY0064/2013 (to F.B. and F.V.P.). S.D. is supported by a postdoctoral fellowship of the Heart and Stroke Foundation of Canada. F.V.P. is a Michael Smith Foundation of Health Research Career Investigator.

Figures

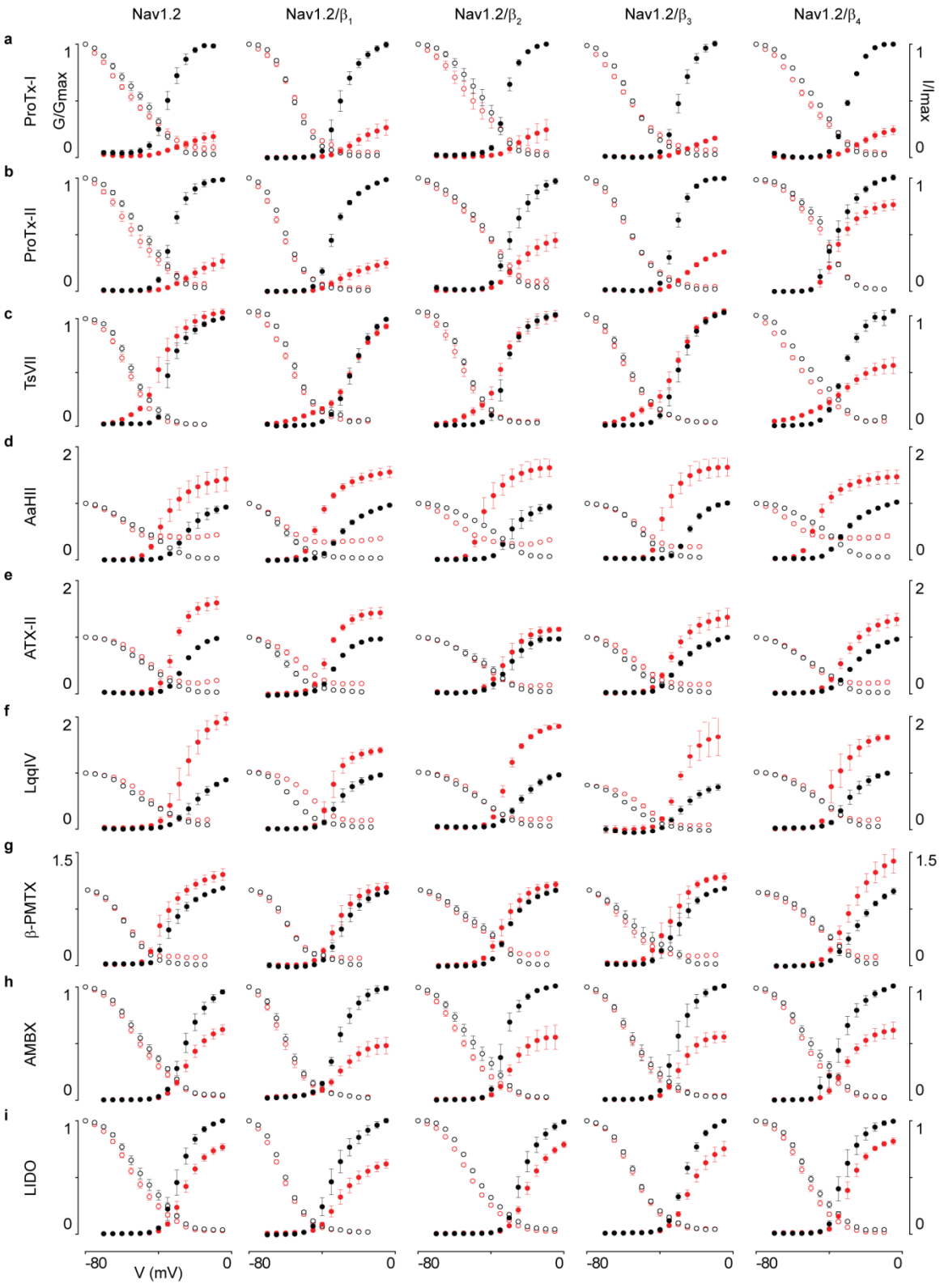
Nav1.2
Nav1.2/β1
Nav1.2/β2
Nav1.2/β3
Nav1.2/β4
a
ProTx-I
b
ProTx-II
c
TsVII
d
AaHII
e
ATX-II
f
LqqIV
g
β-PMTX
h
AMBX
i
LIDO
G/Gmax
I/Imax
V (mV)
-80
0

Figure 2-1: **Influence of β-subunits on the ligand susceptibility of the voltage-gated sodium channel Nav1.2.** Effect of 100 nM ProTx-I (A), 100 nM ProTx-II (B), 500 nM TsVII (C), 100 nM AaHII (D), 500 nM ATX-II (E), 100 nM LqqIV (F), 10 μM β-PMTX (G), 10 mM lidocaine (LIDO) (H), and 500 μM ambroxol (AMBX) (I) (all saturating concentrations) on Nav1.2 without and in the presence of β-subunits. Normalized conductance–voltage relationships (G/Gmax; black filled circle/red filled circle) and steady-state inactivation relationships (I/Imax; black open circle/red open circle) are shown before (black) and after (red) toxin or drug application. Channel-expressing oocytes were depolarized in 5-mV steps from a holding potential of −90 mV. n = 3–5; error bars represent S.E.M.

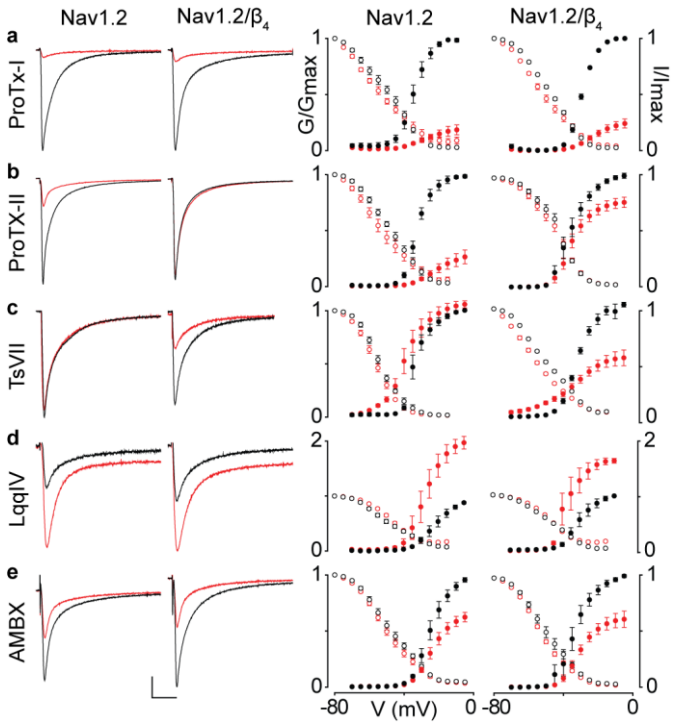

Figure 2-2: Influence of β4 on the ligand susceptibility of $Na_v1.2$. (*A*–*E*) Effect of saturating concentrations [100 nM ProTx-I (*A*), 100 nM ProTx-II (*B*), 500 nM TsVII (*C*), 100 nM LqqIV (*D*), and 500 μM ambroxol (AMBX) (*E*)] [31, 246] on $Na_v1.2$ and $Na_v1.2$/β4. (*Left*) Representative sodium currents are elicited by a depolarization to −20 mV before (black) and after (red) addition of toxin or drug from a holding potential of −90 mV. The *x*-axis is 10 ms; the *y*-axis is ∼0.5 μA. (*Right*) Normalized conductance–voltage relationships (G/G_{max}; black filled circles) and steady-state inactivation relationships (I/I_{max}; black open circles) of the WT $Na_v1.2$ channel with or without β4 coexpression are compared before (black circles) and after (red circles) toxin or drug application. β4 alters $Na_v1.2$ susceptibility to ProTx-II and TsVII, whereas ProTx-I, LqqIV, and AMBX are not affected. Channel-expressing oocytes were depolarized in 5-mV steps from a

holding potential of −90 mV. Boltzmann fit values are reported in Table 2-1. *n* = 3–5; error bars represent S.E.M.

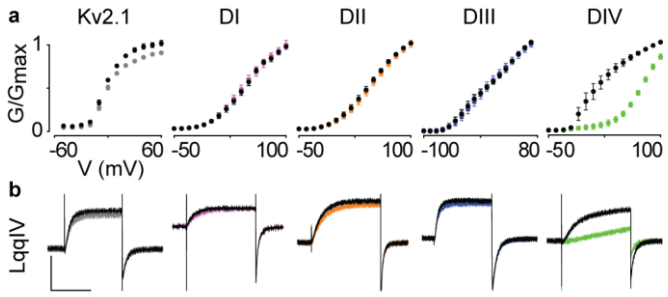

Figure 2-3: Sensitivity of Nav1.2 paddle chimaeras to LqqIV. (A) Effects of 100 nM LqqIV on voltage-gated potassium channel 2.1 (Kv2.1) and chimaeras in which paddle motifs from each of the four domains (DI–IV) were transferred from Nav1.2 into Kv2.1 (1). Normalized tail current–voltage activation relationships are shown, with tail current amplitude plotted against test voltage before (black filled circles) and in the presence of (other colors) toxin. Data reveal that LqqIV selectively targets the paddle motif in DIV of Nav1.2. The holding voltage was −90 mV, test pulse duration was 300 ms, and the tail voltage was −60 mV (−80 mV for DIII). (B) Potassium currents elicited by depolarizations near the foot of the voltage–activation curve for Kv2.1 and chimaeras in the absence and presence of 100 nM LqqIV. The x-axis is 100 ms; the y-axis is ~0.5 μA.

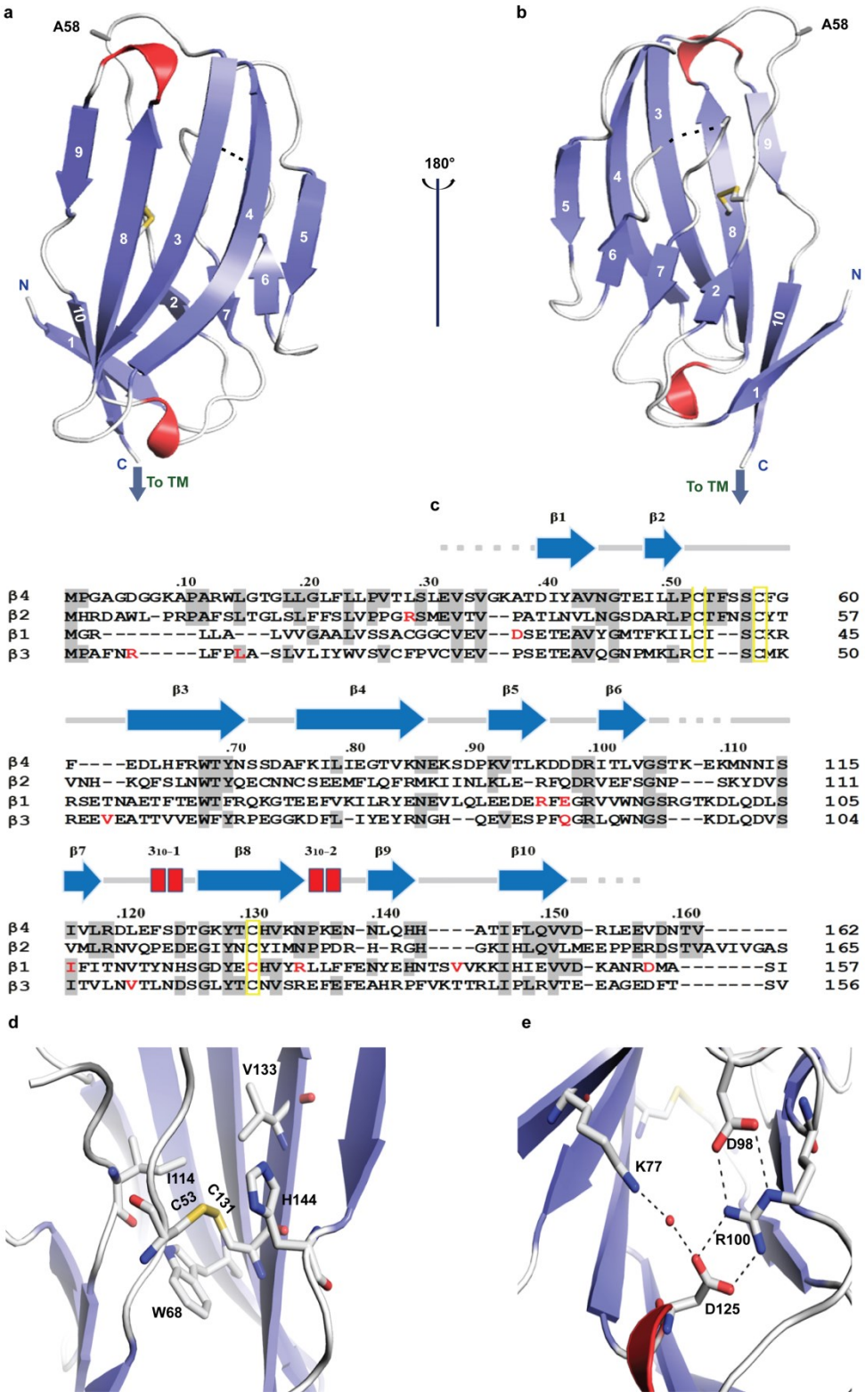
a
A58
9
8
3
4
5
N
10
1
2
7
6
C
To TM
180°
b
A58
3
9
4
5
8
6
7
2
N
10
1
C
To TM
c
β1
β2
.10 .20 .30 .40 .50
β4 MPGAGDGGKAPARWLGTGLLGLFLLPVTLSLEVSVGKATDIYAVNGTEILLPCTFSSCFG 60
β2 MHRDAWL-PRPAFSLTGLSLFFSLVPPGRSMEVTV--PATLNVLNGSDARLPCTFNSCYT 57
β1 MGR--------LLA---LVVGAALVSSACGGCVEV--DSETEAVYGMTFKILCI--SCKR 45
β3 MPAFNR-----LFPLA-SLVLIYWVSVCFPVCVEV--PSETEAVQGNPMKLRCI--SCMK 50
β3
β4
β5
β6
.70 .80 .90 .100 .110
β4 F----EDLHFRWTYNSSDAFKILIEGTVKNEKSDPKVTLKDDDRITLVGSTK-EKMNNIS 115
β2 VNH--KQFSLNWTYQECNNCSEEMFLQFRMKIINLKLE-RFQDRVEFSGNP---SKYDVS 111
β1 RSETNAETFTEWTFRQKGTEEFVKILRYENEVLQLEEDERFEGRVVWNGSRGTKDLQDLS 105
β3 REEVEATTVVEWFYRPEGGKDFL-IYEYRNGH--QEVESPFQGRLQWNGS---KDLQDVS 104
β7
3₁₀-1
β8
3₁₀-2
β9
β10
.120 .130 .140 .150 .160
β4 IVLRDLEFSDTGKYTCHVKNPKEN-NLQHH----ATIFLQVVD-RLEEVDNTV------- 162
β2 VMLRNVQPEDEGIYNCYIMNPPDR-H-RGH----GKIHLQVLMEEPPERDSTVAVIVGAS 165
β1 IFITNVTYNHSGDYECHVYRLLFFENYEHNTSVVKKIHIEVVD-KANRDMA-------SI 157
β3 ITVLNVTLNDSGLYTCNVSREFEFEAHRPFVKTTRLIPLRVTE-EAGEDFT-------SV 156
d
V133
I114
C53
C131
H144
W68
e
D98
K77
R100
D125

Figure 2-4: Crystal structure of the β4 extracellular domain. (*A* and *B*) Two views of the hβ4 extracellular domain, rotated by 180° around a vertical axis. β-Strands are in blue; 3_{10} helices are in red. Dotted lines indicate a flexible region that is invisible in the electron-density map. The conserved cysteine bridge is shown in stick format, with the sulfur atoms colored yellow. The C58A mutation is indicated as A58, and three potential glycosylation sites are shown in as ^{45}Asn (N45), ^{71}Asn (N71), and ^{113}Asn (N113). "To TM" indicates the position at which the single-transmembrane helix starts; N and C specify the N- and C-terminal ends of the structured part of the extracellular domain, respectively. (*C*) Sequence alignment of the extracellular regions of hβ1–4 with the secondary structure of β4 shown above. Amino acids conserved between β4 and other β-subunits are in bold, and known β-subunit–related disease mutations are in red. Conserved cysteines are highlighted by a gray background and the C58A locus by a green background. (*D*) Close-up view of the disulfide bond showing the nearby conserved hydrophobic core. (*E*) Close-up view of the ion-pair network formed by hydrogen bonds between ^{98}Asp and ^{100}Arg, which forms two additional bonds with ^{125}Asp as well as a water-mediated hydrogen bond between ^{77}Lys and ^{125}Asp.

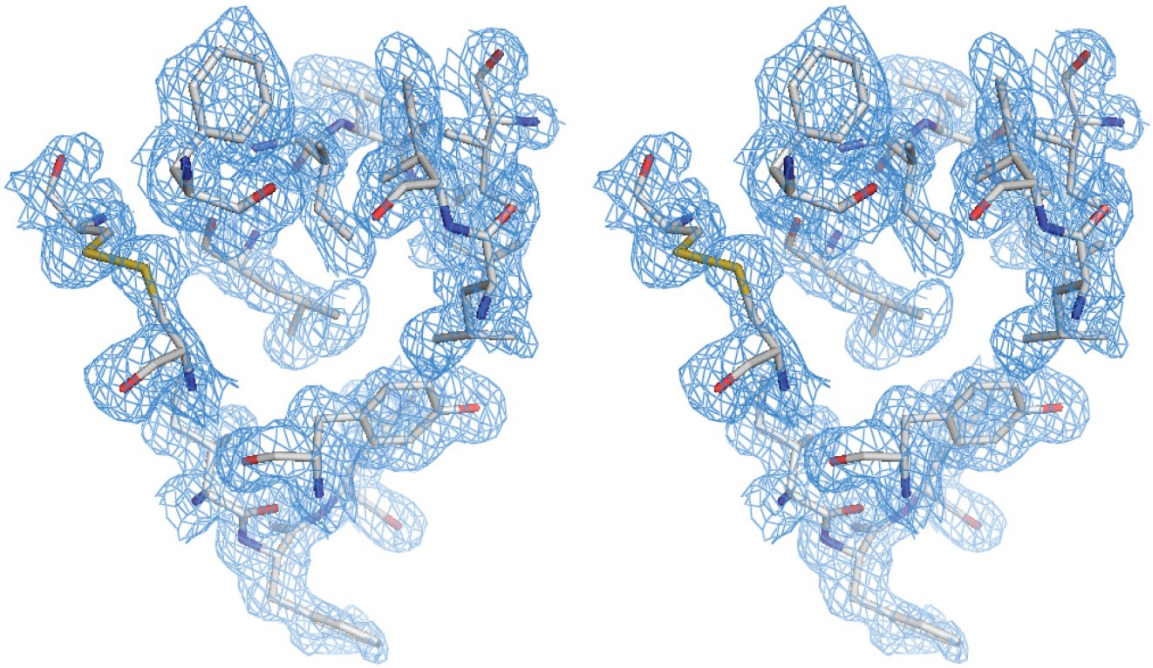

Figure 2-5: Omit map of the β4 core. A stereo view of a simulated annealing composite omit map of the β4 subunit core contoured at 1σ. The ^{53}C–^{131}C disulfide bond (yellow) is present in this view.

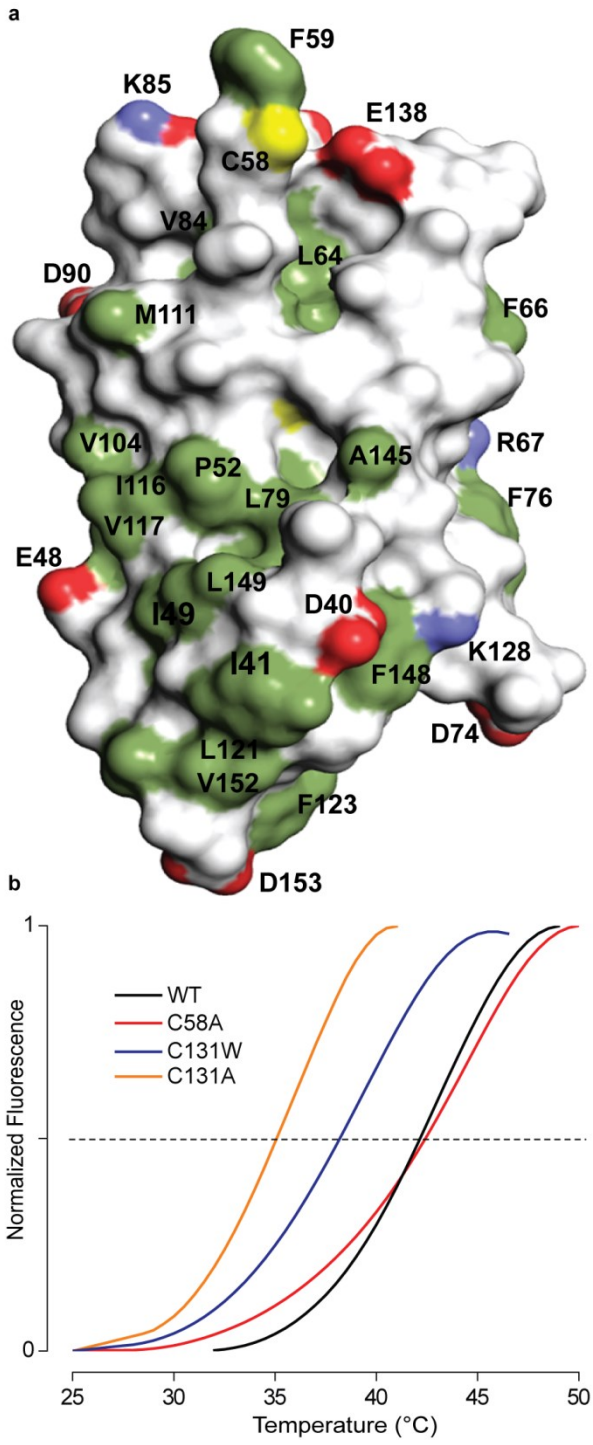

Figure 2-6: Surface representation and thermal stability of the β4 extracellular domain. (*A*) Surface representation of the β4 extracellular domain. Hydrophobic side chains are indicated in green, carboxyl groups of Asp and Glu are shown in red, and the positively charged nitrogen groups of Lys and Arg are

in blue. The position of ^{58}Cys is shown in yellow; other select residues are labeled for reference purposes. (*B*) ThermoFluor experiments showing average melting curves for WT β4 and three mutants under reducing conditions (14 mM 2-ME). The melting temperatures are WT: 42.2 ± 0.1 °C; C58A: 42.2 ± 0.2 °C; C131W: 38.3 ± 1.1 °C; and C131A: 35.1 ± 0.4 °C (SDs are the results of three measurements). The melting curves for C131W and C131A are identical in the absence or presence of 2-ME.

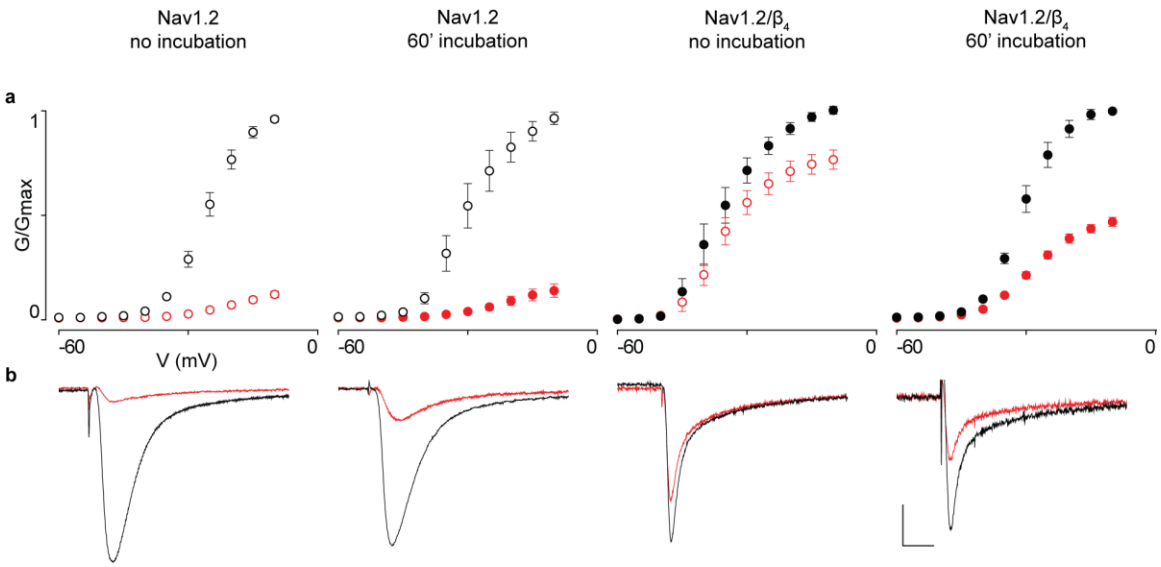

Figure 2-7: Reducing [58]Cys abolishes the effect of β4 on ProTx-II binding. (A) Normalized conductance–voltage relationships (G/G_{max}) of Nav1.2 and Nav1.2/β4- expressing oocytes are shown before (black circles) and after (red circles) the application of 100 nM ProTx-II in control (no incubation; panels 1 and 3) and after 60 min incubation with 200 μM DTT and 100 μM EDTA (panels 2 and 4). As shown in this figure, Nav1.2 opening is not significantly affected by the treatment; however, Cys reduction results in an increased affinity of ProTx-II for the Nav channel in the presence of β4. Channel-expressing oocytes were depolarized in 5- mV steps from a holding potential of −90 mV. n = 3–5; error bars represent S.E.M. (B) Representative sodium currents are elicited by a depolarization to −20 mV before (black) and after (red) the addition of 100 nM ProTx-II from a holding potential of −90 mV. The x-axis is 10 ms; the y-axis is ~0.5 μA.

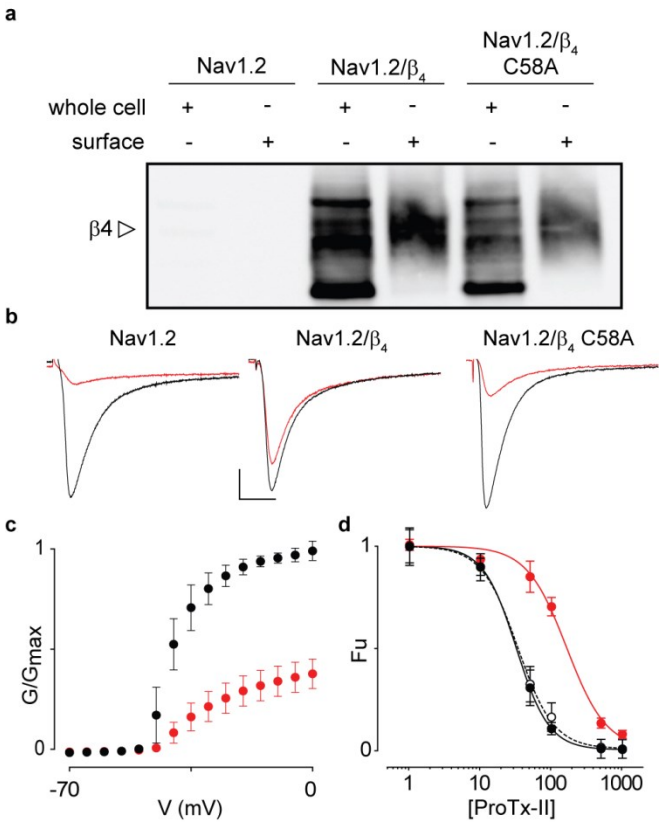

Figure 2-8: Influence of β4 C58A on ProTx-II susceptibility of Nav1.2. (*A*) Correct cellular trafficking of WT β4 and the C58A mutant in oocytes is shown using Western blot analyses by probing for an intracellular β4 Myc-tag combined with primary amine biotinylation of surface proteins. The gel demonstrates that the oocytes produce WT β4 as well as the C58A mutant and that the membrane-inserted protein is heavily glycosylated. The open arrow indicates glycosylated β4. A more detailed gel showing deglycosylated β4 is shown in Fig. 2-9. (*B*) The effect of 100 nM ProTx-II on Nav1.2, Nav1.2/β4, and Nav1.2/β4 C58A. Representative sodium currents are elicited by a depolarization to −20 mV before (black trace) and after (red trace) the addition of ProTx-II from a holding potential of −90 mV. The *x*-axis is 10 ms; the *y*-axis is ~0.5 μA. (*C*) Normalized conductance–voltage relationship (G/G_{max}) of the Nav1.2/β4 C58A channel

without (black filled circles) and in the presence (red filled circles) of ProTx-II. (*D*) Affinity (IC_{50}) of ProTx-II interacting with WT $Na_v1.2$ (black filled circles), Nav1.2/β4 (red filled circles), and Nav1.2/β4 C58A (black open circles connected by the dashed line). The concentration dependence for toxin inhibition is plotted as the fraction of uninhibited channels (Fu). Lines represent a fit with the Hill equation, and IC_{50} values are mentioned in the text. n = 3–5 for each toxin concentration; error bars represent S.E.M.

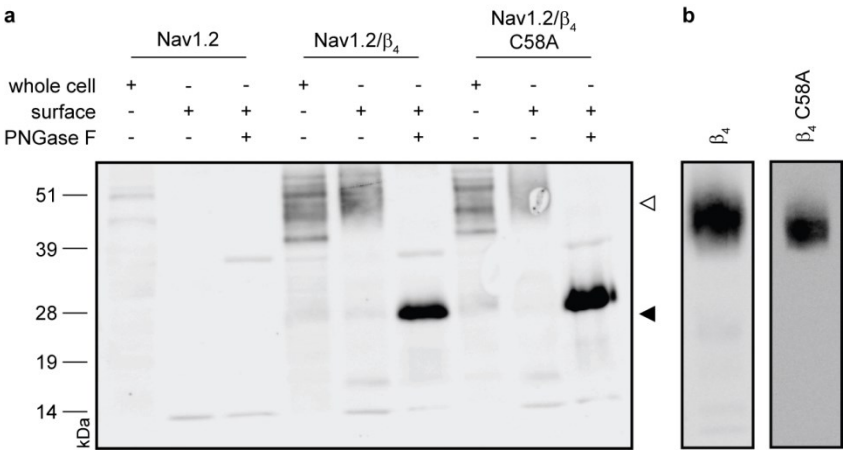

Figure 2-9: β4 and the C58A mutant are glycosylated and traffic to the membrane. (A) Western blot analysis and biotinylation experiments demonstrate the presence of β4 and the C58A mutant on the oocyte membrane surface, albeit in a glycosylated form (open arrowhead). Removing β4 glycosylation using Peptide-N-Glycosidase F (PNGase F) incubation reveals the correct predicted molecular mass of 28 kDa (filled arrowhead).This figure shows data related to that shown in Fig. 4 but over a more extensive range of protein masses. (B) Without Nav1.2, β4 (1) and the C58A mutant still traffic to the oocyte membrane in a glycosylated form. A ladder in kilodaltons (kDa) is shown on the left.

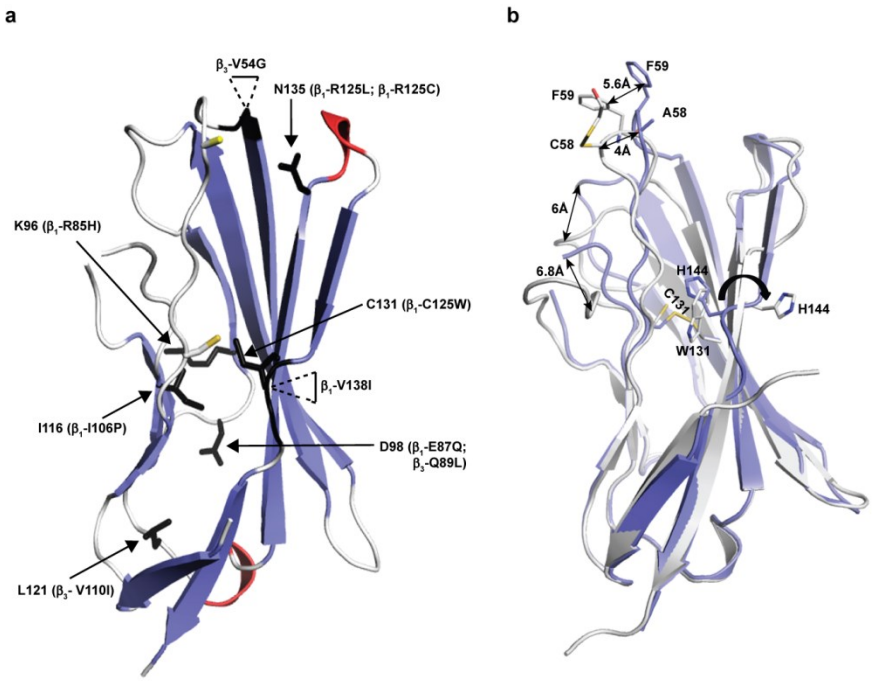

Figure 2-10: Disease-related mutations mapped onto the β4 extracellular domain structure and crystal structure of the β4 C131W variant. (*A*) Arrows indicate the positions of known β1 and β3 disease mutations (summarized in Table 2-3) mapped onto the β4 extracellular domain. The corresponding residue substitutions are shown in parentheses, and the positions of ^{53}Cys and ^{58}Cys are indicated by a yellow stick for reference purposes. Two mutations occur within inserted regions, and the main chains of amino acids next to these insertions are also colored black. (*B*) The crystal structure of the C131W mutant (white) superimposed onto the WT β4 crystal structure (blue). Shifts in the positions of several regions are indicated by double-headed arrows, and select side chains are shown for reference purposes. ^{58}Cys in the C131W structure appears to have a 2-ME molecule attached to it, further highlighting its reactivity. In both *A* and *B*, mutants discussed in this work are displayed in red.

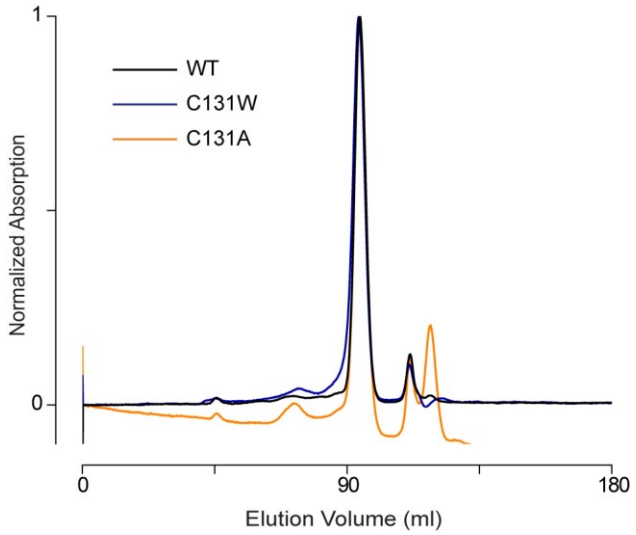

Figure 2-11: Gel-filtration chromatograms of β4, C131W, and C131A. All three chromatograms display a predominant peak corresponding to monomeric protein. Normalized absorption was recorded at 280 nm.

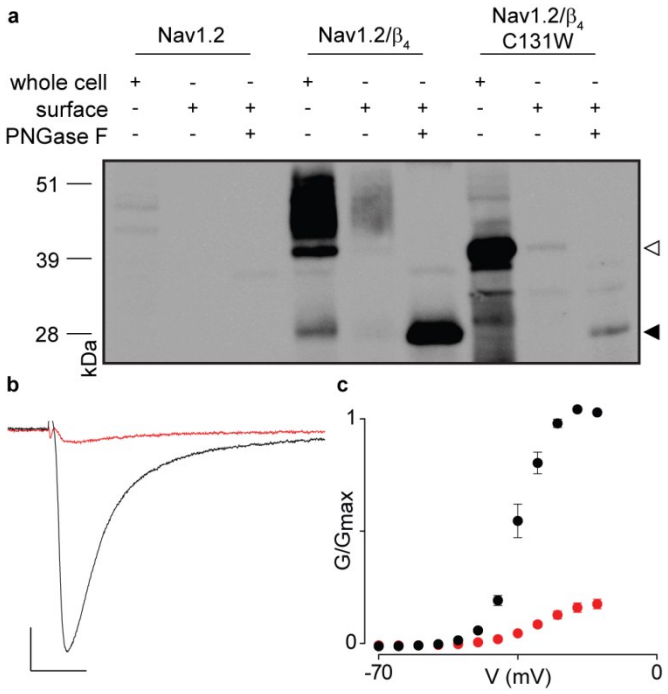

Figure 2-12: Influence of β4 C131W on ProTx-II susceptibility of Nav1.2. (*A*) Cellular trafficking of WT β4 and the C131W mutant in oocytes is shown using nonquantitative Western blot analyses by probing for an intracellular Myc-tag combined with primary amine biotinylation of surface proteins. The gel demonstrates that WT β4, as well as the C131W mutant, is produced and that the membrane-inserted protein is glycosylated. The open arrowhead indicates glycosylated protein, whereas the closed arrowhead represents deglycosylated protein. (*B*) Effect of 100 nM ProTx-II on Nav1.2/β4 C131W. Representative sodium current is elicited by a depolarization to −20 mV before (black trace) and after (red trace) the addition of ProTx-II from a holding potential of −90 mV. The *x*-axis is 10 ms; the *y*-axis is ~0.5 μA. (*C*) Normalized conductance–voltage relationship (G/G_{max}) of the Nav1.2/β4 C131W channel without (black filled circles) and in the presence of (red filled circles) 100 nM ProTx-II. *n* = 3–5; error bars represent S.E.M.

Tables

		Nav1.2		Nav1.2/β_1		Nav1.2/β_2		Nav1.2/β_3		Nav1.2/β_4	
		Before	After	Before	After	Before	After	Before	After	Before	After
ProTx-I	Activation ($V_{1/2}$)	-34.2 ± 1.4mV	-28.0 ± 1.1mV	-29.8 ± 1.5mV	-20.9 ± 0.2mV	-31.8 ± 0.9mV	-22.5 ± 1.8mV	-29.1 ± 1.4mV	-21.3 ± 0.9mV	-29.3 ± 0.2mV	-22.8 ± 0.6mV
	Inactivation ($V_{1/2}$)	-50.2 ± 1.7mV	-58.6 ± 1.4mV	-55.5 ± 0.6mV	-55.8 ± 1.0mV	-45.2 ± 2.6mV	-53.1 ± 4.3mV	-55.7 ± 0.7mV	-61.7 ± 0.7mV	-47.9 ± 0.3mV	-54.1 ± 0.9mV
ProTx-II	Activation ($V_{1/2}$)	-32.3 ± 0.9mV	-22.5 ± 0.2mV	-33.6 ± 0.9mV	-24.8 ± 3.0mV	-27.7 ± 2.1mV	-24.6 ± 2.1mV	-31.7 ± 1.0mV	-24.0 ± 0.9mV	-31.1 ± 3.3mV	-34.6 ± 3.4mV
	Inactivation ($V_{1/2}$)	-49.2 ± 1.3mV	-55.2 ± 2.5mV	-60.0 ± 0.3mV	-63.5 ± 1.0mV	-43.0 ± 0.3mV	-46.3 ± 1.3mV	-56.1 ± 0.5mV	-57.8 ± 0.2mV	-43.2 ± 0.9mV	-44.7 ± 1.5mV
TsVII	Activation ($V_{1/2}$)	-33.5 ± 1.5mV	-38.6 ± 2.1mV	-23.0 ± 1.8mV	-23.4 ± 1.2mV	-32.0 ± 0.9mV	-35.0 ± 0.9mV	-29.6 ± 1.9mV	-31.1 ± 2.4mV	-31.0 ± 1.0mV	-33.0 ± 1.7mV
	Inactivation ($V_{1/2}$)	-54.3 ± 1.0mV	-56.9 ± 1.0mV	-55.4 ± 0.4mV	-58.1 ± 0.8mV	-53.7 ± 0.7mV	-56.8 ± 1.8mV	-57.6 ± 1.2mV	-59.8 ± 1.1mV	-51.8 ± 0.6mV	-59.4 ± 1.5mV
LqqIV	Activation ($V_{1/2}$)	-18.5 ± 0.7mV	-24.4 ± 1.4mV	-28.2 ± 1.7mV	-31.8 ± 1.8mV	-24.5 ± 1.5mV	-32.4 ± 0.8mV	-28.4 ± 1.7mV	-32.3 ± 1.8mV	-30.0 ± 2.3mV	-37.2 ± 3.0mV
	Inactivation ($V_{1/2}$)	-50.5 ± 1.5mV	-48.0 ± 0.8mV	-56.8 ± 0.6mV	-48.1 ± 0.3mV	-47.7 ± 0.5mV	-48.9 ± 0.6mV	-56.9 ± 1.0mV	-50.9 ± 1.0mV	-47.3 ± 0.5mV	-48.0 ± 0.6mV
AMBX	Activation ($V_{1/2}$)	-24.4 ± 1.9mV	-23.3 ± 1.8mV	-30.5 ± 1.7mV	-29.2 ± 1.7mV	-32.8 ± 1.5mV	-29.5 ± 0.6mV	-30.4 ± 2.1mV	-28.4 ± 1.3mV	-34.1 ± 2.7mV	-31.2 ± 1.7mV
	Inactivation ($V_{1/2}$)	-49.1 ± 2.0mV	-51.5 ± 1.5mV	-60.0 ± 1.2mV	-61.9 ± 1.4mV	-50.7 ± 2.6mV	-57.4 ± 1.4mV	-54.3 ± 1.9mV	-55.4 ± 1.3mV	-50.7 ± 2.0mV	-54.2 ± 0.8mV

Table 2-1: Influence of ligands on the gating properties of Nav1.2 and Nav1.2/βx. Results are the average of three to five oocyte recordings and errors are SEM. The table presents data related to Fig. 1 in the main text. *A statistically significant difference before and after toxin addition to Nav1.2 without or in the presence of a particular β-subunit (Student t test with $P < 0.005$).

Data collection		
Space group	$P3_2 2 1$	$P 1 2_1 1$
Cell dimensions		
a, *b*, *c* (Å)	43.44, 43.44, 108.38	31.50, 42.50, 89.20
a, b, g (°)	90.0, 90.0, 120.0	90.0, 91.5, 90.0
Resolution (Å)	27.09 –1.72 (1.77-1.72) [a, b]	29.51 -1.74 (1.77-1.74) [a, b]
R_{sym} or R_{merge}	6.0 (70.1)	6.2 (53.8)
I / sI	21.4 (2.9)	13.6 (2.6)
Completeness (%)	99.9 (98.5)	98.8 (91.4)
Redundancy	10.4 (8.9)	3.6 (3.1)
Refinement		
Resolution (Å)	27.0 –1.72	29.0-1.74
No. reflections	13,205	22,945
R_{work} / R_{free}	17.7/ 21.8	17.0/22.9
No. atoms		
Protein	907	1967
Water	126	280
B-factors		
Protein	30.4	24.7
Water	46.7	38.7
R.m.s. deviations		
Bond lengths (Å)	0.021	0.018
Bond angles (°)	1.925	1.894

Table 2-2: Data collection and refinement statistics. *For each structure, one crystal was used for data collection and structure determination. †Values in parentheses indicate the highest-resolution shell.

	Mutation/ reference	*Disease phenotype*	*β4 residue*	*Location*	*Solvent accesible surface area (Å²)***
Na_Vβ1	R85H[247]	Atrial fibrillation	K96	End of β5	61.9
	E87Q[248]	Cardiac conduction defect	D98	β5- β6 loop	21.4
	I106P[249]	Dravet syndrome	I116	β7, within hydrophobic core	0.7
	C121W[250]	GEFS+	C131	β8. Affects conserved cystine bond. Buried.	0.9
	R125L[251]	GEFS+	N135	End of β8. Lines pocket next to Cys58.	14.3
	R125C[252]	Dravet syndrome	N135	End of β8. Lines pocket next to Cys58.	14.3
	V138I[253]	Idiopathic epilepsy	/	Insertion in β9-β10 loop	/
Na_Vβ3	V54G[254]	Idiopathic ventricular fibrillation	/	Insertion in β2-β3 loop	/
	Q89L[255]	Colorectal cancer*	D98	β5-β6 loop; surface accessible.	21.4
	V110I[256]	Brugada syndrome	L121	β7-3_{10} loop; within hydrophobic core	0

Table 2-3: Disease mutations mapped on the Navβ4 structure

ARCHITECTURE OF THE BETA2/BETA4-NAV CHANNEL SIGNALING COMPLEX

Chapter 3: Binary architecture of the Nav1.2-β2 signaling complex

This chapter adapted from:

Das, S., et al., *Binary architecture of the Nav 1.2-β2 signaling complex.* eLife, 2016. **5**(FEBRUARY2016).

Summary

To investigate the mechanisms by which β-subunits influence Nav channel function, we solved the crystal structure of the β2 extracellular domain at 1.35 Å. We combined these data with known bacterial Nav channel structural insights and novel functional studies to determine the interactions of specific residues in β2 with Nav1.2. We identified a flexible loop formed by ^{72}Cys and ^{75}Cys, a unique feature among the four β-subunit isoforms. Moreover, we found that ^{55}Cys helps to determine the influence of β2 on Nav1.2 toxin susceptibility. Further mutagenesis combined with the use of spider toxins reveals that ^{55}Cys forms a disulfide bond with ^{910}Cys in the Nav1.2 domain II pore loop, thereby suggesting a 1:1 stoichiometry. Our results also provide clues as to which disulfide bonds are formed between adjacent Nav1.2 ^{912}/^{918}Cys residues. The concepts emerging from this work will help to form a model reflecting the β-subunit location in a Nav channel complex.

Contributions: The contents of figures 3-1, 3-2, 3-3, and 3-6 and Table 3-1 were courteously provided by Samir Das and Filip Van Petegem.

Introduction

Nav channels are part of membrane-embedded signaling complexes that initiate the rising phase of action potentials, a crucial event in generating and propagating electrical signals throughout the human body [1, 12]. As key components of these protein assemblies, β-subunits (1) modify Nav channel-gating properties; (2) regulate channel trafficking and localization to distinct surface compartments; and (3) influence channel oligomerization [9, 257]. Moreover, β-subunits can alter the toxin pharmacology of Nav channels [78], a concept that has been exploited to detect their presence in heterologous expression systems or native tissues [213, 258-260]. Structurally, β-subunits are single-transmembrane segment glycoproteins with a short cytoplasmic C-terminal tail and a large V-type immunoglobulin (Ig) extracellular domain that may participate in homophilic and heterophilic interactions, cell adhesion, and cell migration [9, 257, 261]. Although all β-subunits belong to the Ig family, recent atomic resolution information for the β3 and β4 extracellular domain revealed substantial differences in their 3D structure [146, 260]. Given their distinct features and functional roles, it has now become clear that each β-subunit structure should be obtained and assessed separately. Of the four known β-subunits and their splice variants (β1–4; gene names *Scn1b*-*Scn4b*) [138-142], β2 and β4 form a disulfide bond with an unidentified Cys within particular Nav channel isoforms. In contrast, non-covalent interactions underlie β1 and β3 association with Nav channels as well as other members of the voltage-gated ion channel family [9, 147-149, 257]. Aberrant behavior of the ubiquitously expressed

β2 and β4 subunits has been linked to disorders such as long-QT syndrome, atrial fibrillation, sudden infant death syndrome, and epilepsy, possibly through dysregulation of the Nav channel signaling complex [196-200]. Moreover, β2 has been implicated in neurodegenerative disorders and neuropathic pain and is therefore of potential interest for developing novel therapeutic strategies [169, 262]. Finally, β2 is targeted by secretase enzymes, an observation that suggest a potential contribution to Alzheimer's disease [194, 195].

Despite accruing evidence supporting their clinical relevance, fundamental questions on the causal relationship between β2 mutations and disorders remain unanswered. In contrast, auxiliary proteins are the topic of herculean research efforts in other fields where their role as vital contributors to cellular function or in forming drug receptor sites is well established [226, 263-265]. To begin to appreciate β2 function and lay the foundations for constructing an interacting model with Nav channels, we first need to define the mechanism by which β2 regulates Nav channel function. In particular, knowledge of the relative orientation of both partners will help to assess whether a mutation modifies channel function or influences complex assembly. To this end, we solved the crystal structure of the extracellular β2 domain at 1.35 Å and found a ^{55}Cys-containing binding region that modulates Nav1.2 toxin susceptibility by β2. Next, we exploited a combination of Nav channel mutagenesis, biochemistry, and β2-induced alterations in spider toxin pharmacology to uncover a disulfide bond between ^{55}Cys and a partnering Cys located in the domain II S5-S6 pore loop of Nav1.2. Remarkably, Nav1.5 and close relatives Nav1.8/Nav1.9 do not possess

a corresponding Cys, which may explain a lack of β2 effect on Nav1.5 toxin pharmacology. In concert with the available structural information on bacterial Nav channels [16, 17, 45, 46] our results provide conceptual insights into the location of the β2-subunit in the Nav channel-signaling complex.

Results

Crystal structure of the human β2 extracellular region

To begin to understand the functional relationship between human (h)β2 and hNav channels at an atomic level, we solved the crystal structure of the extracellular hβ2 domain at a resolution of 1.35 Å (Fig. 3-1, Table 3-1). The construct encompasses residues 30–153 (Fig. 3-2), and contains a single Cys mutation (C55A) to facilitate crystallization [The C55A mutation is located on the protein surface and therefore unlikely to affect the overall structure (Fig. 3-1*A* and *D*).]. The hβ2 configuration displays an Ig-like fold, consisting of eleven β-strands and three 3_{10} helices. Other than the mutated Cys (C55A), this domain contains four additional cysteines that are arranged in two bonds. The first, intra-subunit bond, is strictly conserved among all four β-subunit isoforms and is mediated by ^{50}Cys and ^{127}Cys buried within the core where it links two opposing faces of the protein. The second intra-subunit bond is located within a loop that spans residues 70–77 and connects strand β5 to β6 via ^{72}Cys - ^{75}Cys (Fig. 3-1*A* and *B*). This loop constitutes a unique feature of hβ2 since corresponding cysteines are absent in β1, β3, and β4. Remarkably, this region displays a dual conformation in the crystal structure which indicates a high degree of flexibility (Fig. 3-1*B*).

Although the overall hβ2 extracellular domain exhibits a similar fold compared to that of the previously reported hβ3 [146] and hβ4 [260] structures, considerable differences are observed. Aside from the distinct ^{72}Cys - ^{75}Cys disulfide bond, there are extensive variances in loop lengths and β strands, indicating that hβ2 and hβ4 have diverged substantially (Fig. 3-2*A* and *C*). Yet, at

a protein sequence level, hβ2 is most closely related to hβ4 (26% identical; 48% conserved) (Fig. 3-2*D* and *E*). Of note is that the N-terminal region of hβ2 is structured rather than disordered in hβ4, adding an additional short β strand (β1) which interacts with the novel β4 strand. The strand following the unique disulfide bond is shortened in hβ2 and two additional 3_{10} helices can be seen, whereas one that is present in hβ4, no longer exists in hβ2. A comparison with the hβ3 structure also shows substantial divergence in loop lengths at particular locations (Fig. 3-2*B* and *C*). The hβ3 extracellular domain misses the additional N-terminal β-strand; instead, its N-terminus is anchored via a disulfide bridge between ^{26}Cys and ^{48}Cys, resulting in positional shifts in excess of 15 Å.

We previously found that ^{58}Cys on the surface of β4 is crucial in modulating Nav1.2 susceptibility to toxins from spider and scorpion venom [260]. The hβ2 subunit possesses a corresponding Cys at position 55 that is located in a longer loop which may result in an altered spatial position of this residue when compared to hβ4 (Fig. 3-2*A* and *C*, Fig. 3-1*D* and *E*). In addition, the residues immediately N-terminal to ^{55}Cys are stabilized through a β-strand interaction between strands β1 and β4, both of which are absent in hβ4. Taken together, these observations suggest that the environment of this key Cys may differ in both isoforms. To further examine the coupling of hβ2 to hNav1.2, we next determined the functional role of ^{55}Cys as well as that of ^{72}Cys and ^{75}Cys.

Mutating ^{55}Cys in hβ2 restores hNav1.2 toxin susceptibility

Previously, we and others discovered that β-subunits can manipulate the pharmacological sensitivities of Nav channels [213, 260, 266]. In particular, β4 is capable of dramatically altering animal toxin binding to rat (r)Nav1.2a [260]. For example, the spider toxin ProTx-II [230] binds to voltage-sensing domains (VSDs) I, II, and IV in rNav1.2a [31], and is ~five-fold less potent when β4 is present. [An intriguing concept is that ProTx-II may also bind directly to β4 [226]; however, our isothermal calorimetry experiments do not support this notion (Fig. 3-3).] To examine whether this protective ability extends to hβ2, we expressed hNav1.2 in *Xenopus* oocytes and measured ProTx-II susceptibility without or in the presence of the β-subunit (Fig. 3-4, Table 3-2). Similar to β4, we observe that the hβ2 subunit expresses abundantly and traffics to the membrane (Fig. 3-5*D*) where it is able to reduce the degree of hNav1.2 current inhibition by ProTx-II. Specifically, 100 nM ProTx-II reduces hNav1.2 conductance to ~17% of peak whereas the current remaining in the presence of hβ2 is typically more than ~64% of peak conductance, thereby demonstrating a protective effect. Other gating parameters such as conductance-voltage (G–V) and channel availability relationships are unaffected (Table 3-2). Next, we sought to determine if ^{55}Cys in hβ2 is involved in reducing hNav1.2 susceptibility to ProTx-II by mutating this residue to an Ala. Indeed, the C55A mutant traffics to the membrane and causes ProTx-II inhibition of hNav1.2 to resemble that of the wild-type (WT) channel without hβ2 present (Fig. 3-4, Fig. 3-5*B* and *C*). Although Ala wields a small side chain and is often employed in mutagenesis studies, we also replaced ^{55}Cys with

a Ser, as it most closely resembles Cys in terms of size and electric properties. Similar to WT hβ2 and C55A, the C55S mutation impaired neither channel expression nor surface trafficking (Fig. 3-5, Fig. 3-5*C*). Moreover, the extent of ProTx-II-induced hNav1.2 inhibition in the presence of C55S is indistinguishable from that of the channel alone (Fig. 3-5*C*, Table 3-2). Altogether, these results support the notion that hβ2 conveys ProTx-II protection to hNav1.2 via ^{55}Cys and may relate to previous work in which the loss of the covalent link between rβ2 and hNav1.1 disrupts the targeting of rβ2 to nodes of Ranvier and to the axon initial segment in hippocampal neurons [144].

In addition to ^{55}Cys, the hβ2 crystal structure reveals a unique motif bearing a protruding disulfide-stabilized loop formed by ^{72}Cys and ^{75}Cys (Fig. 3-1*A* and *B*). Remarkably, this additional loop is highly conserved in almost all species that express β2, suggesting an evolutionary conserved contribution to function (see Fig. 3-2, Fig. 3-6). To determine if this loop regulates the gating or pharmacological influence of hβ2 on hNav1.2, we mutated ^{72}Cys and ^{75}Cys to Ala (C72A C75A) but found that it is functionally indistinguishable from WT hβ2 (Fig. 3-4, Fig. 3-5*C*). The C72A C75A mutant localizes to the oocyte membrane surface without or with hNav1.2 co-expression. Moreover, typical gating parameters and hNav1.2 inhibition by 100 nM ProTx-II in the presence of C72A C75A is similar to that observed for the channel when co-expressed with WT hβ2 (Table 3-2). The lack of effect of the C72A C75A mutant on hNav1.2 function suggests that this disulfide bond is not essential for folding, and that its disruption may not significantly affect the position or environment of ^{55}Cys. To verify this

hypothesis, we produced recombinant hβ2 extracellular domain containing three Cys mutations: C55A, C72A, and C75A. Size exclusion chromatography demonstrates that the mutant produces monomeric protein, indicating that the bond between ^{72}Cys and ^{75}Cys is unessential for folding (Fig. 3-1*F*). Furthermore, we obtained a crystal structure of the triple mutant at 1.85 Å which overlays well onto the C55A structure (Fig. 3-1*C*). The only significant difference is situated in the loop containing both cysteines, which now displays a single conformation. Although the spatial organization of this loop does not seem to impact the ability of hβ2 to modulate hNav1.2 gating or sensitivity to ProTx-II, this region may yet play a functional role in modulating other Nav channel isoforms.

The S5-S6 loop in domain II of hNav1.2 contains an anchoring point for hβ2

Although previous work has postulated the involvement of the domain II (DII) S5-S6 pore loop as the region responsible for forming an inter-subunit disulfide bond between particular Nav channel isoforms and β2 or β4 [144, 267], the precise residue has remained elusive. To explore the possibility of an hβ2 anchoring point in this region, we individually replaced each of the three cysteines found here (^{910}Cys, ^{912}Cys, and ^{918}Cys) with Ser. When expressed without or with WT hβ2, the C910S mutant exhibits the same degree of inhibition by 100 nM ProTx-II, indicating that the protective effect of hβ2 is lost and that ^{910}Cys is a critical residue for hβ2 binding (Fig. 3-7*A* and *B*, Fig. 3-8, and Table 3-3). In contrast, the C918S mutant retains protection from 100 nM ProTx-II by the β-subunit. The C912S mutant displays a split toxin-sensitive population that is consistently observed throughout multiple oocyte batches. One fraction of

experiments reveals hNav1.2 current inhibition as though no hβ2 is present whereas another displays protection against 100 nM ProTx-II, similar to the WT channel and C918S mutant (Fig. 3-7*A*). To verify the presence of hβ2, oocytes were collected after recording and checked for expression by Western blot (see Figure 3-7*B*), thereby indicating that the observed loss-of-protection effects indeed relate to the hNav1.2 mutation.

Altogether, these results hint towards a possibility of mutation-induced shifts in intra-subunit disulfide bond formations, a plausible scenario given the close vicinity of ^{910}Cys, ^{912}Cys, and ^{918}Cys in hNav1.2. To evaluate this hypothesis, we constructed a set of double Cys to Ser mutations (C910S C912S, C910S C918S, and C912S C918S) and examined the effects on ProTx-II susceptibility without and in the presence of hβ2 (Fig. 3-7*A* and *B*, Fig. 3-8, and Table 3-3). According to previous work with rNav1.2a, mutating ^{912}Cys or ^{918}Cys results in a bridge between ^{910}Cys and the remaining intact cysteine [268]. These experiments were carried out without a β2 subunit and with GVIIJ [267], a unique μO§-conotoxin that directly competes for binding to ^{910}Cys; however, the rest of its binding site remains unexplored. In our hands, high concentrations of GVIIJ are needed to achieve an effect, and efficacy towards hNav1.2 is augmented in case of the C910S mutation (Fig. 3-9, Table 3-4), two complicating factors that made us revert to ProTx-II which is more potent and has clearly delineated binding sites within Nav1.2. Our experiments on these double mutants show a much clearer picture wherein hβ2 only protects against ProTx-II when ^{910}Cys is intact: the C912S C918S mutant still has lowered toxin susceptibility whereas

C910S C912S and C910S C918S are completely inhibited by 100 nM ProTx-II, suggesting that these mutants no longer bind hβ2 (Fig. 3-7*A* and *B*, Fig. 3-8). Altogether, these results indicate that ^{910}Cys is the disulfide bond partner of ^{55}Cys in hβ2, while ^{912}Cys and ^{918}Cys could form an intra-subunit bridge. At first sight, the C912S data which show the split population appear in conflict with this interpretation. However, it is conceivable that losing the ^{912}Cys- ^{918}Cys bond results in the formation of a non-native bond between ^{910}Cys and ^{918}Cys (Fig. 3-7*C*). Indeed, when ^{918}Cys is mutated in addition to ^{912}Cys, ^{918}Cys again allows toxin protection by hβ2 similar to WT, suggesting it has become available again. The data also indicate that a non-native disulfide bond between ^{910}Cys and ^{912}Cys may not occur in the C918S mutant, likely because such a Cys-Val-Cys disulfide bond could be too constrained. Importantly, hβ2 cannot protect the C910S C918S or the C910S C912S mutants from 100 nM ProTx-II, indicating that neither ^{912}Cys nor ^{918}Cys can compensate for the loss of ^{910}Cys (Fig. 3-7*C*).

To biochemically verify that Nav1.2 and β2 are covalently bound, we expressed the closely related and well-expressing rat variants (~99% sequence identity) in oocytes and immunoprecipitated the rNav1.2a/rβ2 complex. It is worth noting that WT myc-tagged rβ2 can form higher-order oligomers under non-reducing conditions, which may complicate the interpretation of immunoblots (Fig. 3-10). However, these oligomers disappear upon removal of ^{55}Cys, further highlighting the reactivity of this residue. Notwithstanding this phenomenon, probing crude cell lysates uncovers a clear co-migration of myc-tagged rβ2 with rNav1.2a under non-reducing conditions, since co-expression yields a distinct

myc-stained band above the highest rβ2 oligomer (Fig. 3-11). Substitution of either ^{55}Cys in rβ2 or ^{910}Cys in rNav1.2a with Ser results in the loss of this covalent complex. Furthermore, the presence of DTT completely abolishes the rβ2-rNav1.2a complex as well as the rβ2 oligomers (Fig. 3-11*B*). Thus, these results confirm our toxin experiments and suggest the formation of a disulfide bond between ^{910}Cys in the DII S5-S6 linker of Nav1.2 and ^{55}Cys in β2. In addition to investigating the interaction of rNav1.2a and rβ2 in crude lysate from injected oocytes, we also pulled down rβ2 with an antibody directed against the C-terminal myc-tag and treated with DTT before loading onto a tris-acetate gel (Fig. 3-11*C*). In this experiment, we observe that WT rNav1.2a is present only when co-expressed with WT rβ2. Moreover, both ^{910}Cys within the channel and ^{55}Cys in rβ2 are required for co-immunoprecipitation, thereby pointing to their role in forming a disulfide bond between both subunits (Fig. 3-5, Fig. 3-7).

Next, we were curious to learn whether ^{910}Cys also constitutes an inter-subunit anchoring point for ^{58}Cys in the β4-subunit. To examine this notion, we measured ProTx-II susceptibility of rNav1.2a and its C910S mutant expressed in oocytes without or with the rβ4-subunit (Fig. 3-12*A* and *B*, Table 3-5). Analogous to hβ2, we observe rβ4 protein production in oocytes (Fig. 3-12*C*) where it is able to influence the degree of rNav1.2a current inhibition by ProTx-II. In particular, 100 nM ProTx-II reduces rNav1.2a conductance to ~22% of peak whereas the current remaining in the presence of rβ4 is ~55% of peak conductance. Other gating parameters such as G–V and channel availability relationships are unaffected. In case of the C910S mutant, the presence of rβ4 no longer

decreases ProTx-II efficacy (from ~22% current inhibition to ~17%, respectively, Table 3-5), thus illustrating the likely role of rNav1.2a ^{910}Cys in forming a disulfide bond with rβ4 ^{58}Cys. In concert, (co-)immunoprecipitation experiments with rNav1.2a and rβ4 expressed in oocytes indicate that both partners are covalently bound and that mutating ^{910}Cys in the channel indeed disrupts the disulfide bond (Fig. 3-11).

Aligning the primary sequences of all tetrodotoxin (TTX)-sensitive hNav channel isoforms (Nav1.1–1.7) reveals that the cardiac hNav1.5 channel lacks the cysteine triad while the flanking sequences are highly conserved (Fig. 3-13*A*). Subsequently, it seems unlikely that hNav1.5 forms a covalent bond with hβ2, unless it occurs via a distinct site. However, when applying 100 nM ProTx-II to hNav1.5 without and with the β-subunit, we observe no effects on gating or protection against the toxin, suggesting that hβ2 may not modulate this channel isoform (Fig. 3-13*B*-*E*, Table 3-6). It is worth mentioning that hNav1.8 and hNav1.9, two TTX-resistant isoforms that are evolutionary related to hNav1.5, also lack the cysteine triad and may therefore not interact with hβ2 via a disulfide bond.

Positioning β2 in relation to Nav1.2

Having identified ^{910}Cys within the DII S5-S6 loop of hNav1.2 and ^{55}Cys within hβ2 as inter-subunit disulfide bond partners, we sought to find evidence for a potential locus of the β-subunit in relation to the channel. Although hβ2 seems to be anchored to the DII pore forming region, ProTx-II was previously shown to

target VSDs I, II, and IV [31], suggesting that the protective effect of hβ2 is through occlusion of the ProTx-II binding site in one or more of these regions. In order to determine which one, we assembled a set of animal toxins that, together, interact with VSDI, II, and IV in Nav1.2 [31], and tested whether or not their function is influenced by hβ2 (Fig. 3-14*A*). A previous study in which rNav1.2a S3b-S4 paddle loops from each domain (I-IV) were transplanted into a homotetrameric Kv channel to identify the VSDs with which toxins interact [31], found that the tarantula toxin PaurTx3 and scorpion toxin AahII [269] exclusively target VSDII and VSDIV, respectively. In addition, the tarantula toxins ProTx-I and ProTx-II both interact with the voltage sensor in DII and DIV, whereas ProTx-II also binds to DI with high affinity. Here, we tested these four toxins on hNav1.2 without and with hβ2 to determine if the presence of the subunit impacts toxin function. Aside from ProTx-II, we observe no significant difference in PaurTx3, AahII, or ProTx-I effect which suggests that hβ2 does not impede binding of these toxins to VSDII and VSDIV (Fig. 3-14*B* and *C*, Fig. 3-15, and Table 3-7). Therefore, we speculate that hβ2 primarily influences VSDI and as such, is located near this region (Fig. 3-14*D*). Since μO§-conotoxin GVIIJ function is also influenced by hβ2 [267], it will be interesting to investigate a possible VSDI binding site for this toxin. While our data are limited by the absence of VSDI- and VSDIII-specific toxins and do not exclude the possibility of non-overlapping binding sites for a particular toxin and hβ2 on the same VSD, or of direct competition for binding to the DII S5-S6 loop, they may yet prove valuable as insights into hβ2 function accrue.

Discussion

The goal of this study was to explore the interaction of β2 with Nav1.2 and identify anchoring residues in both partners which will help orient functional motifs within their extracellular domains. Although we obtained the first crystal structure of the hβ4 extracellular region [260], the second reported structure of the corresponding hβ3 domain [146] highlights the unique character of each β-subunit isoform. Since the ability to compare the distinct organizational features of β-subunits will provide valuable information as to their difference in action, we now obtained detailed structural information for the extracellular domain of hβ2 at a resolution of 1.35 Å (Fig. 3-1*A* and *B*, Table 3-1). We identified a flexible loop formed by ^{72}Cys and ^{75}Cys that is a unique feature among β-subunits but with a function that has yet to be elucidated (Fig. 3-1*C*, Fig. 3-2, and Fig. 3-5). Moreover, hβ2 contains a Cys at position 55 that, when mutated, disrupts the influence of hβ2 on hNav1.2 toxin pharmacology (Fig. 3-5*B*-*D*). Next, we combined mutagenesis and biochemical studies with spider and scorpion toxins that target specific VSDs within Nav1.2 [31, 78] to probe the interaction with hβ2. As a result, we found that ^{55}Cys forms a distinct disulfide bond with ^{910}Cys located in the domain II S5-S6 loop of hNav1.2, thereby revealing a 1:1 stoichiometry (Fig. 3-7*A* and *B*, Fig. 3-8, and Table 3-3). We also exploited this toxin-reporter approach to investigate the possibility of intra-subunit disulfide bond formations between ^{910}Cys, ^{912}Cys, and ^{918}Cys in hNav1.2, three reactive residues that are in close vicinity to each other. The outcome of these experiments indicates that ^{912}Cys and ^{918}Cys form an intra-subunit bridge in WT

hNav1.2 (Fig. 3-7). When mutating ^{918}Cys, hβ2 still interacts with ^{910}Cys whereas substituting ^{912}Cys suggests the possibility for bond formation between ^{910}Cys and ^{918}Cys (Fig. 3-7*C*).

Interestingly, hNav1.5 lacks these three cysteines (Fig. 3-13*A*) and as a result, ProTx-II is equipotent without or in the presence of hβ2 (Fig. 3-13*B*-*E*, and Table 3-6) This outcome provides evidence that this particular β-subunit may not modulate hNav1.5 in heterologous systems or that binding occurs through a different mechanism in native tissues. In concert, immunocytochemical studies in the heart and electrophysiological measurements in mammalian cell lines or oocytes disagree on whether hβ2 can modulate hNav1.5 function [154, 170, 270-272]. As opposed to native cardiomyocytes, hNav1.5 may not associate with hβ2 upon heterologous expression, a hypothesis that is supported by co-localization experiments in HEK293 cells where hNav1.5 and hβ2 were mainly found in the endoplasmatic reticulum or plasma membrane, respectively [271].

So far, none of the hβ2 mutations implicated in disorders have been found close to ^{55}Cys, as they are located either in the signal peptide or near the transmembrane region [196-200]. In contrast, amino acid substitutions in the DII S5-S6 pore loop of particular Nav channel variants are linked to diseases. For example, more than 30 mutations have been identified within this region in hNav1.1, several of which relate to Dravet syndrome [2]. This includes C927F (corresponding to ^{918}Cys in hNav1.2), and other variants which introduce an additional Cys that may interfere with local disulfide bond pattern formation.

Therefore, it is conceivable that DII S5-S6 linker mutations may affect channel interactions with hβ2 or hβ4.

Collectively, our results uncover the disulfide link between hβ2 and hNav1.2 which opens up the possibility to assign a potential orientation of this subunit in relation to the channel and provide an experimental basis for future docking efforts (Fig. 3-14*D*). hβ2 may position itself in the gaps between VSDs where it can interact with a voltage sensor as well as anchor to a pore-forming region. One important observation from bacterial Nav channel crystal structures [16, 17, 45, 46] is the domain-swapped architecture of the channel in which the S1-S4 VSD within one subunit is located adjacent to the S5-S6 segments of the next subunit. Such a structural clockwise arrangement has also been consistently observed in prokaryotic and mammalian Kv channels [44, 48]. Since hNav channels may be organized in a similar fashion, the determinants of hβ2-subunit sensitivity can be located in multiple Nav channel domains. For example, we found that hβ2 binds to ^{910}Cys in the S5-S6 loop of DII and influences ProTx-II interaction with VSDI. Although it is challenging to pinpoint its precise location, our data suggest that hβ2 is positioned in the cleft between VSDIV and VSDI or VSDI and VSDII where it is presented with an opportunity to interact with both determinants to influence ProTx-II action (Fig. 3-14*D*). In contrast, the consistent picture emerging from the literature is that Nav channel fast inactivation and voltage-dependence of activation changes substantially when co-expressed with the β1-subunit in heterologous systems [151, 152, 160, 161]. Given the pivotal role of VSDIV in channel fast inactivation [31-35], β1 may be positioned close to

VSDIV where it can also interact with the extracellular S5-S6 pore-loop within DI (Fig. 3-14*D*), a presumed interacting region [150, 151]. Altogether, this model suggests that particular Nav channel isoforms can interact simultaneously with a β1- and β2-subunit [9]. Future experiments will further investigate the possible locations of β3 and β4 in this model as well as allow the incorporation of mutational effects which is essential to uncover the contribution of β-subunit mutations to human disorders or contribute to small molecule screening efforts geared towards disrupting or facilitating subunit interactions.

Materials and methods

Production of the hβ2 extracellular domain

Human β2 (residues 30–153) was cloned into a modified pET28 vector (pET28HMT) [273]. Mutations (C55A and C55/72/75A) were introduced using the Quikchange kit from Agilent Technologies (USA) according to the manufacturer's instructions. Proteins were expressed at 18°C in *E. coli* Rosetta (DE3) pLacI strains (Novagen, USA), induced at an OD600 of ~0.6 with 0.4 mM IPTG, and grown overnight prior to harvesting. Cells were lysed via sonication in buffer A (250 mM KCl and 10 mM HEPES at pH 7.4), supplemented with 25 μg/ml DNaseI and 25 μg/ml lysozyme. After centrifugation, the supernatant was applied to a PorosMC column (Tosoh Biosep, USA), washed with buffer A plus 10 mM imidazole, and eluted with buffer B (250 mM KCl plus 500 mM imidazole pH 7.4). The protein was dialyzed overnight against buffer A and cleaved simultaneously with recombinant TEV protease. Next, the samples were run on another PorosMC column in buffer A, and the flowthrough was collected and dialyzed against buffer C (10 mM KCl plus 10 HEPES at pH 7.4), applied to a HiloadQ column (GE Healthcare, USA), and eluted with a gradient from 0% to 30% buffer D (1 M KCl plus 10 mM HEPES at pH 7.4). Finally, the samples were run on a Superdex200 (GE Healthcare, USA) gel filtration column in buffer A. The protein samples were exchanged to 50 mM KCl plus 10 mM HEPES (pH 7.4), concentrated to ~5 mg/ml using Amicon concentrators (3K MWCO; Millipore USA), and stored at −80°C.

Crystallization, data collection, and structure solution

Crystals were grown using the hanging-drop method at 4°C. Both C55A and C55/72/75A were crystallized in 0.1 M Tris (pH 8), 15–20% (w/v) PEG 6000. Crystals were flash-frozen after transfer to the same solution supplemented with 30% glycerol. The data used to solve the final structures were collected at the Canadian Light Source (Saskatoon) beamline 08ID-1 and datasets were processed using XDS [239] and HKL3000 [274]. A search model was created by using only β-strands from PDB 4 MZ2, and with all side chains truncated to alanine. Molecular replacement was performed using Phaser [240], yielding poor initial phases which were improved via autobuilding in ARP/wARP [241]. The model was completed by successive rounds of manual model building in COOT [275] and refinement using Phenix [276]. A simulated annealing composite omit map was calculated with CNS [244] to verify the absence of residual model bias. 85Met was found to be in a disallowed region of the Ramachandran plot in both structures. All structure figures were prepared using PYMOL (DeLano Scientific, San Carlos, USA).

Accession codes

Coordinates and structure factors have been deposited in the Protein Data Bank under accession codes 5FEB (C55A) and 5FDY (C55/72/75A).

Toxin acquisition and purification

ProTx-I and ProTx-II were acquired from Peptides International (USA), PaurTx3 from Alomone Labs (Israel). AaHII from *Androctonus australis* hector

venom was purified as described [269]. Toxins were kept at -20°C and aliquots were dissolved in appropriate solutions containing 0.1% BSA.

Two-electrode voltage-clamp recording from Xenopus oocytes

The DNA sequence of hNav1.2 (NM_021007.2), rNav1.2a (NM_012647.1), rβ4 (NM_001008880) and hβ2 (NM_004588.4) (acquired from Origene, USA), as well as their mutants was confirmed by automated DNA sequencing and cRNA was synthesized using T7 polymerase (mMessage mMachine kit, Ambion) after linearizing the DNA with appropriate restriction enzymes. Channels were expressed in *Xenopus* oocytes together with a β-subunit (1:5 molar ratio) and studied following 1–2 days incubation after cRNA injection (incubated at 17°C in 96 mM NaCl, 2 mM KCl, 5 mM HEPES, 1 mM $MgCl_2$ and 1.8 mM $CaCl_2$, 50 μg/ml gentamycin, pH 7.6 with NaOH) using two-electrode voltage-clamp recording techniques (OC-725C, Warner Instruments) with a 150 μl recording chamber. The data were filtered at 4 kHz and digitized at 20 kHz using pClamp 10 software (Molecular Devices, USA). Microelectrode resistances were 0.5–1 MΩ when filled with 3 M KCl. The external recording solution contained 100 mM NaCl, 5 mM HEPES, 1 mM $MgCl_2$ and 1.8 mM $CaCl_2$, pH 7.6 with NaOH. The experiments were performed at room temperature (~22°C) and leak and background conductances, identified by blocking the channel with tetrodotoxin (Alomone Labs, Israel), have been subtracted for all Nav channel currents. All chemicals used were obtained from Sigma-Aldrich (USA) unless indicated otherwise.

Analysis of channel activity and toxin–channel interactions

Voltage–activation relationships were obtained by measuring steady-state currents and calculating conductance (G), fitted to the data according to: $G/G_{max} = (1 + e{-}zF(V – V_{1/2})/RT){-}1$ G/Gmax = 1 + e-zF(V - $V_{1/2}$)/RT-1 where G/G_{max} is the normalized conductance, *z* is the equivalent charge, $V_{1/2}$ is the half-activation voltage, *F* is Faraday's constant, R is the gas constant and T is temperature in Kelvin. Occupancy of closed or resting channels by ProTx-II and other toxins was examined using negative holding voltages where open probability was very low, and the fraction of uninhibited channels (F_u) was estimated using depolarizations that are too weak to open toxin-bound channels, as described previously. After addition of the toxin to the recording chamber, the equilibration between the toxin and the channel was monitored using weak depolarizations typically elicited at 5 s intervals. Off-line data analysis was performed using Clampfit 10 (Molecular Devices, USA), and Origin 8 (Originlab, USA).

Qualitative biochemical assessment of hβ2 production in Xenopus oocytes

After each electrophysiological experiment, oocytes expressing hNav1.2, hβ2, and the described mutants were washed with ND100 and incubated with 0.5 mg/ml Sulfo-NHS-LC-biotin (Pierce, USA) for 30 min. Oocytes were thoroughly washed again in ND100 before lysis (by pipetting up and down) in 20 µl/oocyte buffer H (1% Triton X-100, 100 mM NaCl, 20 mM Tris-HCl, pH 7.4) plus protease inhibitors (Clontech, USA). All subsequent steps were performed at 4°C. Lysates were gently shaken for 15 min after which they were centrifuged at 16,200 x *g* for 3 min. The pellet was discarded and the supernatant (SN) transferred to a fresh

1.l Eppendorf tube. 40 µl of SN was stored at -80°C for later use as the whole cell protein aliquot. 200 µl of hydrophilic streptavidin magnetic beads (New England Biolabs, USA) were then added and the sample shaken gently at 4°C overnight. Beads were washed 6 times with buffer H and resuspended in 40 µl buffer H, after which the biotinylated protein was dissociated from the beads through the addition of 1X LDS loading buffer plus reducing agent (10% 2-ME, 50 mM DTT final conc.) and boiling at 95°C for 5 min to generate the surface protein fraction. All samples were appropriately diluted in buffer H to give equal protein concentrations, as measured by a BCA assay (Pierce, USA). 10 µg of the SN was run on a 10% Tris-Glycine Novex Mini-Gel (Thermo Fisher Scientific, USA) with Tris-Glycine running buffer and analyzed by Western analysis. Nitrocellulose membranes were probed overnight at 4°C with 1:1000 mouse anti-myc antibody as primary (Cell Signaling Technologies, USA) and for 45 min at room temperature with 1:10000 goat anti-mouse HRP-conjugated antibody as secondary (Thermo-Fisher Scientific, USA). Membranes were incubated for 5 min with an enhanced chemiluminescent substrate before imaging.

Immunoprecipitation of the Nav1.2/β2 complex

Xenopus oocytes were injected with 5 ng RNA of rβ2, rNav1.2, or both (~1:5 molar ratio) and incubated for 48 hr at 17°C. 30 oocytes were lysed for each condition, using 20 µl lysis buffer (1x PBS, 1% DDM, 10% glycerol, 1 mM EDTA, 1X protease inhibitor cocktail [Clontech, USA]) per oocyte, and homogenized by passing through a 25-gauge syringe [277]. The lysate was rotated for 1 hr at 4°C in a 1.5 ml microfuge tube, after which it was spun for 30

min at 20,000 x *g* at 4°C. Subsequent steps were performed at 4°C or on ice and during all rotations the tube was sealed with parafilm to prevent leakage. A fresh pipette tip was gently swirled in the supernatant to remove the bulk of the white goop by adhering to the tip and supernatant was transferred to a new tube, taking care not to disturb the pellet. The new tube was spun 3 min at 20,000x*g* and again was swirled with a fresh pipette tip to remove the white goop, after which the clear supernatant was transferred to a new tube. Protein concentration was assayed using a BCA protein concentration kit (Pierce, USA). 150 µg protein was brought to 150 µl in lysis buffer and 1.5 µg (1.5 µl of 1 mg/ml) anti-myc mouse antibody (Thermo-Fisher Scientific, USA) was added. The tube was rotated overnight at 4°C after which 30 µl protein G-coated magnetic Dynabeads (Thermo-Fisher Scientific, USA) were added and rotated for 4 hr at 4°C. The tube was spun for 1 min at 20,000x*g* and placed on a magnetic rack for 1 min to collect the beads. Supernatant was removed and stored for optimization and troubleshooting purposes, as were subsequent washes. The beads were washed with 200 µl wash buffer (1x PBS, 0.4% DDM, 10% glycerol, 1 mM EDTA) by pipette mixing and then magnetized to collect beads. The wash process was repeated three times. After the third wash, beads were suspended in 100 µl wash buffer, transferred to another tube, spun for 1 min at 20,000x*g*, and magnetized to collect beads. The tube was then spun again for 1 min at 20,000x*g* and magnetized, followed by removal of the last residual fluid. Protein was eluted in 30 µl elution buffer (50 mM glycine, pH 2.8) by incubating for 3 min at room temperature, followed by magnetization and transfer to the final tube. For

Western blotting of the immunoprecipitate, 17 µl of eluate was combined with 2.5 µl 10X reducing agent (Thermo-Fisher Scientific, USA) and 6.5 µl 4X LDS sample loading buffer (Thermo-Fisher Scientific, USA), heated for 10 min at 37°C, then loaded onto a 1.0 mm 12-well 3–8% Novex Tris-Acetate pre-cast gel (Thermo-Fisher Scientific, USA). A rabbit anti-PanNav antibody (Alomone labs, Israel) and rabbit anti-hβ2 antibody (Cell Signaling Technologies, USA) were chosen to avoid cross-reaction of the Western blot secondary antibody against the mouse antibody used for immunoprecipitation. For Western blotting, the primary antibodies were used at 1:200 and 1:1000 dilutions, respectively, applied for 1 hr at room temperature and incubated for 45 min at room temperature with a 1:10,000 goat anti-rabbit HRP-conjugated secondary antibody (Thermo-Fisher Scientific, USA).

Acknowledgements

We would like to thank Marie-France Martin-Eauclaire and Pierre Bougis (University of Marseille, France) for sharing AaHII; Al Goldin (UCIrvine, USA) for sharing $rNa_v1.2a$; YaWen Lu and Elizabeth Calzada (Johns Hopkins University – School of Medicine, USA) for assistance with biochemistry; Michael Pennington (Peptides International, USA) for sharing ProTx-II used in the ITC experiment; and Baldomero Olivera (University of Utah – Salt Lake City, USA) for sharing GVIIJ. We also wish to thank the staff of the Advanced Photon Source (Chicago, USA) GM/CA-CAT beamline 23-ID-D, the Stanford Synchrotron Radiation Lightsource (Menlo Park, USA), and the Canadian Light Source (Saskatoon, SK, Canada), which is supported by the Natural Sciences and Engineering Research Council of Canada, the National Research Council Canada, the Canadian Institutes of Health Research (CIHR), the Province of Saskatchewan, Western Economic Diversification Canada, and the University of Saskatchewan. Parts of this work are supported by the National Institute of Neurological Disorders And Stroke (NINDS) of the National Institutes of Health (NIH) under Award Number 1R01NS091352 to FB, a Human Frontier Science Program grant to FB and FVP (RGY0064/2013), and a CIHR grant to FVP (MOP-119404). SD is supported by a postdoctoral fellowship of the Heart and Stroke Foundation of Canada and JG by the NINDS/NIH under Award Number F31NS084646. The content is solely the responsibility of the authors and does not necessarily represent the official views of the NIH.

Figures

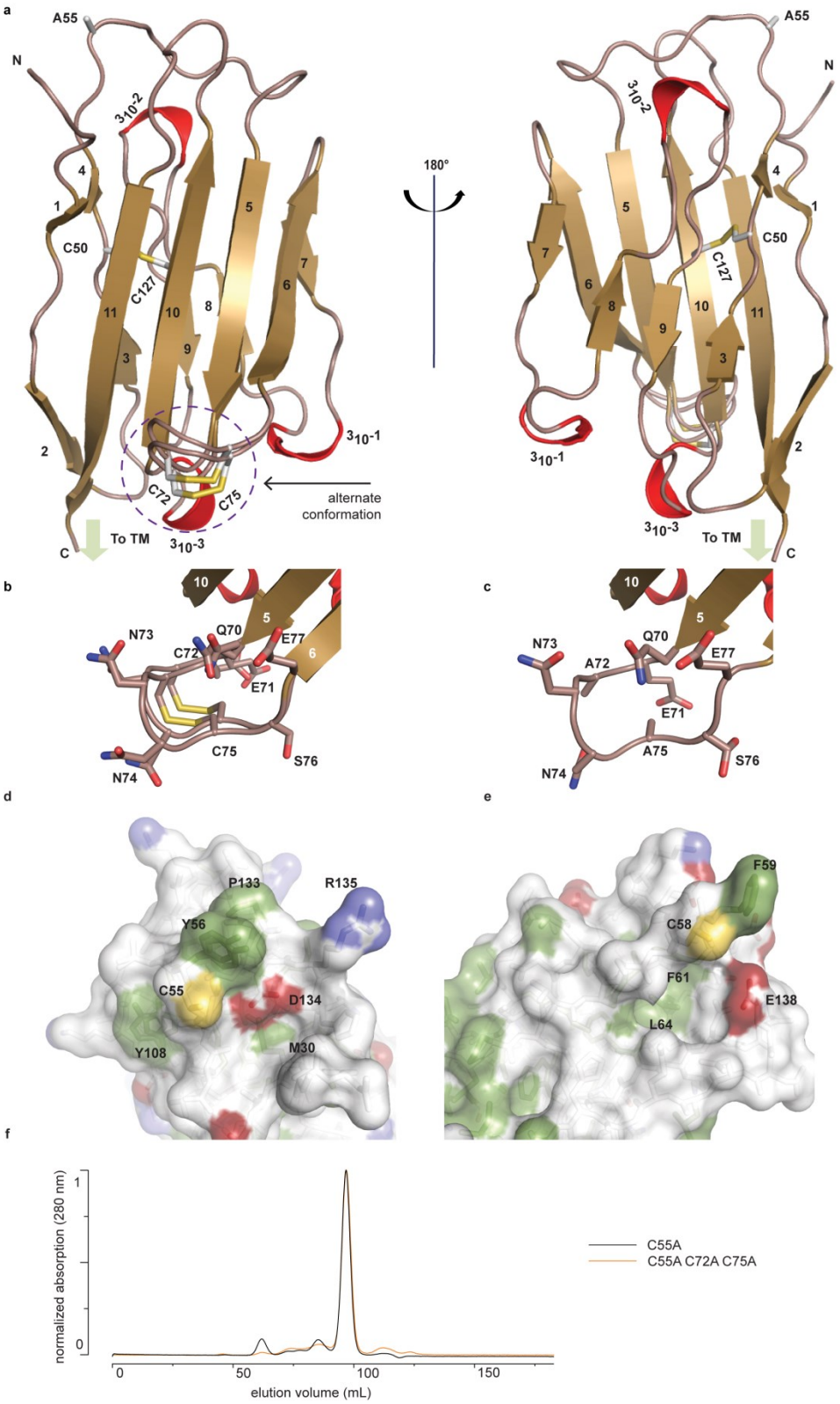
a
A55
N
3_{10}-2
4
1
C50
C127
11
10
8
5
7
6
9
3
2
3_{10}-1
C72
C75
alternate
conformation
C
To TM
3_{10}-3
180°
A55
N
3_{10}-2
4
1
5
C50
7
C127
6
8
10
11
9
3
2
3_{10}-1
3_{10}-3
To TM
C
b
10
5
N73
Q70
E77
C72
6
E71
C75
S76
N74
c
10
5
N73
Q70
A72
E77
E71
A75
S76
N74
d
P133
R135
Y56
C55
D134
Y108
M30
e
F59
C58
F61
E138
L64
f
normalized absorption (280 nm)
1
0
0
50
100
150
elution volume (mL)
C55A
C55A C72A C75A

Figure 3-1: Crystal structure of hβ2. (a) Cartoon representation of the hβ2 (C55A) extracellular domain crystal structure, showing β strands in gold and 3_{10} helices in red. Cysteine side chains, as well as the ^{55}Ala residue, are shown in stick representation. Positions of N-terminus (N) and C-terminus (C) are indicated. The loop containing the ^{72}Cys- ^{75}Cys disulfide bond is modeled in a dual conformation. (b) Detail of the dual conformation of the loop, showing all side chains in stick conformation. (c) Detail of the same loop in the C72A/C75A (C55A) mutant, shown from the same viewpoint as in panel (b). (d,e) Comparison of the surfaces of hβ2 (d) and hβ4 (e) surrounding the reactive cysteines (^{55}Cys and ^{58}Cys, respectively). Side chains of hydrophobic residues are shown in green, negatively charged carboxyl groups in red, and positively charged amino and guanidinium groups in blue. The position of the cysteine (which has been mutated to alanine to allow crystallization) is shown in yellow. (f) Size exclusion chromatograms (Preparative Superdex200) for hβ2 C55A and hβ2 C55/72/75A, which both elute as monomeric species.

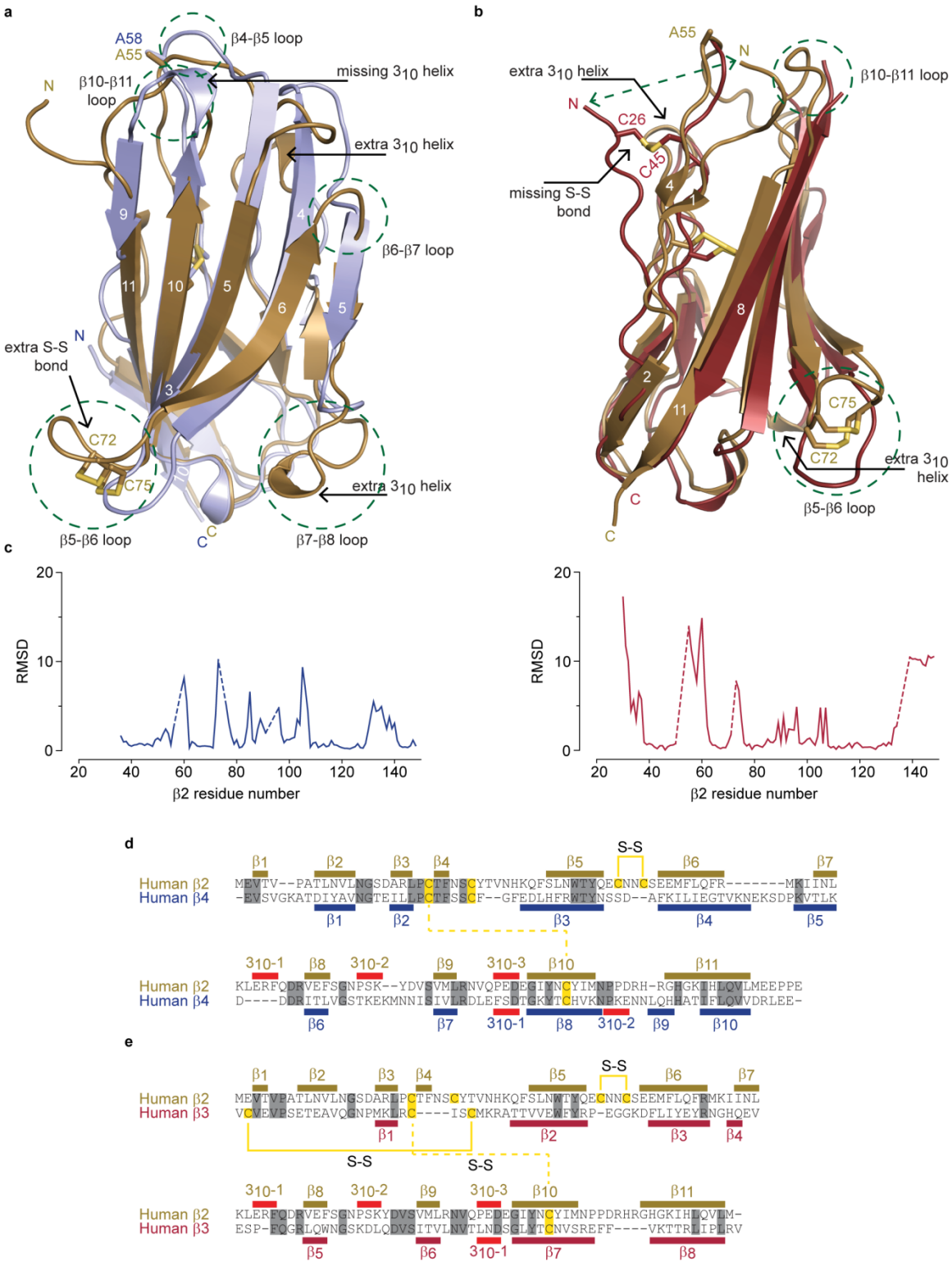
a
A58
A55
β4-β5 loop
missing 310 helix
β10-β11
loop
N
extra 310 helix
β6-β7 loop
extra S-S
bond
C72
C75
extra 310 helix
β5-β6 loop
β7-β8 loop
b
A55
N
β10-β11 loop
extra 310 helix
C26
C45
missing S-S
bond
C72
C75
extra 310
helix
β5-β6 loop
c
RMSD
β2 residue number
d
S-S
Human β2
Human β4
e
Human β2
Human β3
S-S
S-S

Figure 3-2: Structural comparison of hβ2 to hβ3 and hβ4. (a) Superposition of the crystal structures of hβ2 C55A (gold) and hβ4 C58A (blue) in cartoon representation. Cysteines or their equivalent residues (A55 and A58, respectively) are shown in sticks. The major differences are highlighted in the figure. (b) Superposition of crystal structures of hβ2 C55A (gold) and hβ3 (red). (c) Root-mean-square-deviation (RMSD) plots showing the RMSD values per residue for hβ4 C58A (left, blue plot) and hβ3 (right, red plot) relative to hβ2 after a superposition. The residue numbers below correspond to the hβ2 numbers. Sections for which there are no corresponding residues at indicated with dotted lines. (d,e) Shown are sequence alignments of the extracellular domains of (d) hβ2 versus hβ4 and (e) hβ2 versus hβ3. Conserved residues are highlighted in grey, and cysteines in yellow. Observed disulfide bonds are also labeled (S-S). Secondary structure elements found in the corresponding crystal structures are also shown.

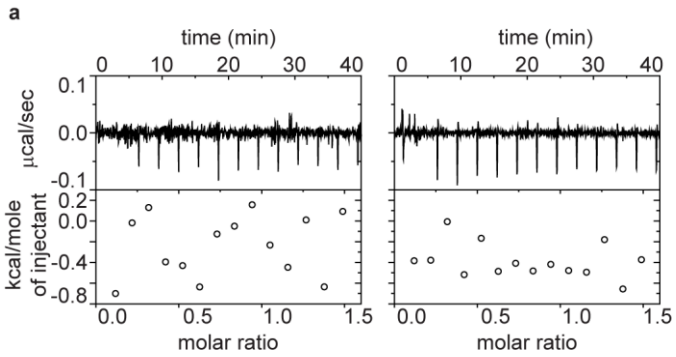

Figure 3-3: ProTx-II does not bind directly to β4. Isothermal calorimetry (ITC) experiments showing titration of 400 µM WT hβ4 extracellular domain into 40 µM ProTx-II (left) and into buffer (right). No significant heat differences are detected.

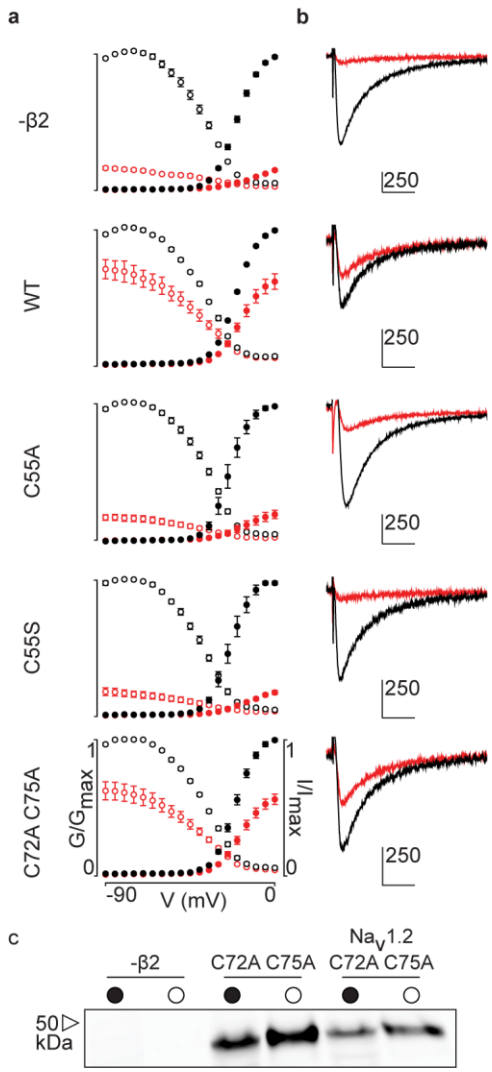

Figure 3-4: G-V and SSI relationships for hβ2 mutants. (a) Conductance-voltage (G-V, filled circles) and steady-state inactivation (SSI, open circles) relationships before 10nM ProTx-II addition are indicated in black and red in the presence of toxin. (b) Representative traces at -15 mV (holding potential of -90 mV) for the corresponding graphs seen in (a). Scale bar is 10 ms along horizontal axis and displayed nA along the vertical axis. (c) Western blot showing that the C72A C75A hβ2 mutant is expressed in whole cell (filled circle) and surface (open circle) fractions either alone (middle column) or with hNav1.2 (right

column). The hβ2 subunit was detected using an antibody against a C-terminal myc-tag.

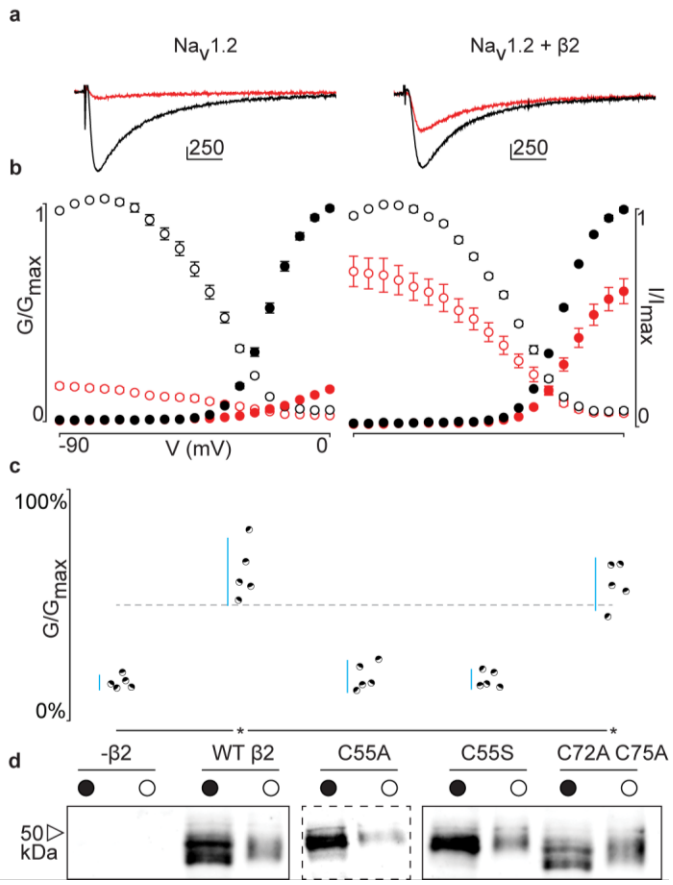

Figure 3-5: Effect of hβ2 on hNav1.2 toxin pharmacology. (a) Co-expression of hNav1.2 with hβ2 decreases the degree of inhibition by 100 nM ProTx-II. Left trace shows ProTx-II strongly inhibiting WT hNav1.2 whereas right trace displays attenuated inhibition in the presence of hβ2. Black trace is control condition without toxin, red is in the presence of ProTx-II. Traces depict a 50 ms depolarization to -15 mV from -90 mV. Scale bar is 10 ms on horizontal axis and given nA vertically. (b) Normalized conductance-voltage (G-V, filled circles) and steady-state inactivation (I-V, open circles) relationships for hNav1.2 with and without hβ2. Pre-toxin values are shown in black and post-toxin in red. Fit values can be found in Table 3-2. (c) Dot plot comparing hβ2 mutations by ability to prevent ProTx-II inhibition of hNav1.2. Black circles represent individual oocytes;

vertical axis shows percent of inhibition by ProTx-II at peak conductance. Blue lines represent a 95% confidence interval. hβ2 mutations are presented underneath the horizontal axis and label the lanes below in (d). Statistical significance ($p < 0.01$) is indicated by an asterisk. (d) Western blot against the C-terminal myc-tag of hβ2. No signal is seen in the negative control but is observed for the WT hβ2 and all mutants, both in whole cell (filled circle) and surface (open circle) fractions.

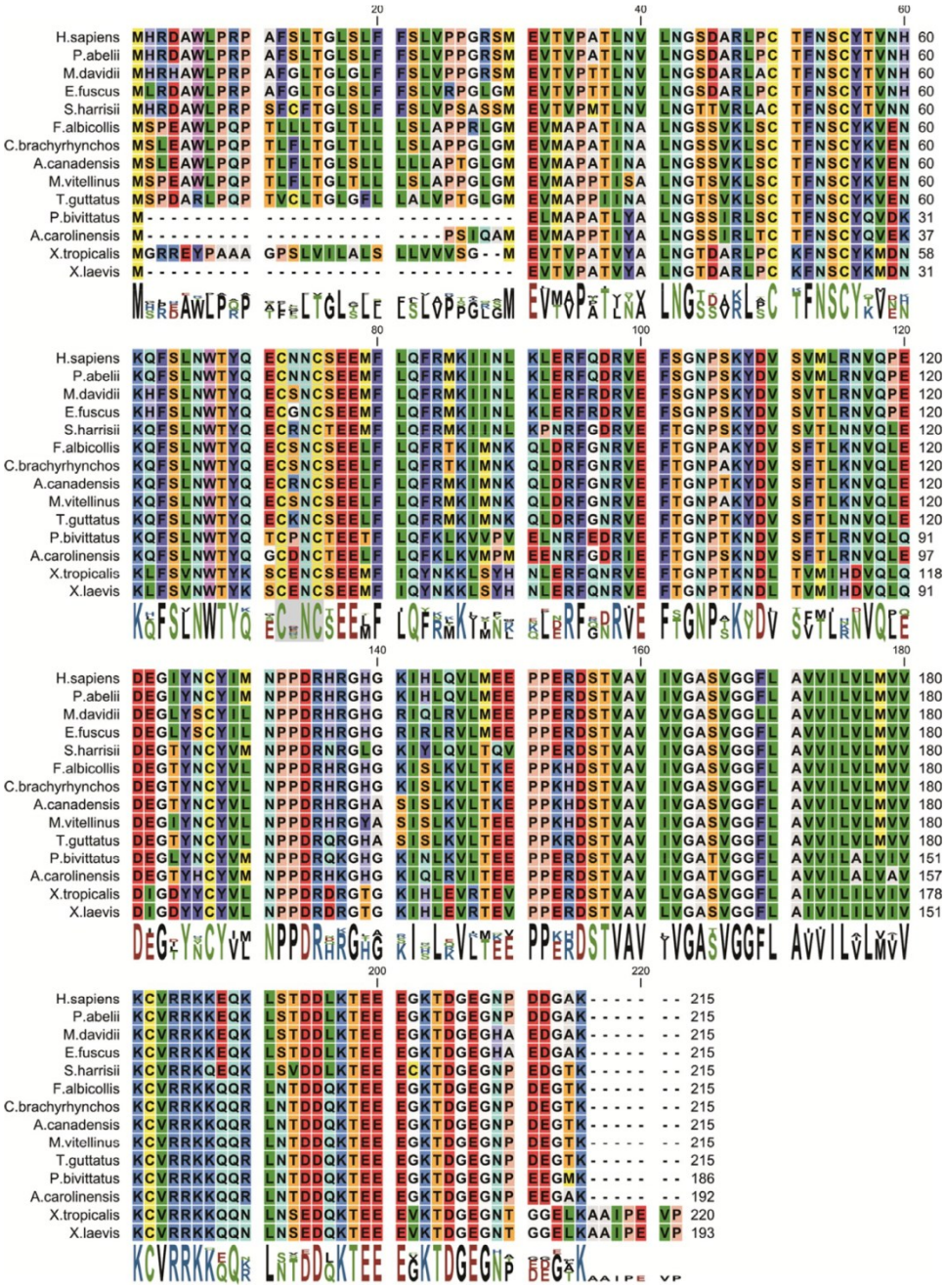

Figure 3-6: Amino acid sequence alignment of the β2 protein found in various organisms. Conserved cysteines ^{72}Cys and ^{75}Cys in hβ2 are indicated with a grey background. Residue numbers in hβ2 above sequences are shown as a reference. Protein accession numbers for sequences used are:

H. sapiens (NP_004579.1),

P. abelii (XP_002822587.1),

M. davidii (XP_006761624.1),

E. fuscus (XP_008148335.1),

S. harrisii (XP_003764204.1),

T. guttatus (XP_010214560.1),

C. brachyrhynchos (XP_008635161.1),

F. albicollis (XP_005058672.1),

A. canadensis (XP_011600162.1),

M. vitellinus (XP_008927155.1),

A. carolinensis (XP_003229016.2),

P. bivittatus (XP_007424304.1),

X. tropicalis (NP_001116903.2),

X. laevis (NP_001088105.2).

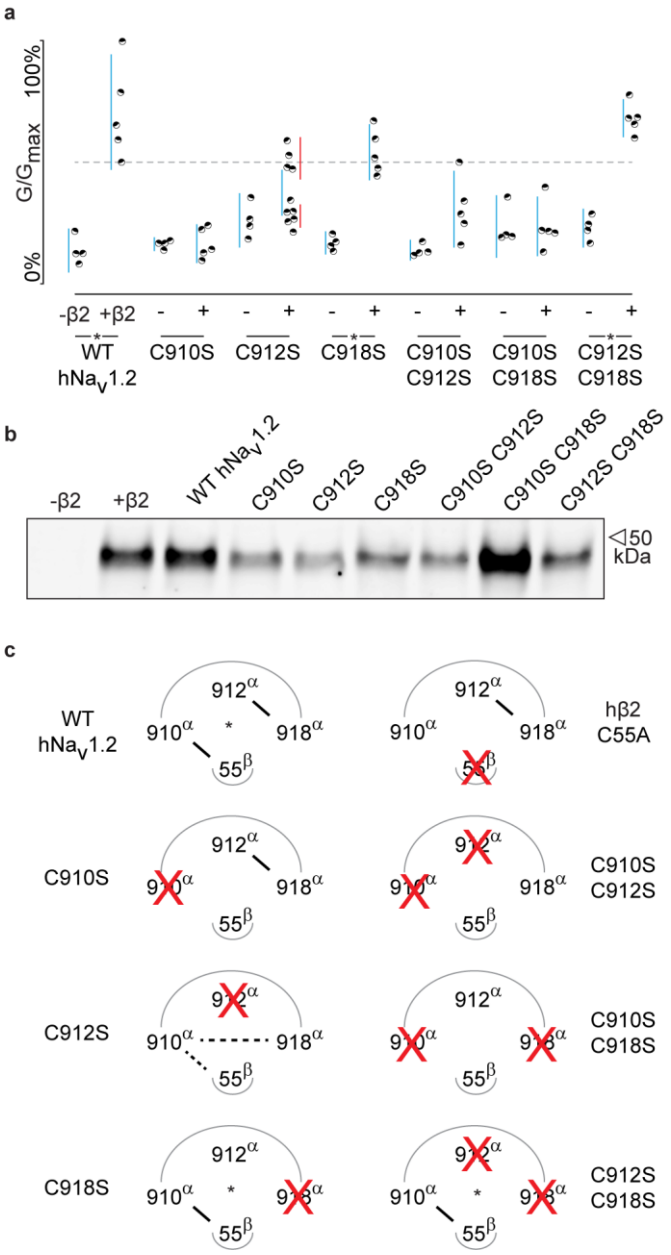

Figure 3-7: hβ2 forms a disulfide bond with ^{910}Cys in hNav1.2. (a) Dot plot showing degree of hNav1.2 mutant inhibition by 100 nM ProTx-II, with and without hβ2. Black circles represent single oocytes expressing the indicated constructs and currents were measured at peak conductance. Blue bars indicate 95% confidence interval, and the red bars are 95% confidence intervals for both populations in the C912S mutant co-expressed with hβ2. Statistical significance

with $p < 0.01$ is shown by an asterisk. (b) Western blot against a myc-tag reveals the presence of hβ2 in whole cell fraction of oocytes co-injected with hβ2 mRNA. (c) Schematic depiction of the proposed disulfide arrangement in hNav1.2 mutants with hβ2. hNav1.2 cysteines are displayed on the top arc with α (pore-forming subunit), while ^{55}Cys of hβ2 is on the bottom arc with β. Black lines represent putative disulfide bonds and dashed lines indicate alternate possibilities. Red X symbolizes a Cys to Ser mutation and an asterisk denotes mutants protected against 100 nM ProTx-II.

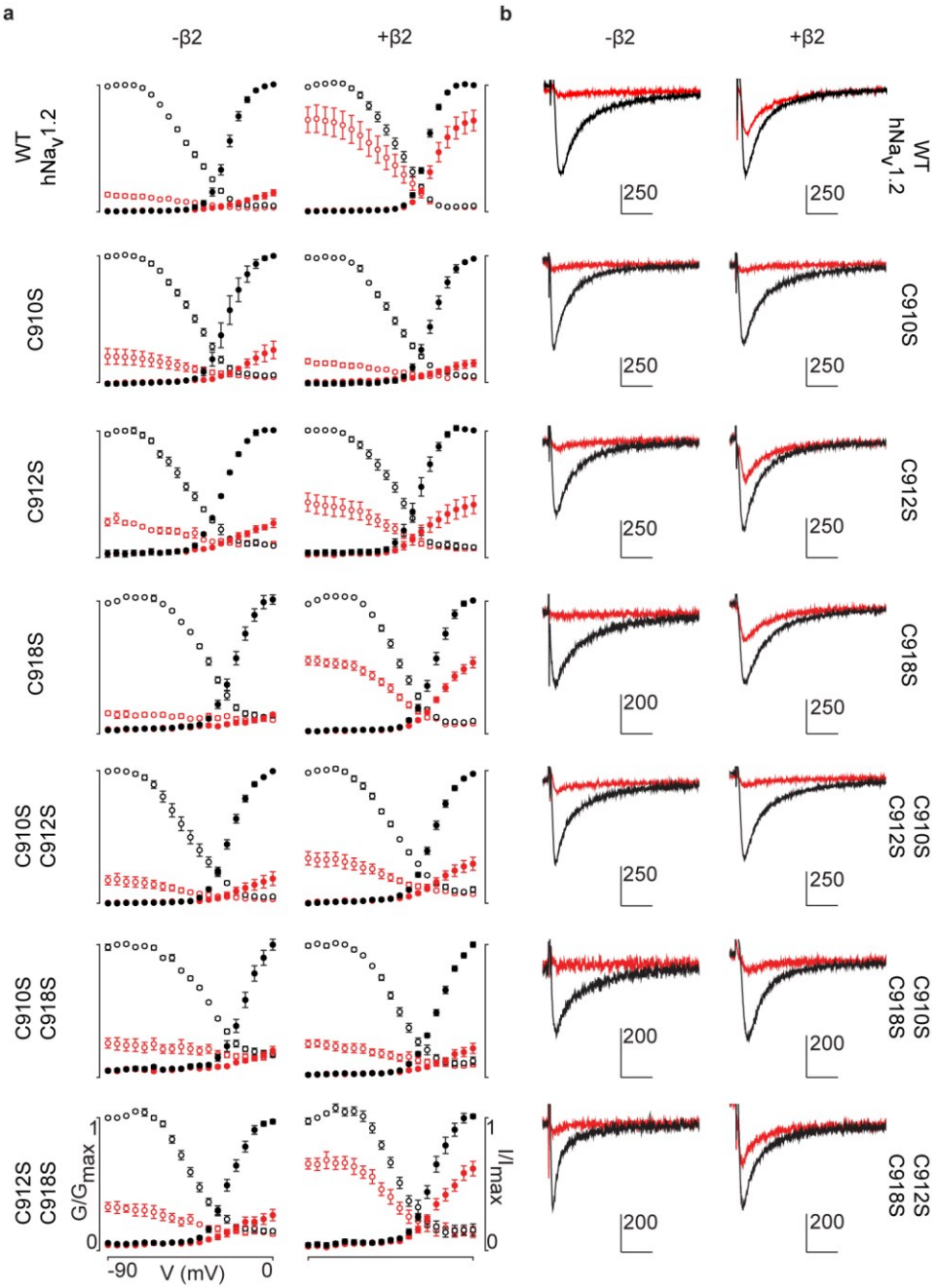

Figure 3-8: G-V and SSI relationships for hNav1.2 mutants. (a) G-V (filled circles) and SSI (open circles) curves are plotted for each of the hNav1.2 Cys to Ser mutants with and without hβ2. Black indicates values before the addition of 100 nM ProTx-II, red shows values after toxin treatment. In the presence of hβ2, the WT hNav1.2, the C918S mutant, and the C912S C918S all show a

diminished susceptibility to ProTx-II whereas the C912S mutant shows a mixed phenotype. (b) Sample traces illustrating the effect of 100 nM ProTx-II on hNav1.2 with and without hβ2 after depolarization to -15 mV from -90 mV. Degree of inhibition reflects the G-V and SSI data shown in (a). Horizontal arm of scale bar is 10 ms and the vertical arm is in nA.

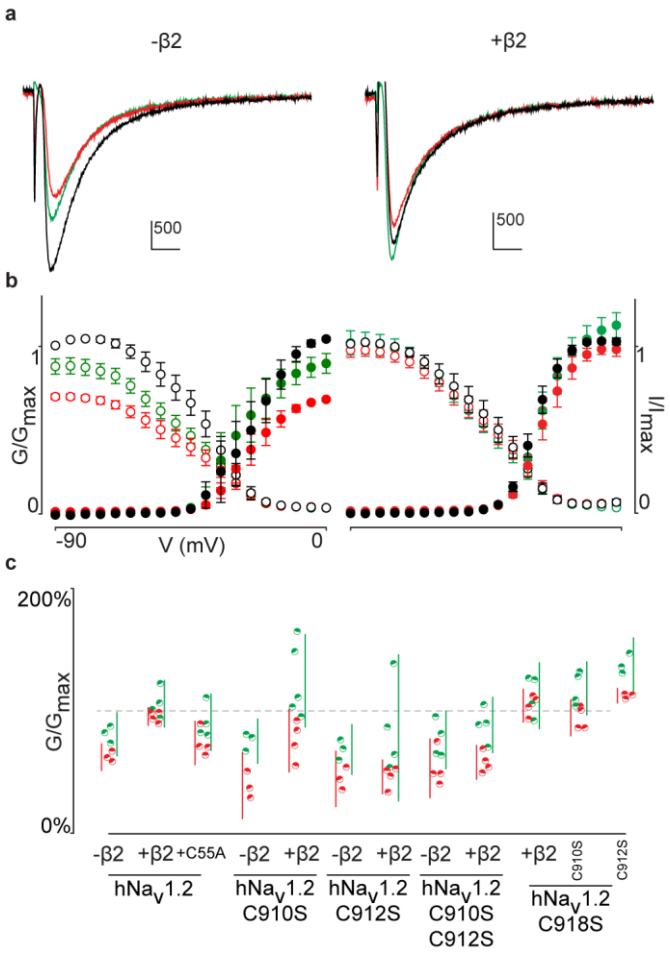

Figure 3-9: Activity of the μO§-conotoxin GVIIJ is affected by hβ2. (a) Representative traces of 5 μM GVIIJ affecting hNav1.2-mediated currents with and without hβ2 in Xenopus oocytes. Control traces are shown in black, red after treatment with 5 μM GVIIJ, and green after a 5-min washout with recording solution. Horizontal bar is 10 ms and vertical bar measures current in nA. The data illustrate that 5 μM GVIIJ can partially block hNav1.2 only when hβ2 is not present. (b) G-V (filled circles) and SSI (open circles) relationships detailing the effect of 5 μM GVIIJ on hNav1.2 with and without hβ2 across a wide voltage range. Color coding is the same as in (a). (c) Dot plot showing the effect of GVIIJ on hNav1.2 Cys to Ser mutants. Red circles indicate fraction of peak control

conductance after addition of 5 μM GVIIJ while green circles represent the same after a 5-min washout. Vertical bars show 95% confidence intervals for color-matched circles. The data clearly illustrate a reduced sensitivity to GVIIJ in the presence of hβ2; however, the results are variable as discussed in the text and led us to pursue ensuing experiments with ProTx-II.

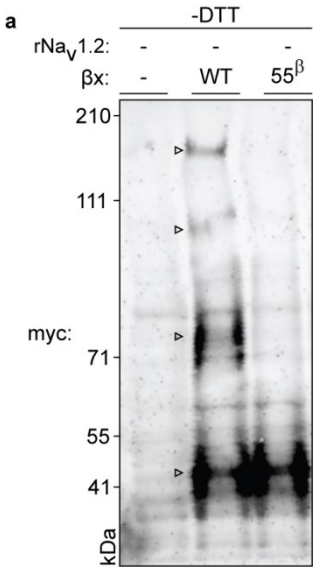

Figure 3-10: Biochemical assessment of rβ2 oligomer formation. Figure represents extended data found in Fig. 3-11. WT myc-tagged rβ2 can form higher-order oligomers under non-reducing conditions (indicated with an open arrow in the middle lane). These oligomers disappear upon removal of ^{55}Cys (right lane), further highlighting the reactivity of this residue. Left lane represents lysate from an uninjected oocyte.

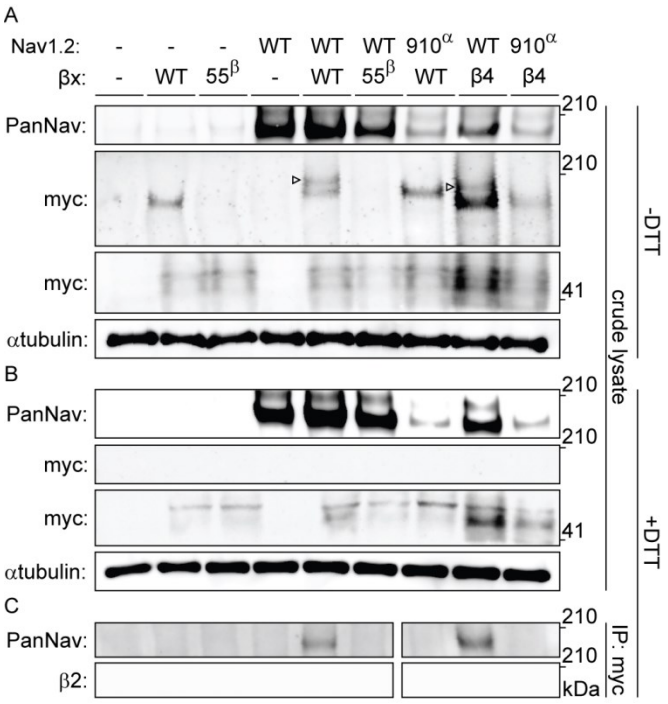

Figure 3-11: Biochemical verification of the β2 and β4 disulfide bond with ^{910}Cys in Nav1.2. Top rows indicate particular Nav channel and β-subunit constructs with which oocytes were injected. WT proteins are indicated as such whereas mutants are noted with a residue number; a superscript letter symbolizes in which partner of the complex pair the mutation is found. rβ2 was loaded in each case except in the two rightmost lanes, where rβ4 was used. Labels on left column indicate which antibody was used to immunoblot the associated slice. (a) Western blot run under non-reducing conditions reveals a fraction of rβ2 migrating with WT rNav1.2a but not after selective cysteine substitution. Crude lysate from injected oocytes was run on a protein gel and probed for both the channel and the myc-tag of the β-subunit. The top PanNav slice and bottom myc slice show the expression of the respective proteins in lysates from oocytes injected with the indicated constructs. Even though equal

quantities of protein was loaded in each lane (10 μg), the C910S channel mutant expresses less bountifully than the WT channel and as a result shows a weaker signal. The WT β-subunit can form redox-sensitive multimers that migrate at an apparent mass similar to that of the Nav channel. Mutation of ^{55}Cys prevents multimer formation and disappearance of the high molecular weight band. Open arrows identify bands representing Nav channel-bound β-subunit and aid in distinguishing them from the multimeric β-subunit. Substituting ^{910}Cys within rNav1.2a with Ser causes a loss of the channel-bound β-subunit band. rβ4 also binds to WT rNav1.2a, as evidenced by a second band, and no longer interacts with the C910S mutant. (b) Addition of DTT prevents both binding of rβ2 to the channel and formation of β-subunit multimers. The absence of myc signal at the same apparent weight as rNav1.2a indicates that binding to the channel is sensitive to reduction. In all cases, α-tubulin was used as a loading control. (c) WT rNav1.2a co-immunoprecipitates with rβ2 and rβ4. The β-subunit was pulled down with an antibody directed against a C-terminal myc-tag and treated with DTT before loading onto the gel. The channel is present only when the WT channel is co-expressed with the WT β-subunit.

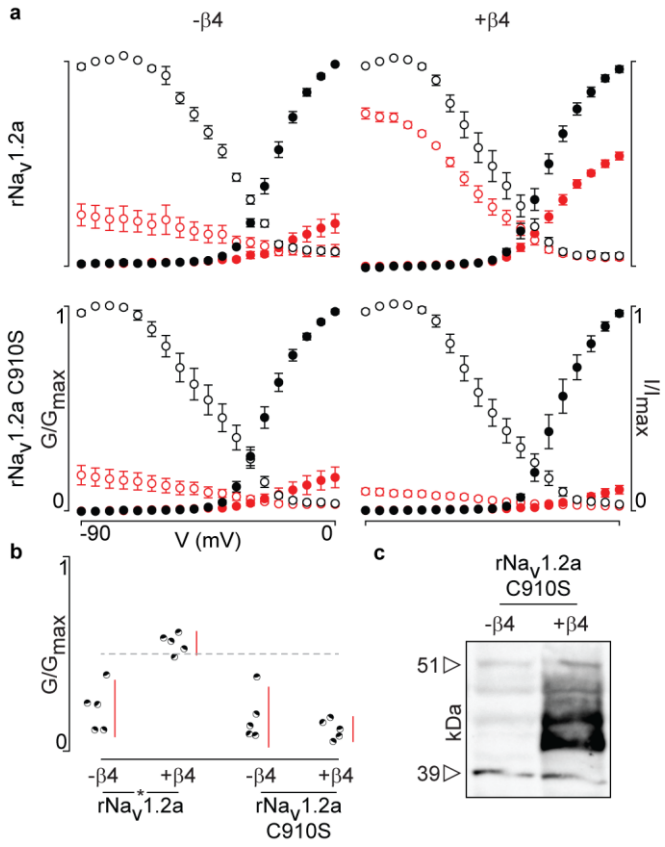

Figure 3-12: Mutation of ^{910}Cys in rNav1.2a disrupts rβ4 influence on ProTx-II effect. (a) Replacement of ^{910}Cys with Ser in rNav1.2a impairs the ability of rβ4 to protect against 100 nM ProTx-II inhibition in a manner similar to that of hβ2. Co-expression of the rNav1.2a isoform with rβ4 minimizes ProTx-II inhibition compared to the channel expressed alone. Graphs compare G-V and SSI relationships, in filled and open circles, respectively. Black color is used for values before the addition of 100 nM ProTx-II and red after. (b) Dot plot comparing the degree of inhibition by 100 nM ProTx-II as a fraction of the pre-toxin peak current. rβ4 confers a high level of a protection against ProTx-II inhibition which is absent in the C910S mutant. (c) Western blot directed against

the C-terminal myc-tag of rβ4 demonstrating its presence in the oocytes measured.

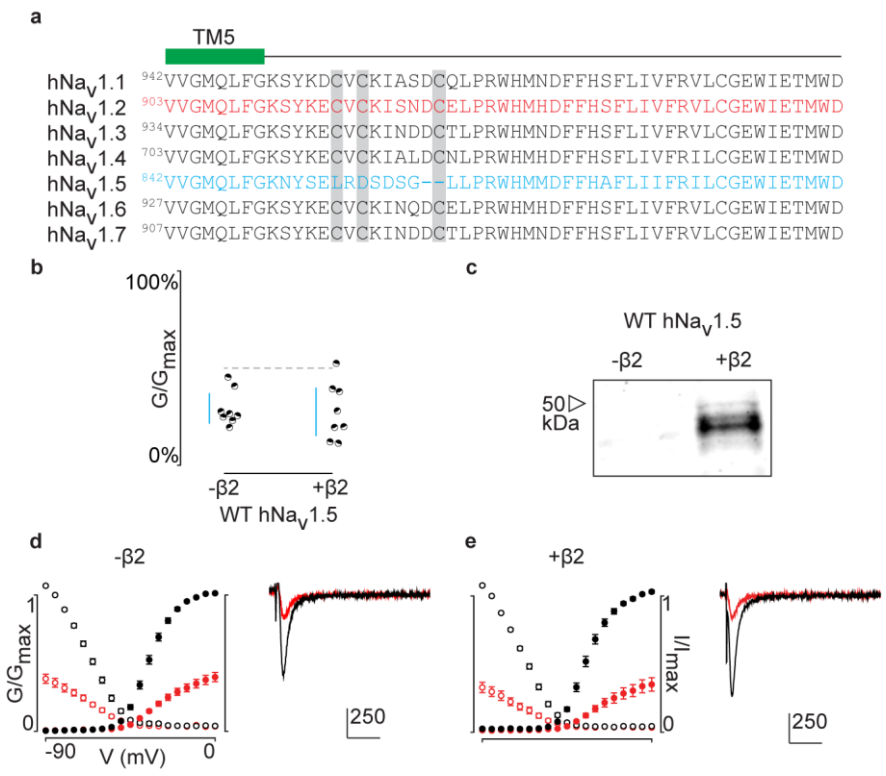

Figure 3-13: ProTx-II inhibits hNav1.5 in the presence of hβ2. (a) Sequence alignment comparing TTX-sensitive hNav channels in the beginning of the S5-S6 (SS1) loop. Green bar indicates the C-terminal portion of the DII transmembrane segment 5 (TM5), and gray background highlights the conserved cysteine triad. The hNav1.2 amino acid sequence is shown in red and hNav1.5 in blue. Residue number of the N-terminal Val for each channel is superscripted. (b) Dot plot showing that hNav1.5 is not protected against inhibition by 100 nM ProTx-II upon co-expressing hβ2. Black circles are individual oocytes of which sodium currents were measured at peak conductance and blue bars show 95% confidence interval. (c) Western blot probing for the C-terminal myc-tag of hβ2 reveals its presence in whole cell oocyte fractions. hNav1.5 sees no change in 100 nM ProTx-II effect in the presence of hβ2. (d, e) G-V (filled circles) and SSI (open

circles) relationships for hNav1.5 with and without hβ2. Black is used for values before ProTx-II addition and red after toxin application. Also shown are representative traces illustrating the lack of effect of hβ2 on hNav1.5 susceptibility to 100 ProTx-II. Horizontal bar indicates 10 ms; vertical bar represents current in nA, with the provided magnitude.

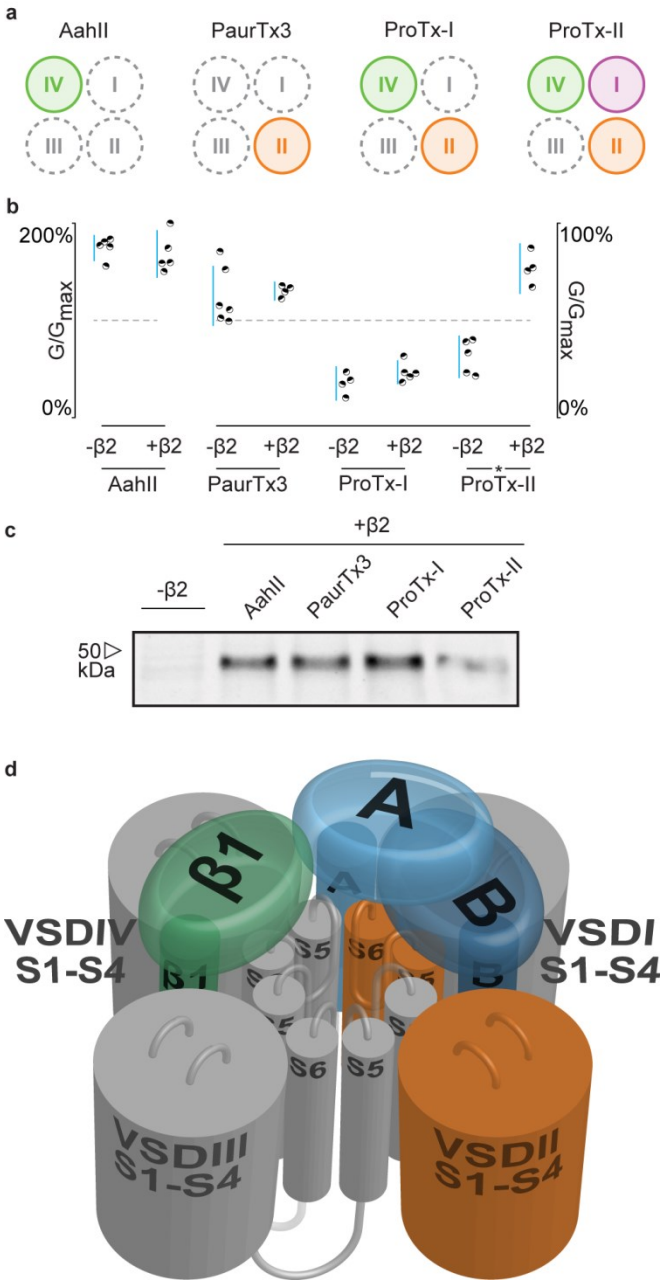

Figure 3-14: hβ2 influences hNav1.2 VSDI toxin pharmacology. (a) Cartoon illustrating the binding site of AaHII, PaurTx3, ProTx-I, and ProTx-II within the VSDs of Nav1.2. Binding to a particular VSD is indicated by coloration. (b) Dot plot showing percent of change in peak conductance for hNav1.2 after treatment by each toxin without or in the presence of hβ2. Blue bars represent 95%

confidence interval and statistical significance ($p < 0.01$) is noted by an asterisk. c) Western blot probing for the C-terminal myc-tag of hβ2, showing its presence in each experimental condition except the negative control. (d) Shown is a Nav channel illustration consisting of the four VSDs I-IV (S1-S4) and the corresponding pore-forming regions (S5-S6) in grey (DI, III, and IV) or orange (DII) in a clockwise orientation which fits with the data reported here. Such an orientation places a S1-S4 voltage sensor of one domain adjacent to the S5-S6 region of the next. A/B (shades of blue) depicts a putative location of hβ2 in the complex where the subunit can interact with the S5-S6 pore region of DII as well as occlude the ProTx-II binding site on VSDI. In contrast, hβ1 (green) may position itself between VSDIV and VSDIII where it can interact with the S5-S6 region of DI and influence VSDIV movement to alter channel fast inactivation.

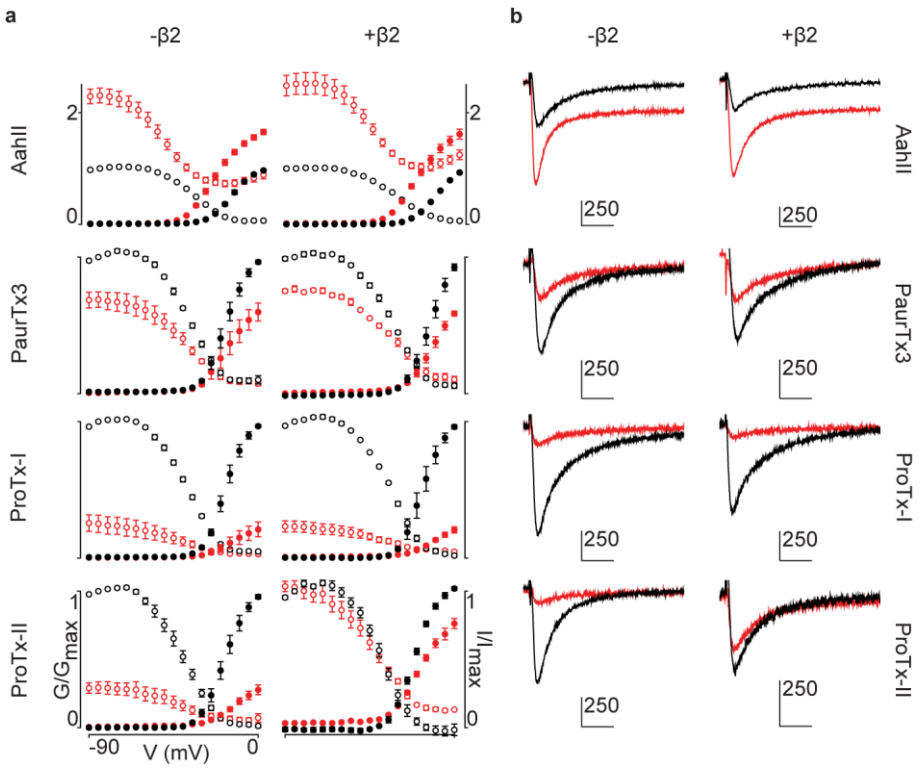

Figure 3-15: Activity of spider and scorpion toxins on hNav1.2. (a) G-V and SSI relationships for hNav1.2, with or without hβ2, treated with toxins (100 nM) with known binding sites. (a) G-V and SSI curves are provided for each of the four toxins tested. Black indicates control values and red illustrates toxin effect. Filled circles are used for G-V curves and open circles for SSI. (b) Representative traces after depolarization to -15 mV from -90 mV for each toxin tested on hNav1.2 with black indicating pre-toxin currents and red showing currents after toxin application. Horizontal scale bar indicates 10 ms whereas vertical bar shows current magnitude in nA, with scale given by the attached number.

Tables

	C55A	C55/72/75A
Data collection		
Space group	$P2_12_12_1$	P 1
Cell dimensions		
a, *b*, *c* (Å)	28.7, 59.4, 71.3	28.4, 36.2, 59.2
α, β, γ (°)	90.0, 90.0, 90.0	89.9, 89.9, 76.4
Resolution (Å)	45.67 –1.35 (1.43-1.35) [a, b]	30.0 -1.85 (1.88-1.85) [a, b]
R_{merge}	7.1 (193.3)	10.0 (32.7)
$CC_{1/2}$ [c]	0.725	0.845
$I / \sigma I$	20.36 (1.81)	14.94 (2.56)
Completeness (%)	99.4 (96.2)	99.0 (90.1)
Redundancy	14.08 (13.8)	3.0 (1.6)
Refinement		
Resolution (Å)	45.67 –1.35	30-1.85
No. reflections	27,539	19,296
R_{work} / R_{free}	16.75/19.25	14.18/19.20
No. atoms		
Protein	2426	A: 1066 B: 1065
Ligand	28	6
Water	174	404
B-factors		
Protein	33.9	A: 16.4 B: 16.5
Ligand	74.5	36.1
Water	42.9	29.8
R.m.s. deviations		
Bond lengths (Å)	0.019	0.007
Bond angles (°)	1.777	0.981

Table 3-1: Data collection and refinement statistics. [a] One crystal for each structure was used for data collection and structure determination. [b] Values in parentheses are for highest-resolution shell. *c* Value is for highest-resolution shell.

			activation		inactivation		peak G_{after}/peak G_{before}
			$V_{1/2}$	V_c	$V_{1/2}$	V_c	
$hNa_V1.2$ WT	-β2	before	-20.2 ± 0.2	5.5 ± 0.1	-37.3 ± 0.8	7.3 ± 0.6	0.17 (0.13, 0.20)
		after	-2.3 ± 3.5	12.2 ± 0.8	-44.1 ± 2.2	13.3 ± 1.3	
	+β2 WT	before	-20.7 ± 0.1	5.5 ± 0.1	-38.0 ± 0.6	8.9 ± 0.6	0.64 (0.50, 0.79)
		after	-17.9 ± 0.6	5.9 ± 0.2	-39.8 ± 1.0	9.3 ± 0.6	
	+β2 C55A	before	-24.0 ± 0.3	5.0 ± 0.1	-36.8 ± 0.8	7.6 ± 0.6	0.19 (0.12, 0.26)
		after	-12.8 ± 2.7	9.1 ± 0.8	-39.9 ± 1.4	9.4 ± 1.0	
	+β2 C55S	before	-24.0 ± 0.5	5.2 ± 0.1	-39.7 ± 0.5	8.4 ± 0.4	0.18 (0.13, 0.22)
		after	-12.6 ± 2.1	9.0 ± 0.7	-43.2 ± 1.3	11.1 ± 1.0	
	+β2 C72A C75A	before	-20.9 ± 0.2	5.3 ± 0.1	-37.7 ± 0.6	8.8 ± 0.5	0.59 (0.47, 0.70)
		after	-18.2 ± 0.6	5.9 ± 0.2	-38.7 ± 0.9	8.9 ± 0.6	

Table 3-2: Table providing values for fits of the data presented in Figure 3-4 and Figure 3-5. G-V and SSI relationship data were fitted by a Boltzmann curve. $V_{1/2}$ provides the midpoint voltage of the calculated curve (in mV) and Vc the unit-less slope, with standard error of the mean (SEM). Right column shows peak conductance after toxin treatment as a fraction of untreated peak conductance with the upper and lower bounds of the 95% confidence interval in parentheses, reflecting the data displayed in the dot plots.

			activation		inactivation		peak G_{after}/peak G_{before}
			$V_{1/2}$	V_c	$V_{1/2}$	V_c	
$hNa_v1.2$ WT	-β2	before	-20.7 ± 0.1	5.5 ± 0.1	-43.9 ± 0.8	9.3 ± 0.6	0.14 (0.05, 0.23)
		after	-6.2 ± 4.9	11.4 ± 1.4	-45.8 ± 1.7	12.7 ± 1.5	
	+β2	before	-21.7 ± 0.2	4.4 ± 0.1	-39.7 ± 1.0	7.8 ± 0.6	0.71 (0.47, 0.94)
		after	-17.8 ± 0.8	5.3 ± 0.3	-39.7 ± 1.3	7.9 ± 0.7	
C910S	-β2	before	-20.7 ± 0.4	6.0 ± 0.2	-41.7 ± 0.5	9.6 ± 0.5	0.16 (0.14, 0.19)
		after	1.3 ± 8.0	12.1 ± 1.4	-46.3 ± 1.2	14.9 ± 0.9	
	+β2	before	-18.3 ± 0.2	6.0 ± 0.1	-41.4 ± 0.7	9.2 ± 0.5	0.17 (0.09, 0.24)
		after	8.9 ± 18.2	19.0 ± 3.3	-44.5 ± 3.2	13.2 ± 2.9	
C912S	-β2	before	-23.8 ± 0.1	6.5 ± 0.1	-43.5 ± 0.7	10.0 ± 0.6	0.26 (0.15, 0.37)
		after	-4.7 ± 10.3	14.3 ± 2.7	-57.2 ± 5.1	16.6 ± 340	
	+β2	before	-26.0 ± 0.5	5.3 ± 0.3	-41.0 ± 0.7	8.92 ± 0.5	0.33 (0.26, 0.39)
		after	-23.3 ± 1.0	7.09 ± 0.5	-43.1 ± 1.0	9.9 ± 0.8	
C918S	-β2	before	-21.2 ± 0.5	5.8 ± 0.3	-36.8 ± 0.9	7.8 ± 0.6	0.17 (0.12, 0.22)
		after	>50	24.6 ± 6.5	-56.8 ± 12.9	16.1 ± 9.8	
	+β2	before	-21.3 ± 0.3	5.3 ± 0.1	-41.1 ± 1.0	6.7 ± 0.6	0.54 (0.43, 0.65)
		after	-17.2 ± 0.7	7.2 ± 0.3	-42.6 ± 0.8	8.7 ± 0.6	
C910S C912S	-β2	before	-22.6 ± 0.3	5.8 ± 0.1	-45.1 ± 0.8	9.1 ± 0.4	0.14 (0.10, 0.18)
		after	-9.2 ± 4.4	11.0 ± 1.0	-53.0 ± 1.9	13.1 ± 1.3	
	+β2	before	-21.7 ± 0.3	6.1 ± 0.2	-42.1 ± 0.5	9.9 ± 0.5	0.32 (0.20, 0.44)
		after	-14.2 ± 3.3	10.6 ± 1.1	-47.2 ± 1.0	13.0 ± 0.7	
C910S C918S	-β2	before	-15.7 ± 0.7	6.1 ± 0.4	-36.1 ± 0.7	10.2 ± 0.7	0.24 (0.11, 0.37)
		after	>50	19.5 ± 7.0	-38.2 ± 3.5	8.0 ± 2.9	
	+β2	before	-18.8 ± 0.3	6.3 ± 0.2	-43.0 ± 0.4	8.3 ± 0.3	0.23 (0.11, 0.36)
		after	-0.23 ± 7.7	14.7 ± 1.6	-47.6 ± 2.6	17.7 ± 2.8	
C912S C918S	-β2	before	-23.5 ± 0.4	5.6 ± 0.2	-43.7 ± 0.8	7.1 ± 0.7	0.23 (0.15, 0.31)
		after	-18.8 ± 2.5	9.4 ± 0.8	-48.0 ± 2.0	10.3 ± 1.5	
	+β2	before	-22.8 ± 0.4	5.3 ± 0.3	-41.9 ± 0.8	6.6 ± 0.7	0.68 (0.60, 0.76)
		after	-17.7 ± 1.9	8.1 ± 0.8	-45.1 ± 0.5	8.3 ± 0.5	

Table 3-3: Table providing values for fits of the data presented in Figure 3-7 and Figure 3-8. G-V and SSI relationship data were fitted by a Boltzmann curve. $V_{1/2}$ provides the midpoint voltage of the calculated curve (in mV) and Vc the unit-less slope, with standard error of the mean (SEM). Right column shows peak conductance after toxin treatment as a fraction of untreated peak

conductance with the upper and lower bounds of the 95% confidence interval in parentheses, reflecting the data displayed in the dot plots.

			activation		inactivation		peak G_{after}/peak G_{before}
			$V_{1/2}$	V_c	$V_{1/2}$	V_c	
$hNa_v1.2$ WT	-β2	before	-30.9 ± 1.0	4.5 ± 0.3	-41.1 ± 1.7	6.7 ± 0.7	0.59 (0.48, 0.71)
		after	-24.1 ± 0.6	5.6 ± 0.2	-44.4 ± 1.1	8.7 ± 0.6	
		recovery	-31.2 ± 1.7	3.8 ± 0.4	-45.2 ± 1.0	8.7 ± 0.5	0.80 (0.61, 0.99)
	+β2	before	-27.5 ± 0.5	4.3 ± 0.2	-44.1 ± 1.1	9.1 ± 0.7	0.95 (0.87, 1.02)
		after	-25.2 ± 0.2	4.5 ± 0.1	-43.9 ± 1.2	9.6 ± 0.9	
		recovery	-25.3 ± 0.6	4.6 ± 0.2	-45.5 ± 1.1	10.4 ± 0.7	1.06 (0.86, 1.27)

Table 3-4: Table providing values for fits of the data presented in Figure 3-9. G-V and SSI relationship data were fitted by a Boltzmann curve. $_{1/2}$ provides the midpoint voltage of the calculated curve (in mV) and Vc the unit-less slope, with standard error of the mean (SEM). Right column shows peak conductance after toxin treatment as a fraction of untreated peak conductance with the upper and lower bounds of the 95% confidence interval in parentheses, reflecting the data displayed in the dot plots.

			activation		inactivation		peak G_{after}/peak G_{before}
			$V_{1/2}$	V_c	$V_{1/2}$	V_c	
$rNa_V1.2a$ WT	-β4	before	-21.2 ± 0.2	6.4 ± 0.2	-39.9 ± 0.6	9.8 ± 0.6	0.22 (0.08, 0.36)
		after	-12.8 ± 0.8	9.4 ± 0.5	-42.4 ± 1.7	11.6 ± 1.7	
	+β4	before	-24.3 ± 0.4	7.3 ± 0.3	-47.6 ± 0.6	10.7 ± 0.6	0.55 (0.49, 0.61)
		after	-21.8 ± 0.3	8.2 ± 0.2	-53.2 ± 0.6	12.1 ± 0.5	
C910S	-β4	before	-23.2 ± 0.3	6.6 ± 0.3	-44.6 ± 0.8	12.1 ± 0.9	0.17 (0.02, 0.32)
		after	-15.5 ± 0.6	9.9 ± 0.4	-47.5 ± 1.4	14.6 ± 1.6	
	+β4	before	-20.9 ± 0.4	6.5 ± 0.4	-47.1 ± 0.7	11.4 ± 0.7	0.11 (0.05, 0.17)
		after	-7.9 ± 1.1	10.4 ± 0.5	-49.9 ± 1.0	13.6 ± 1.0	

Table 3-5: Table providing values for fits of the data presented in Figure 3-12. G-V and SSI relationship data were fitted by a Boltzmann curve. $V_{1/2}$ provides the midpoint voltage of the calculated curve (in mV) and Vc the unit-less slope, with standard error of the mean (SEM). Right column shows peak conductance after toxin treatment as a fraction of untreated peak conductance with the upper and lower bounds of the 95% confidence interval in parentheses, reflecting the data displayed in the dot plots.

			activation		inactivation		peak G_{after}/peak G_{before}
			$V_{1/2}$	V_c	$V_{1/2}$	V_c	
$hNa_v1.5$ WT	-β2	before	-35.6 ± 0.4	5.9 ± 0.2	-67.8 ± 0.7	7.7 ± 0.4	0.29 (0.22, 0.37)
		after	-31.1 ± 0.8	7.3 ± 0.4	-65.0 ± 1.3	6.8 ± 0.8	
	+β2	before	-35.2 ± 0.5	5.9 ± 0.2	-70.3 ± 0.7	7.6 ± 0.4	0.28 (0.15, 0.39)
		after	-28.5 ± 1.1	7.9 ± 0.5	-71.3 ± 1.4	8. 3 ± 0.8	

Table 3-6: Table providing values for fits of the data presented in Figure 3-13. G-V and SSI relationship data were fitted by a Boltzmann curve. $V_{1/2}$ provides the midpoint voltage of the calculated curve (in mV) and Vc the unit-less slope, with standard error of the mean (SEM). Right column shows peak conductance after toxin treatment as a fraction of untreated peak conductance with the upper and lower bounds of the 95% confidence interval in parentheses, reflecting the data displayed in the dot plots.

			activation		inactivation		peak G_{after}/peak G_{before}
			$V_{1/2}$	V_c	$V_{1/2}$	V_c	
AahII	-β2	before	-16.1 ± 0.2	5.5 ± 0.1	-36.5 ± 0.7	7.1 ± 0.6	1.74 (1.61, 1.88)
		after	-24.7 ± 0.6	6.4 ± 0.2	-52.0 ± 1.2	6.7 ± 0.9	
	+β2	before	-11.8 ± 0.3	5.8 ± 0.1	-33.8 ± 0.3	9.7 ± 0.3	1.68 (1.44, 1.93)
		after	-23.1 ± 0.6	5.8 ± 0.2	-46.7 ± 1.3	5.8 ± 1.0	
PaurTx3	-β2	before	-16.0 ± 0.3	5.7 ± 0.1	-37.1 ± 0.7	7.3 ± 0.7	0.63 (0.47, 0.78)
		after	-15.7 ± 1.7	6.2 ± 0.5	-38.6 ± 0.5	8.3 ± 0.4	
	+β2	before	-12.2 ± 0.4	6.1 ± 0.2	-32.9 ± 0.6	8.8 ± 0.6	0.65 (0.60, 0.70)
		after	-7.3 ± 2.9	8.2 ± 0.7	-34.7 ± 0.8	11.5 ± 0.7	
ProTx-I	-β2	before	-16.6 ± 0.4	5.0 ± 0.1	-38.1 ± 0.7	7.4 ± 0.6	0.17 (0.09, 0.26)
		after	-9.2 ± 3.0	7.8 ± 0.7	-42.2 ± 1.1	9.0 ± 0.6	
	+β2	before	-15.6 ± 0.6	5.1 ± 0.2	-34.2 ± 0.7	8.5 ± 0.5	0.23 (0.17, 0.30)
		after	-0.6 ± 7.2	9.3 ± 1.2	-39.2 ± 1.1	10.7 ± 0.9	
ProTx-II	-β2	before	-17.3 ± 0.5	5.4 ± 0.2	-39.3 ± 1.0	7.1 ± 0.6	0.31 (0.20, 0.42)
		after	-9.3 ± 2.5	8.5 ± 0.7	-42.2 ± 0.7	9.6 ± 0.6	
	+β2	before	-21.4 ± 0.3	5.5 ± 0.2	-37.8 ± 1.1	6.8 ± 0.9	0.77 (0.64, 0.90)
		after	-18.9 ± 0.6	6.7 ± 0.3	-42.0 ± 1.0	8.8 ± 0.6	

Table 3-7: Table providing values for fits of the data presented in Figure 3-14 and Figure 3-15. G-V and SSI relationship data were fitted by a Boltzmann curve. $V_{1/2}$ provides the midpoint voltage of the calculated curve (in mV) and Vc the unit-less slope, with standard error of the mean (SEM). Right column shows peak conductance after toxin treatment as a fraction of untreated peak conductance with the upper and lower bounds of the 95% confidence interval in parentheses, reflecting the data displayed in the dot plots.

ARCHITECTURE OF THE BETA2/BETA4-NAV CHANNEL SIGNALING COMPLEX

Chapter 4: Conclusion

Summary of findings

The findings reported here pave the way for a better appreciation of Nav channel/β-subunit interaction and the functional consequences underlying their mutations. Through the tireless efforts of our collaborators, Samir Das and Filip Van Petegem, our group solved the crystal structures of the β2 and β4 subunits and, combined with knowledge of animal toxins, we were able to generate novel architectural insights into Nav channel/β-subunit interaction. The conclusions drawn from our work should provide a greater sense of context in which subsequent investigations can be pursued.

β-subunits affect toxin pharmacology

Supporting prior suggestions [172, 213, 258], we demonstrated that β-subunits can affect the toxin pharmacology of the Nav channel. We screened seven animal toxins (ProTx-I, ProTx-II, AaHII, TsVII, LqqIV, ATX-II, and β-PMTX) on the Nav1.2 channel co-expressed with each of the four β-subunits to evaluate the effects the β-subunit may have on toxin binding. We discovered that several of the β-subunits were able to affect toxin behavior. For example, the β1 subunit causes the α-scorpion toxin LqqIV to induce a depolarizing, leftward shift in the steady-state inactivation (SSI) curve whereas normally it would generate a hyperpolarizing, rightward shift. While the β-scorpion toxin TsVII normally evokes a hyperpolarizing shift in the conductance-voltage (G-V) curve and leaves maximal conductance unaffected, co-expression of the β4 subunit now causes a substantial decrease in maximal conductance in addition to the hyperpolarizing

shift. Most interesting to us was the discovery that both β2 and β4 could diminish Nav1.2 sensitivity to ProTx-II inhibition, a relationship we later exploited to determine both Cys residues involved in forming the disulfide bridge between Nav channel and β-subunit [260, 278].

Beyond the obvious outcome of providing us with novel tools to study β-subunits, this finding brings to light a new means by which the β-subunit may influence the Nav channel; e.g. the possibility that β-subunits could complicate future applications of toxins as therapeutics. Several toxins derived from animal venom have found clinical use [279, 280], but it remains to be seen whether β-subunits could play an antagonistic role, lowering efficacy by blocking their binding sites [259]. Alternatively, toxins could be used to displace mutant β-subunits from the channel that could create disease states.

Lastly, this discovery shows that we must take care when testing toxins on Nav channels in the presence of β-subunits. It is possible that a β-subunit could generate a unique phenotype *a la* TsVII with β4 that would spuriously suggest a unique effect of the toxin on a Nav channel isoform. Alternatively, β-subunits could diminish the sensitivity of the Nav channel to a toxin, erroneously reporting a lower affinity for the toxin than is actually the case. Even greater care must be taken when testing toxins in native tissue, where β-subunit expression may be uncertain and could drastically alter the outcome of experiments if the researchers were caught unaware.

β2 and β4 bind to the Nav1.2 channel through ^{55}Cys and ^{58}Cys, respectively

Harnessing the unique ability of β2 and β4 to diminish ProTx-II inhibition of the Nav channel, we were able to identify the Cys residues of the β-subunit responsible for binding to Nav1.2. Initial experiments with DTT incubation revealed the link between β4 and Nav1.2 was sensitive to reduction and likely mediated through a disulfide interaction. Having observed in crystal structures the free cysteines ^{55}Cys and ^{58}Cys of β2 and β4, respectively, we mutated each to Ala (and Ser, in the case of ^{55}Cys) and witnessed a dramatic loss of protection against ProTx-II. To verify that the disappearance of the β-subunit functional effect was not due to a disappearance of the β-subunit entirely, we verified that the C55A β2 and C58A β4 were both expressed and trafficked to the surface normally, but were otherwise unable to protect the channel against ProTx-II. We used a range of toxin concentrations to determine the IC50 of ProTx-II and saw that while the presence of WT β4 reduced affinity to the channel 5-fold, introduction of the C55A mutation restored toxin sensitivity of the Nav channel to a degree indistinguishable from that of the Nav channel expressed alone.

These results, examined in conjunction with β-subunit crystal structures, allow us to better assess the effect of disease-related β-subunit mutations on binding. For example, compromising the disulfide bond between Nav1.1 and β2 has been shown to affect Nav complex targeting to nodes of Ranvier [144]. By examining how mutations change the local structure of the reactive cysteine, we derive an idea of how they might impact binding of the β-subunit with the Nav channel. In addition, subsequent investigations into the functional interface

between Nav channels and β2/β4 will be better able to orient the two proteins and observe how mutations might perturb the structural conformation. A preliminary depiction of this interaction is shown in Figure 4-1.

Nav1.2 binds to β2 and β4 through ^{910}Cys

Once we had identified the Cys residues of the β-subunits responsible for the disulfide bond with the Nav channel, we then took the next step of locating the corresponding Cys on the Nav channel. Employing the same ProTx-II-based assay used to find the β-subunit cysteine, we mutated a number of extracellular Cys residues of the Nav channel to Ser, targeting the DII S5-S6 region [144, 267]. In doing so, we discovered that the DII S5-S6 C910S mutant of Nav1.2 erased the capacity for β2 and β4 to protect the Nav1.2 against ProTx-II inhibition. To confirm this finding biochemically, we used Western blotting to demonstrate that the WT β2 and β4 subunits co-migrated with the WT Nav1.2 channel. Further, we showed that mutations of the identified cysteines on the β-subunit or the Nav channel prevented this co-migration. We then found that only with WT forms of the proteins could we co-immunoprecipitate the Nav channel with the β-subunit, providing further evidence of the interaction between those residues.

Having established ^{910}Cys as the Nav1.2 site for β-subunit binding, we used several toxins with known binding sites (AaHII DIV, PaurTx3 DII, ProTx-I DII and DIV, ProTx-II DI, DII, and DIV) [31] to see if their effect was impacted by the

presence of the β2 subunit. In fact, only ProTx-II was affected, which would suggest a binding site for the β2 subunit adjacent to VSDI. This is consistent with the domain-swap architecture of the channel that would place the DII S5-S6 adjacent to the DI voltage sensor.

These results suggest a shared binding site for β2 and β4 at ^{910}Cys of Nav1.2, which has a number of implications for β-subunit physiology. Mutations near the ^{910}Cys site could affect binding to the β-subunit and might be a causative disease mechanism for some Nav channel mutations in that region [2]. If the two subunits do, in fact, share a binding site, it would suggest that only one can be bound to the channel at a time, providing insight into β-subunit stoichiometry. Given that β2 KO mice are viable while the β4 KO is embryonically lethal, it would seem that their roles in health must either be exerted distant to the binding site or else are mediated elsewhere in the body. Additionally, this site is distinct from that suggested for β1, with the latter being located between DIII and DIV, based upon cross-linking studies showing an interaction with the DI and DIV pore loops [150, 151]. This is consistent with prior studies suggesting that both β1 and β2 can be simultaneously bound to the channel [9], and raises the question of why the body has expressed each β-subunit where it does. As the roles of β2 and β4 continue to be resolved, the idea of mutual exclusion at VSDI may prove useful in untangling their separate contributions to human physiology.

Avenues to study β-subunit disease mutations

Previous investigations into the pathogenesis of β-subunit-related diseases had no recourse to structural knowledge but with the results of this work we are able to begin making strides into understanding the multidimensional consequences of mutations in the β-subunit. The first identified β-subunit disease mutant was C121W in β1, which leads to a form of epilepsy, generalized epilepsy febrile seizures plus (GEFS+) [188]. Despite linking this mutation to a disease, there is not yet a consensus on the mechanism [221-223]. We generated the corresponding mutant in β4, C131W, and found that a disulfide bond in the protein core was disrupted, thus destabilizing the β-subunit structure. In particular, we discovered that the local conformation surrounding the bridge-forming ^{58}Cys was altered and may have affected binding to the channel, explaining the loss of protection conferred by β4 against ProTx-II inhibition.

Although we examined only a single mutant, we were able to map many more β1 mutations onto the β4 structure and the possibility exists that a similar approach could be used to determine their pathogenic mechanism. However, as three of the four β subunit structures have been solved already [146, 260, 278], it is only a matter of time before the β1 structure is too. With structures in hand, we have the ability to directly observe how mutations may yield structural perturbations and through co-expression with the Nav channel, how these changes generate functional consequences.

Future directions

Although we have identified the residues involved in formation of the disulfide bridge linking Nav1.2 to the β2 and β4 subunits, a great deal more work remains. A toxin assay suggested that the β2 and β4 subunits sit adjacent to the VSDI of Nav1.2 but with our available repertoire of toxins we were unable to determine if the β-subunit rested between DIV and DI or DI and DII. Knowing the exact site would allow us to better understand the functional interface between β-subunit and Nav channel, and to appreciate the pathogenesis of β-subunit mutants. Additionally, the results from this work suggest that toxins could also be used to determine the specific binding site of β1 and β3. The former is believed to sit between DIII and DIV, near the pore domains of both DI and DIV, suggesting that it may share an overlapping binding site with DIV-specific toxins [151]. Furthermore, a similar screen could be employed on the Nav channel co-expressed with β3 in order to determine if the β-subunit shares a binding site with any toxins.

Prior research had indicated that the β-subunit is glycosylated [142, 220] and here we showed that mutating individual Asn residues to Gln could change the glycosylation pattern of β4. Before subsequent investigations into the role of β-subunit glycosylation can take place the nature of glycosylation in heterologous systems must first be reconciled. Glycosylation machinery is known to vary between organisms [281-283] and so first experiments must determine if the *Xenopus* system is suitable for exploring mammalian β-subunit isoforms. Once a

system is established, the logical steps following would involve determination of the extent and composition of N-linked glycosylation at each identified site and the effect of its removal on β-subunit folding and Nav biophysics.

Ultimately, the results presented in this work represent a substantial advance in our understanding of the Nav channel/β-subunit interaction and demonstrate the capable application of a number of research techniques, from molecular biology to electrophysiology to biochemistry. Most importantly, they represent several years under the tutelage of Dr. Frank Bosmans and the cultivation of a critical mind.

Figures

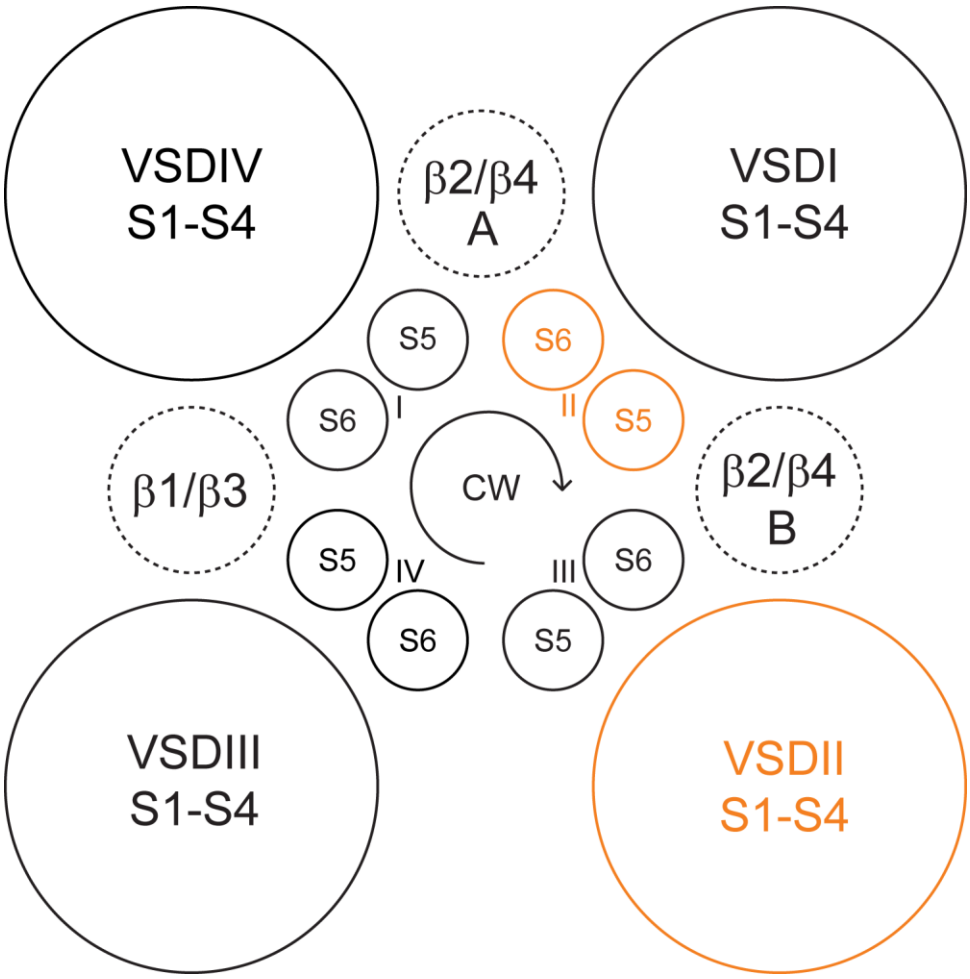

Figure 4-1: Potential location of β-subunits within the Nav channel signaling complex. Potential sites for β2 and β4 indicated by A and B adjacent to VSDI as indicated by toxin screen shown in Figure 3-14. DII highlighted in orange to show S5-S6 pore loop. Presumed location of β1 and β3 indicated between VSDIII and VSDIV.

References

1. Catterall, W.A., *Voltage-gated sodium channels at 60: Structure, function and pathophysiology.* Journal of Physiology, 2012. **590**(11): p. 2577-2589.
2. Claes, L.R.F., et al., *The SCN1A variant database: A novel research and diagnostic tool.* Human Mutation, 2009. **30-10**: p. E904-E920.
3. Dichgans, M., et al., *Mutation in the neuronal voltage-gated sodium channel SCN1A in familial hemiplegic migraine.* The Lancet, 2005. **366**(9483): p. 371-377.
4. Kapplinger, J.D., et al., *An international compendium of mutations in the SCN5A-encoded cardiac sodium channel in patients referred for Brugada syndrome genetic testing.* Heart Rhythm, 2010. **7**(1): p. 33-46.
5. Wang, Q., et al., *Cardiac sodium channel mutations in patients with long QT syndrome, an inherited cardiac arrhythmia.* Human molecular genetics, 1995. **4**(9): p. 1603-1607.
6. Fertleman, C.R., et al., *SCN9A mutations in paroxysmal extreme pain disorder: allelic variants underlie distinct channel defects and phenotypes.* Neuron, 2006. **52**(5): p. 767-774.
7. Drenth, J.P. and S.G. Waxman, *Mutations in sodium-channel gene SCN9A cause a spectrum of human genetic pain disorders.* The Journal of clinical investigation, 2007. **117**(12): p. 3603-3609.
8. Brackenbury, W.J. and L.L. Isom, *Na+ channel β subunits: Overachievers of the ion channel family.* Frontiers in Pharmacology, 2011. **SEP**.

9. Calhoun, J.D. and L.L. Isom, *The role of non-pore-forming b subunits in physiology and pathophysiology of voltage-gated sodium channels*, in *Handbook of Experimental Pharmacology*. 2014. p. 51-89.

10. Isom, L.L., *Sodium channel β subunits: Anything but auxiliary.* Neuroscientist, 2001. **7**(1): p. 42-54.

11. Abriel, H. and R.S. Kass, *Regulation of the voltage-gated cardiac sodium channel Nav1.5 by interacting proteins.* Trends in Cardiovascular Medicine, 2005. **15**(1): p. 35-40.

12. Hille, B., *Ion channels of excitable membranes*. Vol. 507. 2001: Sinauer Sunderland, MA.

13. Favre, I., E. Moczydlowski, and L. Schild, *On the structural basis for ionic selectivity among Na+, K+, and Ca2+ in the voltage-gated sodium channel.* Biophysical Journal, 1996. **71**(6): p. 3110-3125.

14. Sun, Y.M., et al., *On the structural basis for size-selective permeation of organic cations through the voltage-gated sodium channel: Effect of alanine mutations at the DEKA locus on selectivity, inhibition by Ca2+ and H+, and molecular sieving.* Journal of General Physiology, 1997. **110**(6): p. 693-715.

15. Huang, C.J., I. Favre, and E. Moczydlowski, *Permeation of large tetra-alkylammonium cations through mutant and wild- type voltage-gated sodium channels as revealed by relief of block at high voltage.* Journal of General Physiology, 2000. **115**(4): p. 435-453.

16. Payandeh, J., et al., *The crystal structure of a voltage-gated sodium channel.* Nature, 2011. **475**(7356): p. 353-359.

17. Zhang, X., et al., *Crystal structure of an orthologue of the NaChBac voltage-gated sodium channel.* Nature, 2012. **486**(7401): p. 130-134.

18. Kontis, K.J., A. Rounaghi, and A.L. Goldin, *Sodium channel activation gating is affected by substitutions of voltage sensor positive charges in all four domains.* Journal of General Physiology, 1997. **110**(4): p. 391-401.

19. Yarov-Yarovoy, V., et al., *Structural basis for gating charge movement in the voltage sensor of a sodium channel.* Proceedings of the National Academy of Sciences of the United States of America, 2012. **109**(2).

20. Catterall, W.A., *From ionic currents to molecular mechanisms: The structure and function of voltage-gated sodium channels.* Neuron, 2000. **26**(1): p. 13-25.

21. Hartshorne, R.P. and W.A. Catterall, *The sodium channel from rat brain. Purification and subunit composition.* Journal of Biological Chemistry, 1984. **259**(3): p. 1667-1675.

22. Hartshorne, R.P., et al., *The saxitoxin receptor of the sodium channel from rat brain. Evidence for two nonidentical β subunits.* Journal of Biological Chemistry, 1982. **257**(23): p. 13888-13895.

23. Waechter, C.J., J.W. Schmidt, and W.A. Catterall, *Glycosylation is required for maintenance of functional sodium channels in neuroblastoma cells.* Journal of Biological Chemistry, 1983. **258**(8): p. 5117-5123.

24. Catterall, W.A., A.L. Goldin, and S.G. Waxman, *International Union of Pharmacology. XLVII. Nomenclature and structure-function relationships of voltage-gated sodium channels.* Pharmacological Reviews, 2005. **57**(4): p. 397-409.

25. Agnew, W.S., et al., *Purification of the tetrodotoxin-binding component associated with the voltage-sensitive sodium channel from Electrophorus electricus electroplax membranes.* Proceedings of the National Academy of Sciences of the United States of America, 1978. **75**(6): p. 2606-2610.

26. Hille, B., *The receptor for tetrodotoxin and saxitoxin: a structural hypothesis.* Biophysical Journal, 1975. **15**(6): p. 615-619.

27. Gellens, M.E., et al., *Primary structure and functional expression of the human cardiac tetrodotoxin-insensitive voltage-dependent sodium channel.* Proceedings of the National Academy of Sciences, 1992. **89**(2): p. 554-558.

28. Tate, S., et al., *Two sodium channels contribute to the TTX-R sodium current in primary sensory neurons.* Nature neuroscience, 1998. **1**(8): p. 653-655.

29. Frank, H.Y. and W.A. Catterall, *Overview of the voltage-gated sodium channel family.* Genome biology, 2003. **4**(3): p. 207.

30. Ulbricht, W., *Sodium channel inactivation: molecular determinants and modulation.* Physiological reviews, 2005. **85**(4): p. 1271-1301.

31. Bosmans, F., M.F. Martin-Eauclaire, and K.J. Swartz, *Deconstructing voltage sensor function and pharmacology in sodium channels.* Nature, 2008. **456**(7219): p. 202-208.

32. Capes, D.L., et al., *Domain IV voltage-sensor movement is both sufficient and rate limiting for fast inactivation in sodium channels.* Journal of General Physiology, 2013. **142**(2): p. 101-112.

33. Chanda, B. and F. Bezanilla, *Tracking voltage-dependent conformational changes in skeletal muscle sodium channel during activation.* Journal of General Physiology, 2002. **120**(5): p. 629-645.

34. Horn, R., S. Ding, and H.J. Gruber, *Immobilizing the moving parts of voltage-gated ion channels.* Journal of General Physiology, 2000. **116**(3): p. 461-475.

35. Sheets, M.F., et al., *The Na channel voltage sensor associated with inactivation is localized to the external charged residues of domain IV, S4.* Biophysical Journal, 1999. **77**(2): p. 747-757.

36. Kühn, F.J. and N.G. Greeff, *Movement of voltage sensor S4 in domain 4 is tightly coupled to sodium channel fast inactivation and gating charge immobilization.* The Journal of general physiology, 1999. **114**(2): p. 167-184.

37. Stühmer, W., et al., *Structural parts involved in activation and inactivation of the sodium channel.* Nature, 1989. **339**(6226): p. 597-603.

38. Vassilev, P., T. Scheuer, and W.A. Catterall, *Inhibition of inactivation of single sodium channels by a site-directed antibody.* Proceedings of the

National Academy of Sciences of the United States of America, 1989. **86**(20): p. 8147-8151.

39. West, J.W., et al., *A cluster of Hydrophobic amino acid residues required for fast Na+-channel inactivation.* Proceedings of the National Academy of Sciences of the United States of America, 1992. **89**(22): p. 10910-10914.
40. Cha, A., et al., *Voltage sensors in domains III and IV, but not I and II, are immobilized by Na+ channel fast inactivation.* Neuron, 1999. **22**(1): p. 73-87.
41. Eaholtz, G., T. Scheuer, and W.A. Catterall, *Restoration of inactivation and block of open sodium channels by an inactivation gate peptide.* Neuron, 1994. **12**(5): p. 1041-1048.
42. Kuo, C.C. and B.P. Bean, *Na+ channels must deactivate to recover from inactivation.* Neuron, 1994. **12**(4): p. 819-829.
43. Long, S.B., E.B. Campbell, and R. MacKinnon, *Crystal structure of a mammalian voltage-dependent Shaker family K + channel.* Science, 2005. **309**(5736): p. 897-903.
44. Jiang, Y., et al., *X-ray structure of a voltage-dependent K+ channel.* Nature, 2003. **423**(6935): p. 33-41.
45. Payandeh, J., et al., *Crystal structure of a voltage-gated sodium channel in two potentially inactivated states.* Nature, 2012. **486**(7401): p. 135-139.
46. Shaya, D., et al., *Structure of a prokaryotic sodium channel pore reveals essential gating elements and an outer ion binding site common to*

eukaryotic channels. Journal of Molecular Biology, 2014. **426**(2): p. 467-483.

47. Shen, H., et al., *Structure of a eukaryotic voltage-gated sodium channel at near-atomic resolution.* Science, 2017. **355**(6328): p. eaal4326.
48. Long, S.B., et al., *Atomic structure of a voltage-dependent K+ channel in a lipid membrane-like environment.* Nature, 2007. **450**(7168): p. 376-382.
49. Cohen, L., et al., *Design of a specific activator for skeletal muscle sodium channels uncovers channel architecture?* Journal of Biological Chemistry, 2007. **282**(40): p. 29424-29430.
50. Hodgkin, A. and A. Huxley, *The components of membrane conductance in the giant axon of Loligo.* The Journal of physiology, 1952. **116**(4): p. 473-496.
51. Payandeh, J. and D.L. Minor, *Bacterial voltage-gated sodium channels (BacNa<inf>V</inf>s) from the soil, sea, and salt lakes enlighten molecular mechanisms of electrical signaling and pharmacology in the brain and heart.* Journal of Molecular Biology, 2015. **427**(1): p. 3-30.
52. Kink, J.A., et al., *Mutations in paramecium calmodulin indicate functional differences between the C-terminal and N-terminal lobes in vivo.* Cell, 1990. **62**(1): p. 165-174.
53. Liu, C.-j., et al., *Direct interaction with contactin targets voltage-gated sodium channel Nav1. 9/NaN to the cell membrane.* Journal of Biological Chemistry, 2001. **276**(49): p. 46553-46561.

54. Shirahata, E., et al., *Ankyrin-G regulates inactivation gating of the neuronal sodium channel, Nav1. 6.* Journal of neurophysiology, 2006. **96**(3): p. 1347-1357.

55. Nakatani, T., et al., *In vivo genetic evidence for klotho-dependent, fibroblast growth factor 23 (Fgf23)-mediated regulation of systemic phosphate homeostasis.* The FASEB Journal, 2009. **23**(2): p. 433-441.

56. Thimmapaya, R., et al., *Distribution and functional characterization of human Nav1. 3 splice variants.* European Journal of Neuroscience, 2005. **22**(1): p. 1-9.

57. Gong, B., et al., *Type I and type II Na+ channel α-subunit polypeptides exhibit distinct spatial and temporal patterning, and association with auxiliary subunits in rat brain.* Journal of Comparative Neurology, 1999. **412**(2): p. 342-352.

58. Beckh, S., et al., *Differential regulation of three sodium channel messenger RNAs in the rat central nervous system during development.* The EMBO journal, 1989. **8**(12): p. 3611.

59. Plummer, N.W., M.W. McBurney, and M.H. Meisler, *Alternative splicing of the sodium channel SCN8A predicts a truncated two-domain protein in fetal brain and non-neuronal cells.* Journal of Biological Chemistry, 1997. **272**(38): p. 24008-24015.

60. Osteen, J.D., et al., *Selective spider toxins reveal a role for the Nav1. 1 channel in mechanical pain.* Nature, 2016. **534**(7608): p. 494-499.

61. Schaller, K.L., et al., *A novel, abundant sodium channel expressed in neurons and glia.* Journal of Neuroscience, 1995. **15**(5): p. 3231-3242.

62. Whitaker, W.R., et al., *Distribution of voltage-gated sodium channel α-subunit and β-subunit mRNAs in human hippocampal formation, cortex, and cerebellum.* Journal of Comparative Neurology, 2000. **422**(1): p. 123-139.

63. Tzoumaka, E., et al., *Differential distribution of the tetrodotoxin-sensitive rPN4/NaCh6/Scn8a sodium channel in the nervous system.* Journal of neuroscience research, 2000. **60**(1): p. 37-44.

64. Raman, I.M., et al., *Altered subthreshold sodium currents and disrupted firing patterns in Purkinje neurons of Scn8a mutant mice.* Neuron, 1997. **19**(4): p. 881-891.

65. Barchi, R.L., *Protein components of the purified sodium channel from rat skeletal muscle sarcolemma.* Journal of neurochemistry, 1983. **40**(5): p. 1377-1385.

66. Trimmer, J.S., et al., *Primary structure and functional expression of a mammalian skeletal muscle sodium channel.* Neuron, 1989. **3**(1): p. 33-49.

67. White, M.M., et al., *SkM2, a Na+ channel cDNA clone from denervated skeletal muscle, encodes a tetrodotoxin-insensitive Na+ channel.* Molecular pharmacology, 1991. **39**(5): p. 604-608.

68. Sangameswaran, L., et al., *A novel tetrodotoxin-sensitive, voltage-gated sodium channel expressed in rat and human dorsal root ganglia.* Journal of Biological Chemistry, 1997. **272**(23): p. 14805-14809.

69. Akopian, A.N., L. Sivilotti, and J.N. Wood, *A tetrodotoxin-resistant voltage-gated sodium channel expressed by sensory neurons.* Nature, 1996. **379**(6562): p. 257.

70. Dib-Hajj, S., et al., *NaN, a novel voltage-gated Na channel, is expressed preferentially in peripheral sensory neurons and down-regulated after axotomy.* Proceedings of the National Academy of Sciences, 1998. **95**(15): p. 8963-8968.

71. Ahn, H.-S., et al., *Na V 1.7 is the predominant sodium channel in rodent olfactory sensory neurons.* Molecular pain, 2011. **7**(1): p. 32.

72. Dib-Hajj, S.D., et al., *The Na v 1.7 sodium channel: From molecule to man.* Nature Reviews Neuroscience, 2013. **14**(1): p. 49-62.

73. Gilchrist, J. and F. bosmans, *Animal toxins can alter the function of Nav1.8 and Nav1.9.* Toxins, 2012. **4**(8): p. 620-632.

74. Kis-Toth, K., et al., *Voltage-gated sodium channel Nav1. 7 maintains the membrane potential and regulates the activation and chemokine-induced migration of a monocyte-derived dendritic cell subset.* The Journal of Immunology, 2011. **187**(3): p. 1273-1280.

75. Lo, W.-L., D.L. Donermeyer, and P.M. Allen, *A voltage-gated sodium channel is essential for the positive selection of CD4+ T cells.* Nature immunology, 2012. **13**(9): p. 880-887.

76. Carrithers, M.D., et al., *Expression of the voltage-gated sodium channel NaV1. 5 in the macrophage late endosome regulates endosomal acidification.* The Journal of Immunology, 2007. **178**(12): p. 7822-7832.

77. Black, J.A., S. Liu, and S.G. Waxman, *Sodium channel activity modulates multiple functions in microglia.* Glia, 2009. **57**(10): p. 1072-1081.

78. Gilchrist, J., B.M. Olivera, and F. Bosmans, *Animal toxins influence voltage-gated sodium channel function*, in *Handbook of Experimental Pharmacology*. 2014. p. 203-229.

79. Swartz, K.J., *Tarantula toxins interacting with voltage sensors in potassium channels.* Toxicon, 2007. **49**(2): p. 213-230.

80. Bosmans, F. and K.J. Swartz, *Targeting voltage sensors in sodium channels with spider toxins.* Trends in Pharmacological Sciences, 2010. **31**(4): p. 175-182.

81. Miller, J.A., W.S. Agnew, and S.R. Levinson, *Principal glycopeptide of the tetrodotoxin/saxitoxin binding protein from Electrophorus electricus: Isolation and partial chemical and physical characterization.* Biochemistry, 1983. **22**(2): p. 462-470.

82. Beneski, D.A. and W.A. Catterall, *Covalent labeling of protein conponents of the sodium channel with a photoactivable derivative of scorpion toxin.* Proceedings of the National Academy of Sciences of the United States of America, 1980. **77**(1): p. 639-643.

83. Thomsen, W.J. and W.A. Catterall, *Localization of the receptor site for α-scorpion toxins by antibody mapping: Implications for sodium channel*

topology. Proceedings of the National Academy of Sciences of the United States of America, 1989. **86**(24): p. 10161-10165.

84. Tejedor, F.J. and W.A. Catterall, *Site of covalent attachment of α-scorpion toxin derivatives in domain I of the sodium channel α subunit.* Proceedings of the National Academy of Sciences of the United States of America, 1988. **85**(22): p. 8742-8746.

85. Oliveira, J.S., et al., *Binding Specificity of Sea Anemone Toxins to Nav 1.1-1.6 Sodium Channels UNEXPECTED CONTRIBUTIONS FROM DIFFERENCES IN THE IV/S3-S4 OUTER LOOP.* Journal of Biological Chemistry, 2004. **279**(32): p. 33323-33335.

86. Teichert, R.W., et al., *Characterization of two neuronal subclasses through constellation pharmacology.* Proceedings of the National Academy of Sciences of the United States of America, 2012. **109**(31): p. 12758-12763.

87. Teichert, R.W., E.W. Schmidt, and B.M. Olivera, *Constellation pharmacology: a new paradigm for drug discovery.* Annual review of pharmacology and toxicology, 2015. **55**: p. 573-589.

88. Meisler, M.H. and J.A. Kearney, *Sodium channel mutations in epilepsy and other neurological disorders.* Journal of Clinical Investigation, 2005. **115**(8): p. 2010-2017.

89. Jurkat-Rott, K., et al., *Sodium channelopathies of skeletal muscle result from gain or loss of function.* Pflugers Archiv European Journal of Physiology, 2010. **460**(2): p. 239-248.

90. Adsit, G.S., et al., *Channelopathies from mutations in the cardiac sodium channel protein complex.* Journal of molecular and cellular cardiology, 2013. **61**: p. 34-43.

91. Waxman, S.G., *Channel, neuronal and clinical function in sodium channelopathies: from genotype to phenotype.* Nature neuroscience, 2007. **10**(4): p. 405-409.

92. Rhodes, T.H., et al., *Sodium channel dysfunction in intractable childhood epilepsy with generalized tonic–clonic seizures.* The Journal of physiology, 2005. **569**(2): p. 433-445.

93. Claes, L., et al., *De novo mutations in the sodium-channel gene SCN1A cause severe myoclonic epilepsy of infancy.* American Journal of Human Genetics, 2001. **68**(6): p. 1327-1332.

94. Escayg, A., et al., *Mutations of SCN1A, encoding a neuronal sodium channel, in two families with GEFS+ 2.* Nature genetics, 2000. **24**(4): p. 343-345.

95. Harkin, L.A., et al., *The spectrum of SCN1A-related infantile epileptic encephalopathies.* Brain, 2007. **130**(3): p. 843-852.

96. Mantegazza, M., et al., *Voltage-gated sodium channels as therapeutic targets in epilepsy and other neurological disorders.* The Lancet Neurology, 2010. **9**(4): p. 413-424.

97. Holland, K.D., et al., *Mutation of sodium channel SCN3A in a patient with cryptogenic pediatric partial epilepsy.* Neuroscience letters, 2008. **433**(1): p. 65-70.

98. Blumenfeld, H., et al., *Role of hippocampal sodium channel Nav1. 6 in kindling epileptogenesis.* Epilepsia, 2009. **50**(1): p. 44-55.

99. Ragsdale, D.S., *How do mutant Nav1.1 sodium channels cause epilepsy?* Brain Research Reviews, 2008. **58**(1): p. 149-159.

100. Frank, H.Y., et al., *Reduced sodium current in GABAergic interneurons in a mouse model of severe myoclonic epilepsy in infancy.* Nature neuroscience, 2006. **9**(9): p. 1142-1149.

101. Ogiwara, I., et al., *Nav1. 1 localizes to axons of parvalbumin-positive inhibitory interneurons: a circuit basis for epileptic seizures in mice carrying an Scn1a gene mutation.* Journal of Neuroscience, 2007. **27**(22): p. 5903-5914.

102. Kohrman, D.C., et al., *A missense mutation in the sodium channel Scn8a is responsible for cerebellar ataxia in the mouse mutant jolting.* Journal of Neuroscience, 1996. **16**(19): p. 5993-5999.

103. George Jr, A.L., *Inherited disorders of voltage-gated sodium channels.* Journal of Clinical Investigation, 2005. **115**(8): p. 1990-1999.

104. Fontaine, B., et al., *Hyperkalemic Periodic Paralysis and the Adult Muscle Sodium Channel (Alpha)-Subunit Gene.* Science, 1990. **250**(4983): p. 1000.

105. Hayward, L.J., R.H. Brown, and S.C. Cannon, *Inactivation defects caused by myotonia-associated mutations in the sodium channel III-IV linker.* The Journal of general physiology, 1996. **107**(5): p. 559-576.

106. Yang, N., et al., *Sodium channel mutations in paramyotonia congenita exhibit similar biophysical phenotypes in vitro.* Proceedings of the National Academy of Sciences, 1994. **91**(26): p. 12785-12789.

107. Cannon, S.C., *Pathomechanisms in channelopathies of skeletal muscle and brain*, in *Annual Review of Neuroscience*. 2006. p. 387-415.

108. Schott, J.-J., et al., *Cardiac conduction defects associate with mutations in SCN5A.* Nature genetics, 1999. **23**(1): p. 20-21.

109. Tan, H.L., et al., *A sodium-channel mutation causes isolated cardiac conduction disease.* Nature, 2001. **409**(6823): p. 1043-1047.

110. Wang, Q., et al., *SCN5A mutations associated with an inherited cardiac arrhythmia, long QT syndrome.* Cell, 1995. **80**(5): p. 805-811.

111. Makita, N., et al., *Drug-induced long-QT syndrome associated with a subclinical SCN5A mutation.* Circulation, 2002. **106**(10): p. 1269-1274.

112. Chen, Q., et al., *Genetic basis and molecular mechanism for idiopathic ventricular fibrillation.* Nature, 1998. **392**(6673): p. 293-296.

113. Bezzina, C., et al., *A single Na+ channel mutation causing both long-QT and Brugada syndromes.* Circulation Research, 1999. **85**(12): p. 1206-1213.

114. Grant, A.O., et al., *Long QT syndrome, Brugada syndrome, and conduction system disease are linked to a single sodium channel mutation.* The Journal of clinical investigation, 2002. **110**(8): p. 1201-1209.

115. Akai, J., et al., *A novel SCN5A mutation associated with idiopathic ventricular fibrillation without typical ECG findings of Brugada syndrome.* FEBS letters, 2000. **479**(1-2): p. 29-34.

116. Vatta, M., et al., *Genetic and biophysical basis of sudden unexplained nocturnal death syndrome (SUNDS), a disease allelic to Brugada syndrome.* Human molecular genetics, 2002. **11**(3): p. 337-345.

117. Sangwatanaroj, S., C. Ngamchareon, and S. Prechawat, *Pattern of inheritance in three sudden unexplained death syndrome (" Lai-tai") families.* Journal of the Medical Association of Thailand= Chotmaihet thangphaet, 2001. **84**: p. S443-51.

118. Sangwatanaroj, S., et al., *Linkage analyses and SCN5A mutations screening in five sudden unexplained death syndrome (Lai-tai) families.* Journal of the Medical Association of Thailand= Chotmaihet thangphaet, 2002. **85**: p. S54-61.

119. Baron, R.C., et al., *Sudden death among Southeast Asian refugees: an unexplained nocturnal phenomenon.* Jama, 1983. **250**(21): p. 2947-2951.

120. Cox, J.J., et al., *An SCN9A channelopathy causes congenital inability to experience pain.* Nature, 2006. **444**(7121): p. 894-898.

121. Goldberg, Y., et al., *Loss-of-function mutations in the Nav1. 7 gene underlie congenital indifference to pain in multiple human populations.* Clinical genetics, 2007. **71**(4): p. 311-319.

122. Leipold, E., et al., *A de novo gain-of-function mutation in SCN11A causes loss of pain perception.* Nature Genetics, 2013. **45**(11): p. 1399-1407.

123. Hirsch, E., D. Moye, and J.H. Dimon, *Congenital indifference to pain: long-term follow-up of two cases.* Southern medical journal, 1995. **88**(8): p. 851-857.

124. Weiss, J., et al., *Loss-of-function mutations in sodium channel Nav1. 7 cause anosmia.* Nature, 2011. **472**(7342): p. 186-190.

125. Yang, Y., et al., *Mutations in SCN9A, encoding a sodium channel alpha subunit, in patients with primary erythermalgia.* Journal of medical genetics, 2004. **41**(3): p. 171-174.

126. Faber, C.G., et al., *Gain-of-function Nav1. 8 mutations in painful neuropathy.* Proceedings of the National Academy of Sciences, 2012. **109**(47): p. 19444-19449.

127. Huang, J., et al., *Gain-of-function mutations in sodium channel NaV1. 9 in painful neuropathy.* Brain, 2014: p. awu079.

128. Zhang, X.Y., et al., *Gain-of-function mutations in SCN11A cause familial episodic pain.* The American Journal of Human Genetics, 2013. **93**(5): p. 957-966.

129. Latessa, V., *Erythromelalgia: a rare microvascular disease.* Journal of Vascular Nursing, 2010. **28**(2): p. 67-71.

130. Dib-Hajj, S.D., et al., *From genes to pain: Na v 1.7 and human pain disorders.* Trends in neurosciences, 2007. **30**(11): p. 555-563.

131. Dib-Hajj, S.D., J.A. Black, and S.G. Waxman, *Voltage-Gated Sodium Channels: Therapeutic Targets for Pain.* Pain Medicine, 2009. **10**(7): p. 1260-1269.

132. Kerr, B.J., et al., *A role for the TTX-resistant sodium channel Nav 1.8 in NGF-induced hyperalgesia, but not neuropathic pain.* Neuroreport, 2001. **12**(14): p. 3077-3080.

133. Jarvis, M.F., et al., *A-803467, a potent and selective Nav1. 8 sodium channel blocker, attenuates neuropathic and inflammatory pain in the rat.* Proceedings of the National Academy of Sciences, 2007. **104**(20): p. 8520-8525.

134. Payne, C.E., et al., *A novel selective and orally bioavailable Nav1. 8 channel blocker, PF-01247324, attenuates nociception and sensory neuron excitability.* British journal of pharmacology, 2015. **172**(10): p. 2654-2670.

135. Hains, B.C., et al., *Upregulation of sodium channel Nav1. 3 and functional involvement in neuronal hyperexcitability associated with central neuropathic pain after spinal cord injury.* Journal of Neuroscience, 2003. **23**(26): p. 8881-8892.

136. Samad, O.A., et al., *Virus-mediated shRNA knockdown of Nav1. 3 in rat dorsal root ganglion attenuates nerve injury-induced neuropathic pain.* Molecular Therapy, 2013. **21**(1): p. 49-56.

137. Harpaz, Y. and C. Chothia, *Many of the immunoglobulin superfamily domains in cell adhesion molecules and surface receptors belong to a new structural set which is close to that containing variable domains.* Journal of molecular biology, 1994. **238**(4): p. 528-539.

138. Isom, L.L., et al., *Primary structure and functional expression of the β1 subunit of the rat brain sodium channel.* Science, 1992. **256**(5058): p. 839-842.

139. Isom, L.L., et al., *Structure and function of the β2 subunit of brain sodium channels, a transmembrane glycoprotein with a CAM motif.* Cell, 1995. **83**(3): p. 433-442.

140. Morgan, K., et al., *β3: An additional auxiliary subunit of the voltage-sensitive sodium channel that modulates channel gating with distinct kinetics.* Proceedings of the National Academy of Sciences of the United States of America, 2000. **97**(5): p. 2308-2313.

141. Patino, G.A., et al., *Voltage-gated Na + channel β1B: A secreted cell adhesion molecule involved in human epilepsy.* Journal of Neuroscience, 2011. **31**(41): p. 14577-14591.

142. Yu, F.H., et al., *Sodium channel β4, a new disulfide-linked auxiliary subunit with similarity to β2.* Journal of Neuroscience, 2003. **23**(20): p. 7577-7585.

143. Messner, D.J. and W.A. Catterall, *The sodium channel from rat brain. Separation and characterization of subunits.* Journal of Biological Chemistry, 1985. **260**(19): p. 10597-10604.

144. Chen, C., et al., *Identification of the cysteine residue responsible for disulfide linkage of Na+ channel α and β2 subunits.* Journal of Biological Chemistry, 2012. **287**(46): p. 39061-39069.

145. Buffington, S.A. and M.N. Rasband, *Na+ channel-dependent recruitment of Navβ4 to axon initial segments and nodes of Ranvier.* Journal of Neuroscience, 2013. **33**(14): p. 6191-6202.

146. Namadurai, S., et al., *Crystal structure and molecular imaging of the Nav channelβ3 subunit indicates a trimeric assembly.* Journal of Biological Chemistry, 2014. **289**(15): p. 10797-10811.

147. Marionneau, C., et al., *The sodium channel accessory subunit Navβ1 regulates neuronal excitability through modulation of repolarizing Voltage-gated K+ channels.* Journal of Neuroscience, 2012. **32**(17): p. 5716-5727.

148. Nguyen, H.M., et al., *Modulation of voltage-gated K+ channels by the sodium channel β1 subunit.* Proceedings of the National Academy of Sciences of the United States of America, 2012. **109**(45): p. 18577-18582.

149. Deschênes, I., et al., *Post-transcriptional gene silencing of KChIP2 and Navβ1 in neonatal rat cardiac myocytes reveals a functional association between Na and Ito currents.* Journal of Molecular and Cellular Cardiology, 2008. **45**(3): p. 336-346.

150. Makita, N., P.B. Bennett, and A.L. George Jr, *Molecular determinants of β1 subunit-induced gating modulation in voltage-dependent Na+ channels.* Journal of Neuroscience, 1996. **16**(22): p. 7117-7127.

151. Qu, Y., et al., *Functional roles of the extracellular segments of the sodium channel α subunit in voltage-dependent gating and modulation by β1 subunits.* Journal of Biological Chemistry, 1999. **274**(46): p. 32647-32654.

152. McCormick, K.A., et al., *Molecular determinants of Na+ channel function in the extracellular domain of the β1 subunit.* Journal of Biological Chemistry, 1998. **273**(7): p. 3954-3962.

153. Johnson, D., et al., *The sialic acid component of the β1 subunit modulates voltage-gated sodium channel function.* Journal of Biological Chemistry, 2004. **279**(43): p. 44303-44310.

154. Johnson, D. and E.S. Bennett, *Isoform-specific effects of the β2 subunit on voltage-gated sodium channel gating.* Journal of Biological Chemistry, 2006. **281**(36): p. 25875-25881.

155. Sharkey, R.G., D.A. Beneski, and W.A. Catterall, *Differential labeling of the alpha and beta 1 subunits of the sodium channel by photoreactive derivatives of scorpion toxin.* Biochemistry, 1984. **23**(25): p. 6078-6086.

156. Aman, T.K., et al., *Regulation of persistent na current by interactions between β subunits of voltage-gated na channels.* Journal of Neuroscience, 2009. **29**(7): p. 2027-2042.

157. Ho, C., et al., *Differential expression of sodium channel β subunits in dorsal root ganglion sensory neurons.* Journal of Biological Chemistry, 2012. **287**(18): p. 15044-15053.

158. Cusdin, F.S., et al., *The sodium channel β3-subunit induces multiphasic gating in Na V1.3 and affects fast inactivation via distinct intracellular regions.* Journal of Biological Chemistry, 2010. **285**(43): p. 33404-33412.

159. Patton, D.E., et al., *The adult rat brain beta 1 subunit modifies activation and inactivation gating of multiple sodium channel alpha subunits.* Journal of Biological Chemistry, 1994. **269**(26): p. 17649-17655.

160. Chen, C. and S.C. Cannon, *Modulation of Na+channel inactivation by the β1 subunit: A deletion analysis.* Pflügers Archiv European Journal of Physiology, 1995. **431**(2): p. 186-195.

161. Isom, L.L., et al., *Functional co-expression of the β1 and type IIA α subunits of sodium channels in a mammalian cell line.* Journal of Biological Chemistry, 1995. **270**(7): p. 3306-3312.

162. Chanda, B., O.K. Asamoah, and F. Bezanilla, *Coupling Interactions between Voltage Sensors of the Sodium Channel as Revealed by Site-specific Measurements.* Journal of General Physiology, 2004. **123**(3): p. 217-230.

163. O'Malley, H.A. and L.L. Isom, *Sodium channel β subunits: Emerging targets in channelopathies*, in *Annual Review of Physiology*. 2015. p. 481-504.

164. Meadows, L., et al., *The intracellular segment of the sodium channel β1 subunit is required for its efficient association with the channel α subunit.* Journal of Neurochemistry, 2001. **76**(6): p. 1871-1878.

165. Spampanato, J., et al., *A novel epilepsy mutation in the sodium channel SCN1A identifies a cytoplasmic domain for β subunit interaction.* Journal of Neuroscience, 2004. **24**(44): p. 10022-10034.

166. Lopez-Santiago, L.F., et al., *Sodium channel Scn1b null mice exhibit prolonged QT and RR intervals.* Journal of Molecular and Cellular Cardiology, 2007. **43**(5): p. 636-647.

167. Chen, C., et al., *Mice Lacking Sodium Channel β1 Subunits Display Defects in Neuronal Excitability, Sodium Channel Expression, and Nodal Architecture.* Journal of Neuroscience, 2004. **24**(16): p. 4030-4042.

168. Qin, N., et al., *Molecular cloning and functional expression of the human sodium channel β1B subunit, a novel splicing variant of the β1 subunit.* European Journal of Biochemistry, 2003. **270**(23): p. 4762-4770.

169. Lopez-Santiago, L.F., et al., *Sodium channel β2 subunits regulate tetrodotoxin-sensitive sodium channels in small dorsal root ganglion neurons and modulate the response to pain.* Journal of Neuroscience, 2006. **26**(30): p. 7984-7994.

170. Maier, S.K.G., et al., *Distinct Subcellular Localization of Different Sodium Channel α and β Subunits in Single Ventricular Myocytes from Mouse Heart.* Circulation, 2004. **109**(11): p. 1421-1427.

171. Chen, C., et al., *Reduced sodium channel density, altered voltage dependence of inactivation, and increased susceptibility to seizures in mice lacking sodium channel β2-subunits.* Proceedings of the National Academy of Sciences of the United States of America, 2002. **99**(26): p. 17072-17077.

172. Uebachs, M., et al., *Efficacy loss of the anticonvulsant carbamazepine in mice lacking sodium channel β subunits via paradoxical effects on*

persistent sodium currents. Journal of Neuroscience, 2010. **30**(25): p. 8489-8501.

173. Meadows, L.S., et al., *Functional modulation of human brain Nav1.3 sodium channels, expressed in mammalian cells, by auxiliary β1, β2 and β3 subunits.* Neuroscience, 2002. **114**(3): p. 745-753.

174. Moran, O., F. Conti, and P. Tammaro, *Sodium channel heterologous expression in mammalian cells and the role of the endogenous β1-subunits.* Neuroscience letters, 2003. **336**(3): p. 175-179.

175. Moran, O., M. Nizzari, and F. Conti, *Endogenous expression of the β1A sodium channel subunit in HEK-293 cells.* FEBS letters, 2000. **473**(2): p. 132-134.

176. Takahashi, N., et al., *Expression of auxiliary β subunits of sodium channels in primary afferent neurons and the effect of nerve injury.* Neuroscience, 2003. **121**(2): p. 441-450.

177. Hakim, P., et al., *Scn3b knockout mice exhibit abnormal sino-atrial and cardiac conduction properties.* Acta Physiologica, 2010. **198**(1): p. 47-59.

178. Hakim, P., et al., *Scn3b knockout mice exhibit abnormal ventricular electrophysiological properties.* Progress in Biophysics and Molecular Biology, 2008. **98**(2-3): p. 251-266.

179. Bant, J.S. and I.M. Raman, *Control of transient, resurgent, and persistent current by open-channel block by Na channel β4 in cultured cerebellar granule neurons.* Proceedings of the National Academy of Sciences of the United States of America, 2010. **107**(27): p. 12357-12362.

180. Vassar, R., et al., *The β-secretase enzyme BACE in health and Alzheimer's disease: regulation, cell biology, function, and therapeutic potential.* Journal of Neuroscience, 2009. **29**(41): p. 12787-12794.

181. Miyazaki, H., et al., *Singular localization of sodium channel β4 subunit in unmyelinated fibres and its role in the striatum.* Nature communications, 2014. **5**.

182. Kazarinova-Noyes, K., et al., *Contactin associates with Na+ channels and increases their functional expression.* Journal of Neuroscience, 2001. **21**(19): p. 7517-7525.

183. Srinivasan, J., M. Schachner, and W.A. Catterall, *Interaction of voltage-gated sodium channels with the extracellular matrix molecules tenascin-C and tenascin-R.* Proceedings of the National Academy of Sciences of the United States of America, 1998. **95**(26): p. 15753-15757.

184. Malhotra, J.D., et al., *Sodium channel β subunits mediate homophilic cell adhesion and recruit ankyrin to points of cell-cell contact.* Journal of Biological Chemistry, 2000. **275**(15): p. 11383-11388.

185. Malhotra, J.D., et al., *Structural requirements for interaction of sodium channel β1 subunits with ankyrin.* Journal of Biological Chemistry, 2002. **277**(29): p. 26681-26688.

186. McEwen, D.P. and L.L. Isom, *Heterophilic interactions of sodium channel β1 subunits with axonal and glial cell adhesion molecules.* Journal of Biological Chemistry, 2004. **279**(50): p. 52744-52752.

187. Yereddi, N.R., et al., *The immunoglobulin domain of the sodium channel β3 subunit contains a surface-localized disulfide bond that is required for homophilic binding.* FASEB Journal, 2013. **27**(2): p. 568-580.

188. Wallace, R.H., et al., *Febrile seizures and generalized epilepsy associated with a mutation in the Na+-channel β1 subunit gene SCN1B.* Nature Genetics, 1998. **19**(4): p. 366-370.

189. Fendri-Kriaa, N., et al., *New mutation c.374C>T and a putative disease-associated haplotype within SCN1B gene in Tunisian families with febrile seizures.* European Journal of Neurology, 2011. **18**(5): p. 695-702.

190. Patino, G.A., et al., *A functional null mutation of SCN1B in a patient with Dravet syndrome.* Journal of Neuroscience, 2009. **29**(34): p. 10764-10778.

191. Ogiwara, I., et al., *A homozygous mutation of voltage-gated sodium channel βi gene SCN1B in a patient with Dravet syndrome.* Epilepsia, 2012. **53**(12).

192. Scheffer, I.E., et al., *Temporal lobe epilepsy and GEFS+ phenotypes associated with SCN1B mutations.* Brain, 2007. **130**(1): p. 100-109.

193. Watanabe, H., et al., *Sodium channel β1 subunit mutations associated with Brugada syndrome and cardiac conduction disease in humans.* Journal of Clinical Investigation, 2008. **118**(6): p. 2260-2268.

194. Kim, D.Y., et al., *Presenilin/γ-secretase-mediated cleavage of the voltage-gated sodium channel β2-subunit regulates cell adhesion and migration.* Journal of Biological Chemistry, 2005. **280**(24): p. 23251-23261.

195. Gersbacher, M.T., et al., *Identification of BACE1 cleavage sites in human voltage-gated sodium channel beta 2 subunit.* Molecular Neurodegeneration, 2010. **5**(1).

196. Li, R.G., et al., *Mutations of the SCN4B-encoded sodium channel β4 subunit in familial atrial fibrillation.* International Journal of Molecular Medicine, 2013. **32**(1): p. 144-150.

197. Medeiros-Domingo, A., et al., *SCN4B-encoded sodium channel β4 subunit in congenital long-QT syndrome.* Circulation, 2007. **116**(2): p. 134-142.

198. Tan, B.H., et al., *Sudden infant death syndrome-associated mutations in the sodium channel beta subunits.* Heart Rhythm, 2010. **7**(6): p. 771-778.

199. Baum, L., et al., *Case-control association study of polymorphisms in the voltage-gated sodium channel genes SCN1A, SCN2A, SCN3A, SCN1B, and SCN2B and epilepsy.* Human Genetics, 2014. **133**(5): p. 651-659.

200. Watanabe, H., et al., *Mutations in Sodium Channel β1- and β2-Subunits Associated With Atrial Fibrillation.* Circulation: Arrhythmia and Electrophysiology, 2009. **2**(3): p. 268-275.

201. Olesen, M.S., et al., *Mutations in sodium channel β-subunit SCN3B are associated with early-onset lone atrial fibrillation.* Cardiovascular Research, 2011. **89**(4): p. 786-793.

202. Ishikawa, T., et al., *Novel SCN3B mutation associated with brugada syndrome affects intracellular trafficking and function of Nav1.5.* Circulation Journal, 2013. **77**(4): p. 959-967.

203. Hu, D., et al., *A Mutation in the β3 Subunit of the Cardiac Sodium Channel Associated With Brugada ECG PhenotypeCLINICAL PERSPECTIVE.* Circulation: Cardiovascular Genetics, 2009. **2**(3): p. 270-278.

204. Wilde, A.A. and R. Brugada, *Phenotypical manifestations of mutations in the genes encoding subunits of the cardiac sodium channel.* Circulation research, 2011. **108**(7): p. 884-897.

205. Oyama, F., et al., *Sodium channel β4 subunit: Down-regulation and possible involvement in neuritic degeneration in Huntington's disease transgenic mice.* Journal of Neurochemistry, 2006. **98**(2): p. 518-529.

206. Chioni, A.M., et al., *A novel adhesion molecule in human breast cancer cells: Voltage-gated Na+ channel β1 subunit.* International Journal of Biochemistry and Cell Biology, 2009. **41**(5): p. 1216-1227.

207. Schreibmayer, W., M. Wallner, and I. Lotan, *Mechanism of modulation of single sodium channels from skeletal muscle by the β1-subunit from rat brain.* Pflügers Archiv European Journal of Physiology, 1994. **426**(3-4): p. 360-362.

208. Zhang, Z.N., et al., *The voltage-gated Na+ channel Nav1.8 contains an ER-retention/retrieval signal antagonized by the β3 subunit.* Journal of Cell Science, 2008. **121**(19): p. 3243-3252.

209. Kazen-Gillespie, K.A., et al., *Cloning, localization, and functional expression of sodium channel β1A subunits.* Journal of Biological Chemistry, 2000. **275**(2): p. 1079-1088.

210. Diss, J.K.J., et al., *β-Subunits of voltage-gated sodium channels in human prostate cancer: Quantitative in vitro and in vivo analyses of mRNA expression.* Prostate Cancer and Prostatic Diseases, 2008. **11**(4): p. 325-333.

211. Wong, H.K., et al., *β subunits of voltage-gated sodium channels are novel substrates of β-site amyloid precursor protein-cleaving enzyme (BACE1) and γ-secretase.* Journal of Biological Chemistry, 2005. **280**(24): p. 23009-23017.

212. Brackenbury, W.J. and L.L. Isom, *Voltage-gated Na+ channels: Potential for β subunits as therapeutic targets.* Expert Opinion on Therapeutic Targets, 2008. **12**(9): p. 1191-1203.

213. Wilson, M.J., et al., *Navβ subunits modulate the inhibition of Nav1.8 by the analgesic gating modifier μO-conotoxin MrVIB.* Journal of Pharmacology and Experimental Therapeutics, 2011. **338**(2): p. 687-693.

214. Zhang, M.M., et al., *Pharmacological fractionation of tetrodotoxin-sensitive sodium currents in rat dorsal root ganglion neurons by μ-conotoxins.* British Journal of Pharmacology, 2013. **169**(1): p. 102-114.

215. Rogers, J.C., et al., *Molecular determinants of high affinity binding of α-scorpion toxin and sea anemone toxin in the S3-S4 extracellular loop in domain IV of the Na+ channel α subunit.* Journal of Biological Chemistry, 1996. **271**(27): p. 15950-15962.

216. Xiao, Y., et al., *The tarantula toxins ProTx-II and huwentoxin-IV differentially interact with human Nav1.7 voltage sensors to inhibit channel*

activation and inactivation. Molecular Pharmacology, 2010. **78**(6): p. 1124-1134.

217. Marcotte, P., et al., *Effects of Tityus serrulatus scorpion toxin γ on voltage-gated Na+ channels.* Circulation Research, 1997. **80**(3): p. 363-369.

218. Liu, Z., et al., *Crystal structure of the extracellular domain of human myelin protein zero.* Proteins: Structure, Function and Bioinformatics, 2012. **80**(1): p. 307-313.

219. Karshikoff, A. and R. Ladenstein, *Ion pairs and the thermotolerance of proteins from hyperthermophiles: A 'traffic rule' for hot roads.* Trends in Biochemical Sciences, 2001. **26**(9): p. 550-556.

220. Zhou, T.T., et al., *Glycosylation of the sodium channel β4 subunit is developmentally regulated and involves in neuritic degeneration.* International Journal of Biological Sciences, 2012. **8**(5): p. 630-639.

221. Baroni, D., et al., *Functional modulation of voltage-dependent sodium channel expression by wild type and mutated C121W-β1 subunit.* Journal of Bioenergetics and Biomembranes, 2013. **45**(4): p. 353-368.

222. Egri, C., Y.Y. Vilin, and P.C. Ruben, *A thermoprotective role of the sodium channel β 1 subunit is lost with the β 1(C121W) mutation.* Epilepsia, 2012. **53**(3): p. 494-505.

223. Meadows, L.S., et al., *Functional and biochemical analysis of a sodium channel β1 subunit mutation responsible for generalized epilepsy with febrile seizures plus type 1.* Journal of Neuroscience, 2002. **22**(24): p. 10699-10709.

224. Wimmer, V.C., et al., *Axon initial segment dysfunction in a mouse model of genetic epilepsy with febrile seizures plus.* Journal of Clinical Investigation, 2010. **120**(8): p. 2661-2671.

225. Jover, E., et al., *The correlation between Na+ channel subunits and scorpion toxin-binding sites. A study in rat brain synaptosomes and in brain neurons developing in vitro.* Journal of Biological Chemistry, 1988. **263**(3): p. 1542-1548.

226. Gee, N.S., et al., *The novel anticonvulsant drug, gabapentin (neurontin), binds to the α2δ subunit of a calcium channel.* Journal of Biological Chemistry, 1996. **271**(10): p. 5768-5776.

227. Lenkowski, P.W., et al., *Lidocaine block of neonatal Nav1.3 is differentially modulated by co-expression of β1 and β3 subunits.* European Journal of Pharmacology, 2003. **467**(1-3): p. 23-30.

228. Makielski, J.C., et al., *Intrinsic lidocaine affinity for Na channels expressed in Xenopus oocytes depends on α (hH1 vs. rSkM1) and β1 subunits.* Cardiovascular Research, 1999. **42**(2): p. 503-509.

229. Farmer, C., et al., *Splice variants of Nav1.7 sodium channels have distinct β subunit-dependent biophysical properties.* PLoS ONE, 2012. **7**(7).

230. Middleton, R.E., et al., *Two tarantula peptides inhibit activation of multiple sodium channels.* Biochemistry, 2002. **41**(50): p. 14734-14747.

231. Konno, K., et al., *Isolation and structure of pompilidotoxins, novel peptide neurotoxins in solitary wasp venoms.* Biochemical and Biophysical Research Communications, 1998. **250**(3): p. 612-616.

232. Béress, L., R. Béress, and G. Wunderer, *Isolation and characterisation of three polypeptides with neurotoxic activity from Anemonia sulcata.* FEBS Letters, 1975. **50**(3): p. 311-314.

233. Céard, B., et al., *Purification of the main β-toxin from Tityus serrulatus scorpion venom using high-performance liquid chromatography.* Toxicon, 1992. **30**(1): p. 105-110.

234. Martin, M.F. and H. Rochat, *Large scale purification of toxins from the venom of the scorpion Androctonus australis Hector.* Toxicon, 1986. **24**(11-12): p. 1131-1139.

235. Kopeyan, C., G. Martinez, and H. Rochat, *Primary structure of toxin IV of Leiurus quinquestriatus quinquestriatus. Characterization of a new group of scorpion toxins.* FEBS Letters, 1985. **181**(2): p. 211-217.

236. Auld, V.J., et al., *A rat brain na+ channel α subunit with novel gating properties.* Neuron, 1988. **1**(6): p. 449-461.

237. Navas Díaz, A., F. García Sanchez, and J.A. González García, *Hydrogen peroxide assay by using enhanced chemiluminescence of the luminol-H2O2-horseradish peroxidase system: Comparative studies.* Analytica Chimica Acta, 1996. **327**(2): p. 161-165.

238. Lobo, P.A., et al., *The deletion of exon 3 in the cardiac ryanodine receptor is rescued by β strand switching.* Structure, 2011. **19**(6): p. 790-798.

239. Kabsch, W., *XDS.* Acta Crystallographica Section D: Biological Crystallography, 2010. **66**(2): p. 125-132.

240. McCoy, A.J., et al., *Phaser crystallographic software.* Journal of Applied Crystallography, 2007. **40**(4): p. 658-674.

241. Langer, G., et al., *Automated macromolecular model building for X-ray crystallography using ARP/wARP version 7.* Nature Protocols, 2008. **3**(7): p. 1171-1179.

242. Emsley, P. and K. Cowtan, *Coot: Model-building tools for molecular graphics.* Acta Crystallographica Section D: Biological Crystallography, 2004. **60**(12 I): p. 2126-2132.

243. Murshudov, G.N., A.A. Vagin, and E.J. Dodson, *Refinement of macromolecular structures by the maximum-likelihood method.* Acta Crystallographica Section D: Biological Crystallography, 1997. **53**(3): p. 240-255.

244. Brunger, A.T., et al., *Crystallography and NMR system: A new software suite for macromolecular structure determination.* Acta Crystallographica Section D: Biological Crystallography, 1998. **54**(5): p. 905-921.

245. Nettleship, J.E., et al., *Methods for protein characterization by mass spectrometry, thermal shift (ThermoFluor) assay, and multiangle or static light scattering.* Methods in molecular biology (Clifton, N.J.), 2008. **426**: p. 299-318.

246. Weiser, T. and N. Wilson, *Inhibition of tetrodotoxin (TTX)-resistant and TTX-sensitive neuronal Na+ channels by the secretolytic ambroxol.* Molecular Pharmacology, 2002. **62**(3): p. 433-438.

247. Watanabe, H., et al., *Mutations in sodium channel beta1- and beta2-subunits associated with atrial fibrillation.* Circulation. Arrhythmia and electrophysiology, 2009. **2**(3): p. 268-75.

248. Watanabe, H., et al., *Sodium channel beta1 subunit mutations associated with Brugada syndrome and cardiac conduction disease in humans.* The Journal of clinical investigation, 2008. **118**(6): p. 2260-8.

249. Ogiwara, I., et al., *A homozygous mutation of voltage-gated sodium channel beta(I) gene SCN1B in a patient with Dravet syndrome.* Epilepsia, 2012. **53**(12): p. e200-3.

250. Wallace, R.H., et al., *Febrile seizures and generalized epilepsy associated with a mutation in the Na+-channel beta1 subunit gene SCN1B.* Nature genetics, 1998. **19**(4): p. 366-70.

251. Fendri-Kriaa, N., et al., *New mutation c.374C>T and a putative disease-associated haplotype within SCN1B gene in Tunisian families with febrile seizures.* European journal of neurology : the official journal of the European Federation of Neurological Societies, 2011. **18**(5): p. 695-702.

252. Patino, G.A., et al., *A functional null mutation of SCN1B in a patient with Dravet syndrome.* The Journal of neuroscience : the official journal of the Society for Neuroscience, 2009. **29**(34): p. 10764-78.

253. Orrico, A., et al., *Mutational analysis of the SCN1A, SCN1B and GABRG2 genes in 150 Italian patients with idiopathic childhood epilepsies.* Clinical genetics, 2009. **75**(6): p. 579-81.

254. Valdivia, C.R., et al., *Loss-of-function mutation of the SCN3B-encoded sodium channel {beta}3 subunit associated with a case of idiopathic ventricular fibrillation.* Cardiovascular research, 2010. **86**(3): p. 392-400.

255. Sjoblom, T., et al., *The consensus coding sequences of human breast and colorectal cancers.* Science, 2006. **314**(5797): p. 268-74.

256. Ishikawa, T., et al., *Novel SCN3B mutation associated with brugada syndrome affects intracellular trafficking and function of Nav1.5.* Circulation journal : official journal of the Japanese Circulation Society, 2013. **77**(4): p. 959-67.

257. Namadurai, S., et al., *A new look at sodium channel β subunits.* Open Biology, 2015. **5**(1).

258. Zhang, M.M., et al., *Co-expression of NaVβ subunits alters the kinetics of inhibition of voltage-gated sodium channels by pore-blocking μ-conotoxins.* British Journal of Pharmacology, 2013. **168**(7): p. 1597-1610.

259. Wilson, M.J., et al., *α- And β-subunit composition of voltage-gated sodium channels investigated with μ-conotoxins and the recently discovered μO§-conotoxin GVIIJ.* Journal of Neurophysiology, 2015. **113**(7): p. 2289-2301.

260. Gilchrist, J., et al., *Crystallographic insights into sodium-channel modulation by the β4 subunit.* Proceedings of the National Academy of Sciences of the United States of America, 2013. **110**(51).

261. Brackenbury, W.J., M.B.A. Djamgoz, and L.L. Isom, *An emerging role for voltage-gated Na+ channels in cellular migration: Regulation of central*

nervous system development and potentiation of invasive cancers. Neuroscientist, 2008. **14**(6): p. 571-583.

262. O'Malley, H.A., et al., *Loss of Na+ channel β2 subunits is neuroprotective in a mouse model of multiple sclerosis.* Molecular and Cellular Neuroscience, 2009. **40**(2): p. 143-155.

263. Copits, B.A. and G.T. Swanson, *Dancing partners at the synapse: Auxiliary subunits that shape kainate receptor function.* Nature Reviews Neuroscience, 2012. **13**(10): p. 675-686.

264. Milstein, A.D. and R.A. Nicoll, *Regulation of AMPA receptor gating and pharmacology by TARP auxiliary subunits.* Trends in Pharmacological Sciences, 2008. **29**(7): p. 333-339.

265. Dolphin, A.C., *Calcium channel auxiliary α 2 δ and β subunits: Trafficking and one step beyond.* Nature Reviews Neuroscience, 2012. **13**(8): p. 542-555.

266. Doeser, A., et al., *The effects of eslicarbazepine on persistent Na+ current and the role of the Na+ channel β subunits.* Epilepsy Research, 2014. **108**(2): p. 202-211.

267. Gajewiak, J., et al., *A disulfide tether stabilizes the block of sodium channels by the conotoxin μOS-GVIIJ.* Proceedings of the National Academy of Sciences of the United States of America, 2014. **111**(7): p. 2758-2763.

268. Zhang, M.M., et al., *Probing the Redox States of Sodium Channel Cysteines at the Binding Site of μO§-Conotoxin GVIIJ.* Biochemistry, 2015. **54**(25): p. 3911-3920.

269. Martin, M.F., et al., *Use of high performance liquid chromatography to demonstrate quantitative variation in components of venom from the scorpion Androctonus australis hector.* Toxicon, 1987. **25**(5): p. 569-573.

270. Zimmer, T. and K. Benndorf, *The intracellular domain of the β2 subunit modulates the gating of cardiac Nav1.5 channels.* Biophysical Journal, 2007. **92**(11): p. 3885-3892.

271. Zimmer, T., et al., *The β1 subunit but not the β2 subunit colocalizes with the human heart NA+ channel (hH1) already within the endoplasmic reticulum.* Journal of Membrane Biology, 2002. **186**(1): p. 13-21.

272. Malhotra, J.D., et al., *Characterization of sodium channel α- and β-subunits in rat and mouse cardiac myocytes.* Circulation, 2001. **103**(9): p. 1303-1310.

273. Van Petegem, F., et al., *Structure of a complex between a voltage-gated calcium channel β-subunit and an α-subunit domain.* Nature, 2004. **429**(6992): p. 671-675.

274. Minor, W., et al., *HKL-3000: The integration of data reduction and structure solution - From diffraction images to an initial model in minutes.* Acta Crystallographica Section D: Biological Crystallography, 2006. **62**(8): p. 859-866.

275. Emsley, P., et al., *Features and development of Coot.* Acta Crystallographica Section D: Biological Crystallography, 2010. **66**(4): p. 486-501.

276. Adams, P.D., et al., *PHENIX: A comprehensive Python-based system for macromolecular structure solution.* Acta Crystallographica Section D: Biological Crystallography, 2010. **66**(2): p. 213-221.

277. Yu, Y., et al., *Molecular mechanism of the assembly of an acid-sensing receptor ion channel complex.* Nature Communications, 2012. **3**.

278. Das, S., et al., *Binary architecture of the Nav 1.2-β2 signaling complex.* eLife, 2016. **5**(FEBRUARY2016).

279. Stix, G., *A toxin against pain.* Scientific American, 2005. **292**(4): p. 88-93.

280. Veiseh, M., et al., *Tumor paint: a chlorotoxin: Cy5. 5 bioconjugate for intraoperative visualization of cancer foci.* Cancer research, 2007. **67**(14): p. 6882-6888.

281. COLMAN, A., et al., *The influence of topology and glycosylation on the fate of heterologous secretory proteins made in Xenopus oocytes.* European Journal of Biochemistry, 1981. **113**(2): p. 339-348.

282. Santacruz-Toloza, L., et al., *Glycosylation of shaker potassium channel protein in insect cell culture and in Xenopus oocytes.* Biochemistry, 1994. **33**(18): p. 5607-5613.

283. Tate, C.G., et al., *Comparison of seven different heterologous protein expression systems for the production of the serotonin transporter.*

Biochimica et Biophysica Acta (BBA)-Biomembranes, 2003. **1610**(1): p. 141-153.

Curriculum Vitae

John Michael Gilchrist

Born 21 August 1988

Olongapo, the Philippines

Education and research experience

2011 – 2017: Ph.D., Cellular and Molecular Physiology, lab of Frank Bosmans, Department of Physiology, Johns Hopkins University, Baltimore, MD

Research interests: the role of auxiliary beta-subunits in the voltage-gated sodium channel signaling complex

Thesis committee: Frank Bosmans, Kenton Swartz, Michael Caterina, Jeremy Nathans, David Yue (former)

2009 – 2010: M.S., Forensic Toxicology (degree uncompleted), University of Colorado, Colorado Springs, CO

2006 – 2009: B.S., Microbiology Colorado State University, Fort Collins, CO

2007 – 2009: Undergraduate Research, lab of Alan Schenkel, Department of Microbiology, Immunology, and Pathology, Colorado State University, Fort Collins, CO

Research interests: use of a PECAM-KO mouse to study idiopathic pulmonary fibrosis

Professional activities

2016 – present: International Society on Toxinology, *member*

2013 – 2015: American Association for the Advancement of Science, *member (Program for Excellence in Science)*

2013 – present: Society for General Physiology, *member*

2012 – present: Biophysical Society, *member*

2009 – 2012: Phi Kappa Phi, *member*

Teaching experience

University level

2013 – 2014: Teaching Assistant (Pathways and Regulation, Organ Physiology), Department of Physiology, Johns Hopkins University, Baltimore, MD

2008: MIP384 Supervised College Teaching (Introduction to Microbiology Lab), Department of Microbiology, Immunology, and Pathology, Colorado State University, Fort Collins, CO

High school level

2009 – 2011: Substitute Teacher (Biology, Chemistry, DNA Science)

Academy School District 20, Colorado Springs, CO

Publications

Research papers

(* indicates [co-]first authorship)

• Wingerd J, Mozar C, Üssing C, Murali S, Chin Y, Cristofori-Armstrong B, Durek T, Gilchrist J, Vaughn C, Bosmans F, Adams D, Lewis R, Alewood P, Mobli M, Christie M, and Rash L. *Sci Rep* (in revision).

• Ikonomopoulou M, Smith J, Herzig V, Pineda S, Dziemborowicz S, Er S-Y, Durek T, Gilchrist J, Alewood P, Nicholson G, Bosmans F, and King G. “Isolation of two insecticidal toxins from venom of the Australian theraphosid spider *Coremiocnemis tropix*”. *Toxicon* 123 (2016):62-70.

• Herzig V, Ikonomopoulou M, Smith J, Dziemborowicz, Gilchrist J, Kuhn-Nentwig L, Nicholson G, Bosmans F, and King G. “Molecular basis of the remarkable species selectivity of an insecticidal sodium channel toxin with from the African spider *Augacephalus ezendami*”. *Sci Rep* 6 (2016):29538.

• Osteen J, Herzig V, Gilchrist J, Emrick J, Zhang C, Wang X, Castro J, Garcia-Caraballo S, Grundy L, Rychkov G, Dekan Z, Undheim E, Alewood P, Brierley S, Basbaum A, Bosmans F, King G, and Julius D. “Subtype-selective spider toxins implicate Nav1.1 voltage-gated sodium channels in mechanical pain”. *Nature* 534.7608 (2016):494-9.

• *Das S, Gilchrist J, Bosmans F, and Van Petegem F. “Binary architecture of the Nav1.2-β2 signaling complex”. *eLife* 5 (2016):e10960.

• Bende N, Dziemborowicz S, Mobli M, Herzig V, Gilchrist J, Wagner J, Nicholson G, King G, and Bosmans F. “A distinct sodium channel voltage-sensor locus determines insect selectivity of the spider toxin Dc1a”. *Nat Commun* 5 (2014).

• Lishnevsky M, Young L, Woods S, Groshong S, Basaraba R, Gilchrist J, Higgins D, Gonzalez-Juarrero, Bass T, Muller W, and Schenkel A. "Microhemorrhage is an Early Event in the Pulmonary Fibrotic Disease of PECAM-1 Deficient FVB/n Mice". *Exp Mol Pathol* 97.1 (2014):128-36.

• *Gilchrist J, Dutton S, Diaz-Bustamante M, McPherson A, Olivares N, Kalia J, Escayg A, and Bosmans F. “Nav1.1 modulation by a novel triazole compound attenuates epileptic seizures in rodents”. *ACS Chem Biol* 9.5 (2014):1204-12.

• *Gilchrist J, Das S, Van Petegem F, and Bosmans F. “Crystallographic insights into sodium channel modulation by the β4 subunit”. *Proc Natl Acad Sci U S A* 110.51 (2014):5016-24.

• Schroeder W, Mitrescu L, Hart L, Unnithan R, Gilchrist J, Smith E, Shanley C, Benedict K, Taraba L, Volckens J, Basaraba R, and Schenkel A. “Flexible low-cost system for small animal aerosol inhalation exposure to drugs, proteins, inflammatory agents, and infectious agents”. *Biotechniques* 46.3 (2009):3-8.

• Early M, Lishnevsky M, Gilchrist J, Higgins D, Orme I, Muller W, Gonzalez-Juarerro M, and Schenkel A. “Non-invasive diagnosis of early pulmonary disease in PECAM-deficient mice using infrared pulse oximetry”. *Exp Mol Pathol* 87.2 (2009):152-8.

Reviews

• *Gilchrist J and Bosmans F. "Animal Toxins Can Alter the Function of Nav1.8 and Nav1.9." *Toxins* 4.8 (2012):620-32.

• *Gilchrist J, Olivera B, and Bosmans F. *Handbook of Experimental Pharmacology – voltage-gated sodium channels* (Editor: Peter Ruben). (2013)

Conference Presentations

Abstracts

• Gilchrist J, Das S, Van Petegem F, and Bosmans F. “β-subunits in context: an illustrative model of sodium channel/β-subunit interactions”. Biophysical Society 2017 Annual Meeting (2017), New Orleans, LA.

• Gilchrist J, Das S, Van Petegem F, and Bosmans F. “Proposed architecture of the Nav channel/β-subunit signaling complex”. XII Congress of the Pan American Section of the International Society of Toxinology (2016), Miami, FL.

• Gilchrist J, Das S, Van Petegem F, and Bosmans F. “Binary architecture of the Nav1.2-β2 signaling complex”. Gordon Research Conference, 2016 Ion Channels (2016), Mount Holyoke College, MA.

• Gilchrist J, Das S, Van Petegem F, and Bosmans F. “Binary architecture of the Nav1.2-β2 signaling complex”. Biophysical Society 2016 Annual Meeting (2016), Los Angeles, CA.

• Gilchrist J and Bosmans F. “Rufinamide modifies the gating process of human voltage-gated sodium channels”. Biophysical Society 2013 Annual Meeting (2013), Philadelphia, PA.

• Gilchrist J and Schenkel A. “The Role of T-Regulatory Lymphocytes in a Murine Model of Idiopathic Pulmonary Fibrosis.” Celebrate Undergraduate Research and Creativity (2008), Fort Collins, CO.

Presentations

• Gilchrist J, Das S, Van Petegem F, and Bosmans F. “β4 Modulates Nav1.2 Toxin Pharmacology”. Platform: Voltage-gated Na Channels. Biophysical Society 2014 Annual Meeting (2014), San Francisco, CA.

Department of Physiology Seminar Series:

• “Binary architecture of the Nav1.2- β2 signaling complex” (2016)

• “Crystallographic insights into sodium-channel modulation by the β2 subunit” (2015)

• “β4 modulates Nav1.2 toxin pharmacology” (2013)

• “The anticonvulsant rufinamide modifies gating characteristics of voltage-gated sodium channels” (2012)

Funding support

2013 – 2017: 1F31NS084646-01A1 (NIH)

The role of auxiliary subunits in the sodium channel signaling complex.